T-4013

A HETEROGENEOUS PETROPHYSICAL MODEL FOR POROUS MEDIA

by

Robert L. Elliott

T-4013

A thesis submitted to the Faculty and the Board of Trustees of the Colorado School of Mines in partial fulfillment of the requirements for the degree of Master of Science (Geophysics).

Golden, Colorado
Date March 31, 1992

Signed: Robert L. Elliott
Robert L. Elliott

Approved: Guy Towle
Dr. Guy H. Towle
Thesis Advisor

Golden, Colorado
Date April 2, 1992

P R Romig
Dr. Phillip R. Romig
Professor and Head,
Department of Geophysics

ABSTRACT

Existing theoretical models for conductance and storage have given limited insight into pore space controls on petrophysical properties and their interrelationships. Few have been rigorously compared to empirical data. In this research, a cellular heterogeneous rock properties model is developed. Simultaneous computer simulation is accomplished for the following array of integrated petrophysical properties: porosity, formation factor, permeability, irreducible water saturation, residual oil saturation, resistivity index, cementation and saturation exponents, relative permeabilities, capillary pressure, bulk density, and surface area per unit volume.

The natural complexity and variability of the pore space is developed through Monte Carlo simulation of a network with individual cells acting in parallel. Three cell geometries were proposed: the Tube Model, the Tube Vug Model, and the Dual Tube Vug Model. Stochastic input parameters directly corresponded to microelements in the rock. Intuitive equations were derived through direct relation to geologic parameters and physical processes.

Over 350 preliminary simulations were run to 1) test the effects of varying pore space parameters on the modelled properties, 2) determine the most appropriate internal cell structure, and 3) invert experimental petrophysical data to yield pore space information.

The introduction of non-conductive pore volumes and oil-retaining pore volumes resulted in reasonable irreducible water saturations and residual oil saturations, which provide assymptotic limits on the simulated capillary pressure and relative permeability curves. The proportion of vuggy pore space to total pore space was seen to strongly influence calculated porosities, cementation exponents, and values of S_V. The shapes of the capillary pressure curves were uniquely determined by the average pore size, the range

of pore size, and to a lesser extent, the shape of the pore size distribution. The Tube Model succeeded in matching F, ϕ, k, m, n, I, P_c, and ρ_b data as accurately as the Tube Vug and Dual Tube Vug Models, with a minimum of input variables. The Dual Vug Model provided limited improvement in calculated relative permeability curves.

By adjusting the input distributions of the pore space parameters, data from nonreservoir Facies 1 and reservoir Facies 2.3 of the North Sea Fulmar Sandstone have been accurately simulated. The Monte Carlo method yielded results that were able to correctly simulate the natural heterogeneities of the formation factors, porosities, permeabilities, and cementation exponents. The model data for Facies 1 exhibited the moderate to high porosities, low permeabilities, highly variable pore throat sizes, high irreducible water saturations, and gently sloping capillary pressure curves seen in the empirical data. Likewise, the high porosities, high permeabilities, narrow range of pore sizes, very low irreducible water saturations, and steeply-sloping flat-plateaued capillary pressure curves of Facies 2. 3 were matched.

Based upon pore geometry and conductance parameters provided from pseudo-inversion of empirical data, Facies 1 has been interpreted as a low-energy marine shaly siltstone, and Facies 2.3 as a VF - F grained moderate-energy marginal marine argillaceous sandstone.

This modelling paradigm can serve as a "stand-alone" framework or, with significant computer resources, as an integral part of a reservoir simulation package. Detailed reservoir characterization of reservoir-nonreservoir-fluid systems can thus be substantially improved by microscopic attention to the pore network. The modelling framework can aid in 1) extrapolating known data sets, 2) determining the microstructure of real rock through inversion of petrophysical data, and 3) delineation and evaluation of productive facies.

TABLE OF CONTENTS

LIST OF FIGURES

LIST OF TABLES

ACKNOWLEDGEMENTS

I would like to express my deep appreciation to Dr. Guy Towle, my thesis advisor, for his helpful guidance and encouragement. The enthusiasm he expressed for this project, as well as his invaluable experience and intuitive conveyance of the science of petrophysics, were a source of great inspiration. The conceptual framework for the abstract model was developed by him, and many of the applied concepts came from our many enlightening discussions. I would also like to thank Dr. Walt Whitman and Dr. Tom Davis for participating as members of my graduate committee.

I also wish to extend my gratitude to the Center for Well Logging and Petrophysics for the financial support for my graduate studies; to the Department of Geophysics for the teaching assistantships that were awarded to me; and to Shell UK Exploration & Production for providing the data used in my research project.

I would especially like to thank my mother, Karen Elliott, and my grandparents, Larry and Luella Barber, for their love and encouragement throughout my life. My greatest appreciation goes to them, whose support and understanding have made this research possible.

GLOSSARY

Latin Symbol	Definition
A	Bulk area of network in square μm
a_i	Cross-sectional area of unit cell in square μm
C	Conversion constant, 1.0133×10^8 (cp/p) (dyne/cm^2/atm)
C_i, C_b	Individual cell and bulk conductances in ohms
C_{extra}	Extra conductance of network in mhos of wetting phase saturated cells, clay water, or surface conduction
F	Formation Factor
I	Resistivity Index
k	Absolute permeability in darcies
kr_{nw}	Relative permeability to non-wetting phase
kr_w	Relative permeability to wetting phase
L	Length of cell in direction parallel to flow in μm
Le	Effective length along tortuous tube path in μm
M	Index of cell with highest displacement pressure that is saturated with non-wetting fluid
m	Cementation exponent
NC	Number of cells in network
n	Saturation exponent
P	Pressure
P_c	Capillary pressure in psig
P_d	Displacement pressure in psig
Q	Volume rate of flow in cm^3/sec

R_i	Vug radius of unit cell in μm
R_o	Resistivity of rock that is 100% water saturated in Ωm
R_t	Resistivity of partially saturated rock in Ωm
R_w	Resistivity of water in Ωm
r_i	Tube radius of unit cell in μm
rl_i	Large tube radius of unit cell in μm
rs_i	Small tube radius of unit cell in μm
So_{res}	Residual oil saturation
S_v	Surface area per unit volume
Sw	Water saturation
Sw_{irr}	Irreducible water saturation
V_{ext}	Extraneous pore volume
V_{tube}, V_{vug}	Pore volume related to tubes and vugs

Greek Symbol	**Definition**
α	Ratio of extraneous pore volume to total pore volume
γ	Ratio of volume of residual oil to total pore volume
μ	Viscosity of fluid
ρ_b	Bulk density in g/cm^3
ρ_m	Matrix density in g/cm^3
ρ_o	Oil density in g/cm^3
ρ_w	Water density in g/cm^3
τ_i	Tortuosity of tube in unit cell; L_e / L
τl_i	Tortuosity of large tube in unit cell

τs_i	Tortuosity of small tube in unit cell

Subscript Symbol	**Definition**
b	Bulk rock property of the network
i	Rock property of individual cell
j	Summation in series and parallel Darcy equations
T	Tube Model
TV	Tube Vug Model
DTV	Dual Tube Vug Model

CHAPTER 1. INTRODUCTION

The most important technological areas which depend primarily on the properties of porous media are hydrology and petroleum exploration and production. Hydrology utilizes these properties as they relate to water movement in earth material, such as flow to wells from aquifers, intrusion of sea water into coastal areas, dam projects, and filter beds for the purification of water. The petroleum industry is mainly concerned with exploration and production of oil and natural gas, well logging, and well drilling and development.

Theoretical models for conductance and storage have attempted to simulate a wide range of hydrological and petrophysical properties by representation of the pore space. These have given limited insight into the pore space controls on the physical properties of rocks and how these properties are interrelated.

Porous rocks are often viewed at the macroscopic scale as an entirely homogeneous body; this, however, is too simplistic to develop rock models at the scale to simulate and interpret such properties as porosity and permeability. A microscopic treatment of the essentially heterogeneous nature of the pore space aids in producing improved results that are applicable to the fields of hydrology and petroleum engineering, and scientifically valid. At a large enough scale, the material indeed appears homogeneous; this is a manifestation of the Law of Large Numbers in probability theory. Embedded network theory (Madden, 1976) defines how this can be broken down into sub-networks that show small statistical variation about the bulk homogeneous property. The process can be continued down to elemental fragments, or phenomenological points, with full statistical variation of the material properties.

It is the purpose of this research to develop a conceptual and mathematical framework for a cellularly-based heterogeneous rock properties model. By preserving natural statistical variations in the input parameters of the model, which are associated with their correlative physical attributes in the pore space, the model will rationalize the bulk properties that are observed by engineering and geophysical techniques.

Section 1.1 Motivational Background

This research will apply the model specifically to its application in petroleum exploration and production. Both the exploration and primary and enhanced recovery processes continue to require more accurate and integrated reservoir description to reduce wildcat, development, and drilling risks. Detailed simulations and interpretations also provide the input data for economic investment analysis of development proposals. Mathematical models and simulations of reservoir performance have generally in the past lacked realistic rock-fluid descriptions; this can potentially lead to suboptimal management decisions.

An optimal model will be able to contribute to the many facets of the petroleum business. It can aid in the delineation and evaluation of new reserves in a detailed reservoir rock description that is appropriate in content and detail. Knowledge of the depositional/diagenetic processes that control the reservoir and non-reservoir rock can be incorporated into the input process. This can lead to better estimates of (1) hydrocarbons-in-place, through porosity and fluid saturations, and (2) recoverable reserves, through relative permeabilities.

In the logging phase, a better knowledge of the interrelationships between rock properties can lead to a reduction in the number of geophysical measurements. It may also illuminate petrophysical properties that are not directly measurable, such as permeability and water saturation. It may also permit more accurate and salient measurements as the physical and chemical properties of the rock-fluid system are gradually more understood.

As the production phase of petroleum development progresses, a refined rock properties simulator can model vertical or horizontal fluid flow, or permeability barriers. Zones of unusually high permeability, either production "fingers" or "thief" zones, can likewise be simulated. Therefore, a microscopically-scaled heterogeneous rock model will provide a synergistic integration between geology (via stratigraphy), geophysics (through petrophysical analysis), and petroleum engineering (applied to reservoir simulation) that can provide the best description of macroscopic reservoir properties and megascopic continuity.

Section 1.2 Historical Perspective

The objective of petrophysical modeling by networks has been to describe the geophysical phenomena that have been observed and, ideally, to predict phenomena that have not yet been observed. Previous network models have had various degrees of applicability over wider or narrower ranges of circumstances. The developments of these models have followed from either the introduction of theoretical concepts or advances in technology. The chart in Figure 1 shows the historical development of these models from

Technology	***Theory***	***Network Models***
	Modelling of relationship of only two properties	
Analog electrical resistor network		
	Two-dimensional network modeling	
		Tube model
		Bundle-of-tubes model
	Tortuosity concepts	
		Tube-vug model
Advances in computing power		
	Computer solution of network flow equations	
	Monte Carlo solutions	
	Both theoretical and empirical modelling	
		Sphere pack modelling
	Empirical, geometrical, and shape correction factors	
		Three-dimensional network modelling
	Fluid permeability	
	Two-phase flow	
	Application to dynamic and static flow characteristics	
	Ka, Kr, Pc with hysteresis, I-Sw relation	
	Percolation theory	
	Random processes	
	Network theory	
	Non-uniqueness qualities of resistor networks	
	Miscible vs. immiscible flow	
Image analysis of pore geometries		
Optical data processing and Fourier transforms		
	Realistic pore size distributions in network	
		Statistical pore models
		Unified rock properties model
More advances in computing power		
	Inversion of rock properties models	
	Attention to non-Archie rocks	

Figure 1. The historical development of petrophysical networks and statistical rock properties models.

syntheses of technological or academic breakthroughs, progressing from the 1940s at the top to the 1990s at the bottom.

In 1942, Gus Archie of Shell Oil inspired attempts to derive relationships between various petrophysical properties based upon empirical evidence. Electrical resistivity measurements on 100% brine saturated and partially hydrocarbon saturated rocks established empirical relations between F and ϕ, and I and Sw. Analysis and confirmation of these two relationships were undertaken by Wyllie and Rose (1950) and Winsauer et al. (1951). Wyllie and Rose concluded that the saturation exponent must vary with Sw due to pore tortuosities, while Winsauer et al derived a similar F-ϕ formula to Archie's, $F = a\phi^{-m}$. Empirically derived values of a=0.62 and m=2.15 resulted in the Humble Equation.

Analog resistor networks allowed the calculation of transport properties through various versions of Ohm's Law. Owen (1952) and Fatt (1956a,b,c) recognized the need for an improved conceptual representation of the pore space over previous capillary tube models. Owen's model consisted of smaller pore tubes connecting larger pore vugs (Figure 2). This view of the pore space reduced the tortuosities of 5-72 (Wyllie and Spangler, 1952) to believable levels of 1-5. This fact was later substantiated through ion tracer studies (Winsauer et al., 1952), percolation theory (Kirkpatrick, 1973), and geometrical considerations (Dullien, 1975, 1976). A network of tubes model (Figure 3) was proposed by Fatt in various 2-D array patterns to give interconnectedness to the previous bundle-of-tubes concepts. The pore elements were cylindrical pore tubes whose radii were distributed randomly from given distributions. The permeability could then be calculated via the Poiseuille pipe flow law and hydraulic analogy to Ohm's Law. This network had limited success in predicting capillary hysteresis and relative permeability curves.

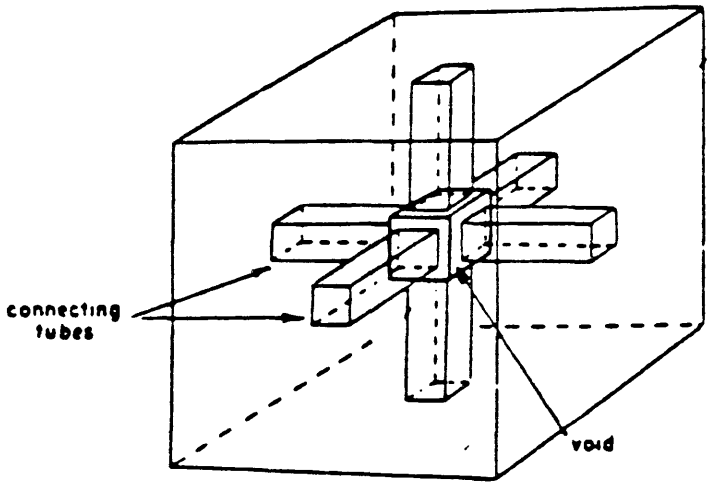

Figure 2. Pore space representation by nodes and tubes (Owen, 1952).

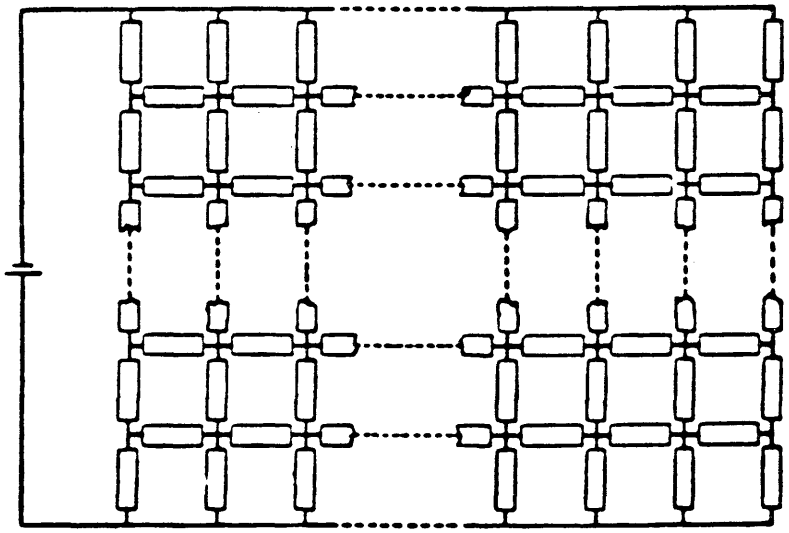

Figure 3. Two-dimensional network of capillary tubes (Fatt, 1956a,b,c).

With advances in computing power came the capability to solve network flow equations (Rose [1968] and Nicholson and Petropoulos [1971]) and the reduction in 2-D model computation times (Rink and Schopper, 1968). The results approached Archie relations as the size of these networks increased (Greenberg and Brace, 1969). Monte Carlo methods were then utilized (Dodd and Kiel, 1959) to study fluid displacement and wettability. It become apparent, however, that pore interconnection is a fundamental aspect of porous rock, and 3-D networks and sphere packs were studied to accommodate two-phase flow phenomena (Nicholson and Petropoulos, 1971). Kirkpatrick (1973) and Larson et al. (1977) investigated three-dimensional conduction through clusters of pores, rather than through single pore channels. Representation in 2-D has been proved as producing valid results for the properties under consideration (Winsauer et al. [1952], Fatt [1956]). Although flow takes place in 3-D, the spatial average obtained from the 2-D input parameters can be effective, provided the statistical representivity of the simulated rock is achieved. That is, changes in network form, radius distribution, and other aspects will influence the modelled properties in the same qualitative manner as in a 3-D network. Fatt (1956a) approached this by adding additional channels in the 2-D network to account for cross-connections in the third dimension.

Sphere pack models (Figure 4) from particle size distributions yielded tube radii distributions (Dodds and Lloyd, 1971) and permeability relations (Iczkowski, 1970). Yale (1984) expanded this concept by investigating the effects of pressure upon the grain-pore boundaries and its subsequent effect upon hydraulic and electrical conduction. Spherical packing models, however, have pore space configurations which are analytically complex and computationally-intensive.

In the late 1960's and early 1970's, advances in computer power also paved the way for application of recent work in percolation theory, network theory, and the study of random processes. Shante and Kirkpatrick (1971) and Kirkpatrick (1973) determined coordination numbers and percolation thresholds from optimum two-phase flow through particular networks. Capillary hysteresis was also modelled via percolation theory, although the theory gives inadequate representations in 2-dimensional networks. The extension from immiscible to miscible flow was studied by Dodds and Lloyd (1971) and Simon and Kelsey (1971), with the inclusion of annular flow (Somerton and Wood, 1988). Significant improvements over Fatt's model in the simulation of permeabilities and relative permeabilities were also achieved using network applications.

Madden (1976), in his treatment of network theory, substantiated the results that physical properties can be modelled by a wide variety of non-unique networks. Preston and Davis (1976) followed with the observation that the physical properties of a stochastic process can be modelled, requiring the equivalence of the autocovariance functions. This conclusion supports the non-uniqueness axiom of network theory.

Statistical pore models began to improve with fully random networks (Haring and Greenkorn, 1970) in which the tube radii, the lengths, and the exact position in space are randomly assigned. The pore geometry became more representative than the regular lattice networks; however, random field theory rather than electrical network theory had to be employed. Furthermore, capillary pressure could not be modelled through the diffusion and dispersion theoretical equations.

Further research on capillary pressure curves revealed the primary controlling factor, the tube radius distribution. Realizing the stochastic nature of the pore space, Dullien et al (1975, 1976) utilized photomicrographs and mercury porisimetry to provide

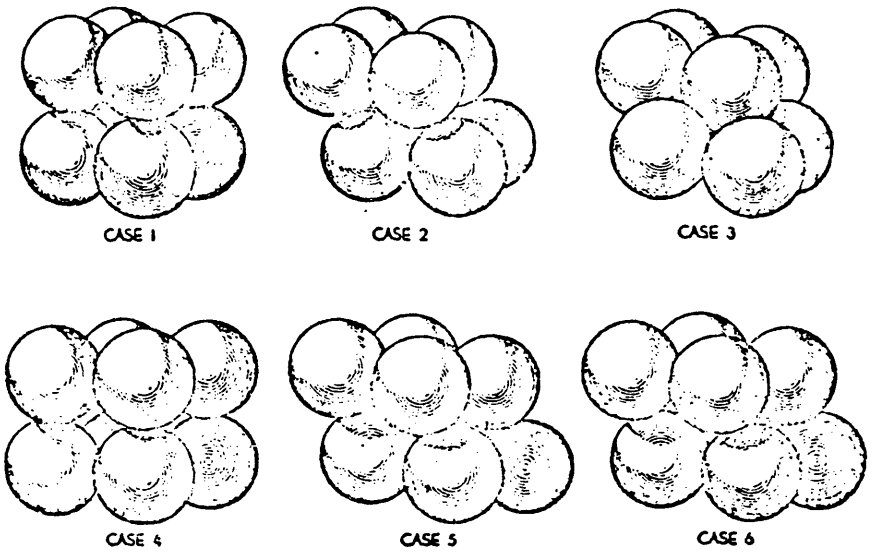

Figure 4. Six possible arrangements in sphere pack representations of the pore space (from Graton and Fraser, 1935).

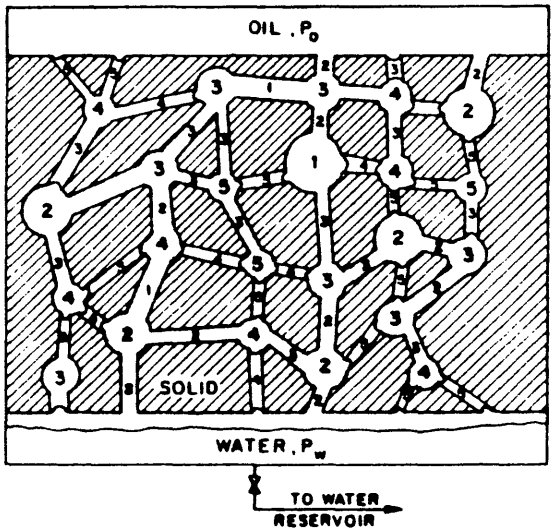

Figure 5. Irreducible water saturation from a two-dimensional pore network (Chatzis,1978).

empirical evidence of pore diameter distributions. He concluded that the constriction of entrances to the pores is an important aspect of the pore space. The network models of Dullien et al (1975a, 1978) incorporate tube networks of arbitrary orientation to macroscopic flow (Figure 5). Dullien's models integrate the permeability (the hydraulic conductivity) and the formation factor (reflecting the electrical conductivity) into statistical equations which produce excellent results. However, the lack of connectivity leads to differences in the capillary characteristics from real rocks.

Unified models (Kwon [1976] and Yale [1984]) were aimed at unifying the various rock property simulations into a comprehensive modelling of storage, and electrical and hydraulic conductivity. This simultaneous modeling leads to a more realistic and integrated representation of the pore space, and also encourages a better understanding of pore space controls on petrophysical properties and their interrelationships. Additionally, it balances the empirical and rational elements that play complementary roles in the understanding of geophysical measurements.

Section 1.3 Scope of Research

By developing a model that utilizes the natural complexity and variability of the pore space, and the stochastic nature of the replacement of one fluid with another in a porous medium, it is hoped that the research will yield the following results:

1.) Model simulations that match empirical petrophysical data;

2.) Insight into the pore space controls on various properties and the interrelationships between these properties;

3.) Simple, intuitive equations that define the model;

4.) Empirical and/or theoretical prediction of such saturation-dependent properties as relative permeability, capillary pressure, resistivity index, saturation exponent, irreducible water saturation, and residual oil saturation;

5.) Pseudo-inversion that may reveal natural statistical variations of pore space parameters in real rocks;

6.) A method of computer simulation that can be constructed in a reasonable amount of time on computers of modest capabilities;

7.) A framework with which to model all types of lithologies, from carbonates to siliciclastics, both consolidated and unconsolidated.

CHAPTER 2. DEVELOPMENT OF THE HRP MODEL

The heterogeneous rock properties (HRP) model is a conceptual and mathematical model for the simultaneous computer simulation of a wide array of integrated petrophysical properties. The initial proposal in 1989 of the abstract model is credited to Dr. Guy Towle at the Colorado School of Mines. This thesis details the application of this model to the most common and useful properties in exploration and production geophysics. These define the storage, geometric, gravimetric, saturation, and electrical and hydraulic conductivities of the rock. This model includes:

1) Porosity - ϕ
2) Formation Factor - F
3) Absolute Permeability - k
4) Water Saturation - Sw
   : Irreducible water saturation - Sw_{irr}
   : Residual oil saturation - So_{res}
5) Resistivity Index - I
6) Cementation Exponent - m
7) Saturation Exponent - n
8) Relative Permeabilities
   : Wetting phase - Kr_w
   : Non-wetting phase - Kr_{nw}
9) Capillary Pressure - Pc

10) Bulk Density - ρ_b

11) Surface area/ Volume - S_V

The model is comprised of many individual cells acting in parallel, with the bulk rock properties being calculated from a composite of the cells that form the network. The pore system as a series of parallel circuits is justified inasmuch as interconnections at high angles contribute little to bulk conductivity (Etris et al., 1989). The abstract model is conceptual and does not refer to any particular internal cell geometry. The applied model, upon which the results of this thesis is based, defines specific geometries of the matrix and the pore space in each cell. Furthermore, it employs input parameters that can directly correspond to microelements in the rock.

Section 2.1 The Abstract HRP Model

This model will utilize calculations from a 2-dimensional network to represent 3-dimensional flow phenomena. Based on the rationale supported by the authors cited in Chapter 1, the statistical representitivity of the 3-D rock may be achieved by 2-D analysis. Therefore, the HRP model will apply parameter distributions in a 2-D framework that will attempt to emulate 3-dimensional conditions.

Within the abstract framework, the individual cell properties can be completely independent of one another. One can then define the statistical distribution of cell permeabilities, for example. The individual cell properties are henceforth referred to with a

subscript "i", while the bulk property of the composite network is denoted with a subscript "b".

The faces of each cell have area a_i, and the total area of the network, in the dimension perpendicular to fluid flow, is $\Sigma a_i = A$. The cells in the abstract model may have any shape desired. The length of each cell is given by L and all cells have the same length. The direction along which L is measured is the dimension along which flow can proceed. A physical conception of this parallel network is shown in Figure 6. Within each cell, there exists pore space through which there can be conductance of electricity and/or fluids. Electrical conduction and water flow occurs only through the cells which are saturated with the wetting phase. The matrix is assumed non-conductive and therefore does not account for the cation exchange capacity of clays or conductance through minerals such as silver, copper, or pyrite. The pore space can be described mathematically as either cylindrical tubes or spherical vugs. Contrasted to this pore space is an additional pore volume that does not allow flow of either fluids or electricity. This is referred to as extraneous pore volume or extraneous porosity. The quantity of extraneous porosity is represented by the parameter α, which is the ratio of extraneous pore volume to the total pore volume. Therefore,

$$\alpha = V_{ext}/V_p = V_{ext}/(V_{tubes} + V_{vugs} + V_{ext}),$$

and the extraneous volume is related to α by

$$V_{ext} = \frac{\alpha}{(1-\alpha)} (V_{tubes} + V_{vugs}).$$

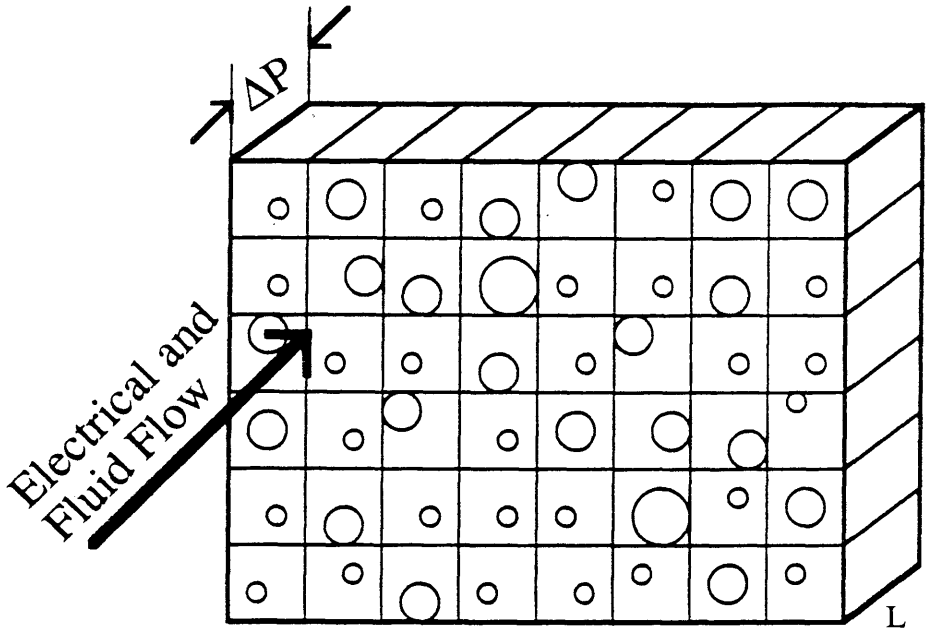

Figure 6. Parallel network of unit cells with pore tubes aligned in direction of current flow.

Note that when the extraneous volume is water saturated, this volume of water cannot leave the network under pressure flow. Thus it can approximate the irreducible water saturation by not having hydraulic communication with the bulk volume of water. Even at the highest capillary pressures, the volume of this water will be independent of further increases in pressure. These fluids may be trapped as pendular rings or in clusters of fine pores.

A reduced volume of nonwetting phase which is entrapped when the capillary pressure is decreased during imbibition is termed the residual oil saturation. This results in a hysteresis effect that can be identified from capillary pressure and relative permeability curves. The fraction of pore space that is occupied by trapped residual phase is proportional to the ratio of viscous to capillary forces within the system (Larson, Scriven,

and Davies, 1977). Pickett et al. (1966) cite pore size distribution, pore configurations, interfacial properties, and initial saturation as affecting So_{res}. Local pore geometry, topology, and fluid properties can cause the rupture of oil connections. In a similar development to Sw_{irr}, the residual oil saturation can be accommodated by definition of the parameter β, the ratio of the volume of residual oil to the total pore volume:

$$\beta = V_{oil} / V_p = V_{oil} / (V_{tubes} + V_{vugs} + V_{ext})$$

$$V_{oil} = \beta \left(1 + \frac{\alpha}{1-\alpha}\right) (V_{tubes} + V_{vugs}) .$$

The properties of the model which are not dependent upon fluid saturations, namely the porosity, formation factor, absolute permeability, cementation exponent, and surface area/volume, can be calculated based upon statistical distributions of either the cell properties or geometric parameters which determine those properties.

With an increasing capillary pressure differential across the network, cells which are initially saturated with the wetting phase (water) are progressively saturated with non-wetting fluid (oil). This enables Pc, Kr, I, n, and ρ_b curves, as a function of water saturation, to be constructed. The succession of cells saturate according to their capillary displacement pressures, with those associated with the lowest displacement pressures imbibing the non-wetting phase first. The parametric index M represents the index of the cell with the highest displacement pressure that is saturated with non-wetting fluid. The total number of cells in the network is NC. When M = 0, the network is completely water-saturated; when M = NC, the network contains oil as a single phase.

Each cell can hold either the wetting phase or the non-wetting phase. Electrical conductivity and permeability to the wetting phase is possible only if the cell is water-saturated. Conversely, if the cell is oil-saturated, there exists permeability to the non-wetting phase, but no electrical conductivity. By this paradigm, the curves of the saturation-dependent properties can be constructed as parametric equations of either Sw or M.

Section 2.2 The Applied HRP Model

The application of the model to a computer-based format is facilitated by defining the internal pore and matrix geometry for the individual cells. The actual pore space of rocks is too complex to be fully described; yet, the salient features of the pore space should be preserved so that the petrophysical properties can be accurately simulated. The equations defining the models should remain simple enough to intuitively reveal how the pore space parameters influence the properties. Three cell sub-models are proposed, based on preliminary research on the behavior of each: (1) The Tube model; (2) The Tube Vug model; and (3) The Dual Tube Vug model.

The Tube Model

This cell consists of a tortuous cylindrical tube, with a constant radius r_i, that travels through a nonconductive matrix volume (Figure 7). The cross-

sectional area of the cell for the applied model, a_i, is square and the radius of the tube is not allowed to exceed 0.5 $(a_i)^{1/2}$. The ratio of the effective length along the tube, Le, to the length of the cell, L, is termed the tortuosity and is signified by τ_i. It will be shown later that this model is not determined by L, which is assigned a constant value between the cells, but by τ alone. This definition of the parameter τ equates it to both the electric and hydraulic tortuosities. Statistical distributions of the four parameters $\{a_i, r_i, \tau_i, \alpha\}$ between the cells of the network can then define the bulk properties of the rock.

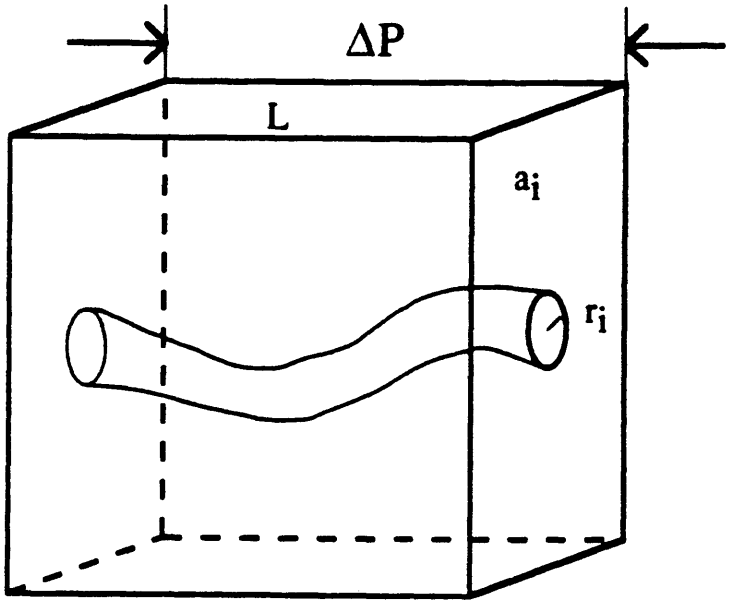

Figure 7. Physical conception of Tube Model individual cell.

The Tube Vug Model

A representative cell of this model (Figure 8) is composed of the same elements as the Tube Model, with the addition of a large spherical vug, or node, through which the tube passes. The radius of the individual vug is R_i and, like the tube, $R_i < 0.5\ (a_i)^{1/2}$. This model, therefore, has two additional degrees of freedom, having the five variables $\{a_i, r_i, R_i, \tau_i, L, \alpha\}$.

The Dual Tube Model

Building upon the Tube Vug model, this representation of the pore space has one additional tube intersecting the vug, in a direction parallel to fluid flow (Figure 9). The radii of the larger of the two and the smaller of the two are rl_i and rs_i, respectively. Likewise, the tortuosities are denoted τl_i and τs_i. This model has the highest degree of freedom with the input parameter suite $\{a_i, rl_i, rs_i, R_i, \tau l_i, \tau s_i, L, \alpha\}$.

The cell and bulk properties for each of these sub-models will now be derived. Subscripts "T", "TV", and "DTV" will differentiate between the equations for the three models.

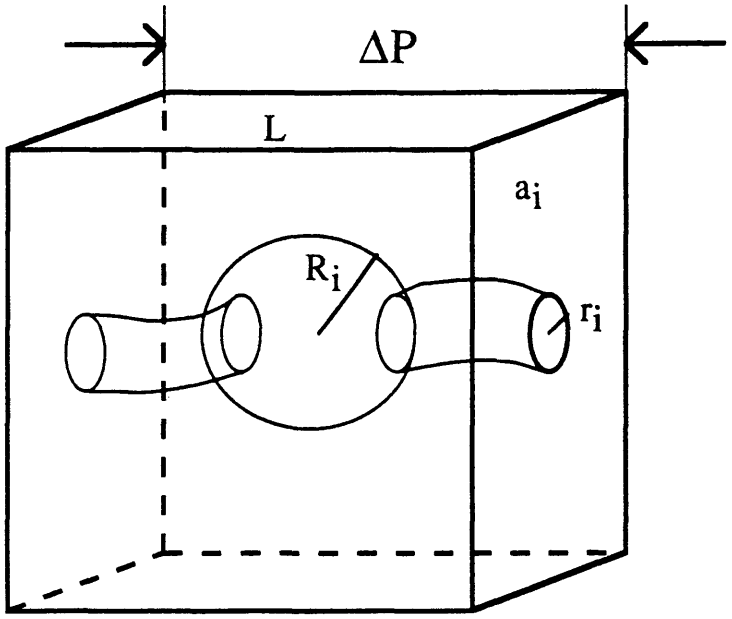

Figure 8. Physical conception of the Tube Vug Model.

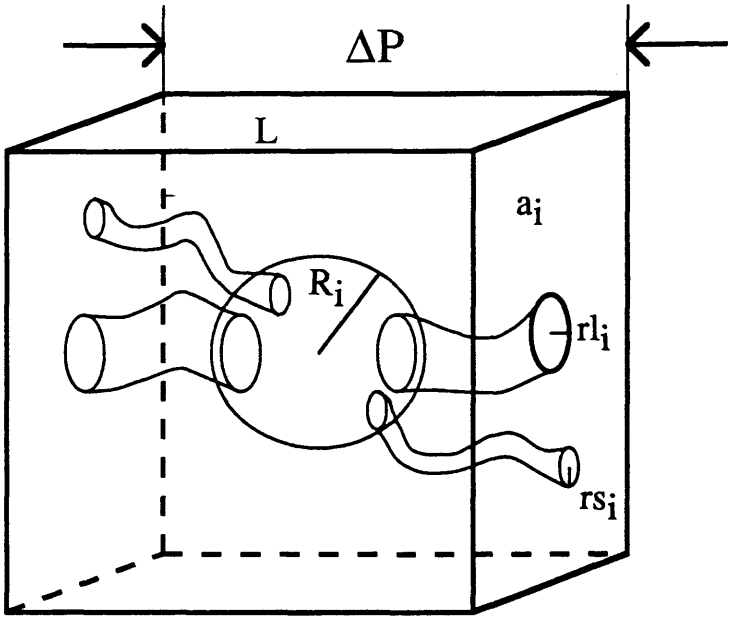

Figure 9. Physical conception of the Dual Tube Vug Model.

Section 2.2.1 Porosity

The porosity of the individual cell is defined as the ratio of the pore volume to the bulk cell volume,

$$\phi_i = (V_{tubes} + V_{vugs} + V_{ext}) / (L\, a_i)$$

The bulk porosity of the network of cells would then be given by the ratio of the total pore volume of the individual cells to the network bulk volume,

$$\phi_b = (\sum_{i=1}^{NC} \phi_i\, L\, a_i)/(L\ A) = (\sum_{i=1}^{NC} \phi_i\, a_i)/A.$$

The porous space within the Tube model is given by the sum of the extraneous porosity and that of the tube itself; therefore, the porosity for this model is given by,

$$\phi_i = \frac{V_{tube} + V_{vug} + V_{ext}}{L\ a_i} = \frac{V_{tube} + V_{vug} + \frac{\alpha}{1-\alpha}(V_{tube} + V_{vug})}{L\ a_i}$$

$$= \frac{(V_{tube} + V_{vug})(1 + \frac{\alpha}{1-\alpha})}{L\ a_i}$$

which, for the Tube model, is reduced to

$$\phi_{i(T)} = [(\pi\, r_i^2\, L_e + 0)(1 + \frac{\alpha}{1-\alpha})]/\ (L\ a_i) = \frac{\pi\, r_i^2\, \tau_i}{a_i} + \frac{\alpha}{1-\alpha}\ \frac{\pi\, r_i^2\, \tau_i}{a_i}$$

$$= \frac{\pi r_i^2 \tau_i (1-\alpha) + \alpha\pi r_i^2 \tau_i}{a_i (1-\alpha)} = \frac{\pi r_i^2 \tau_i}{a_i (1-\alpha)},$$

$$\phi_{b(T)} = (\sum_{i=1}^{NC} \phi_i a_i) / A = \sum_{i=1}^{NC} \pi r_i^2 \tau_i /[A (1-\alpha)] ;$$

and for the Tube Vug model,

$$\phi_{i(TV)} = [\pi r_i^2 \tau_i (L - 2R_i) + \frac{4}{3}\pi R_i^3] (1 + \frac{\alpha}{1-\alpha}) / (L a_i)$$

$$= \frac{\pi r_i^2 \tau_i (L - 2R_i) + \frac{4}{3}\pi R_i^3}{L a_i (1 - \alpha)}$$

$$\phi_{b(TV)} = (\sum_{i=1}^{NC} \phi_i a_i) / A = [\sum_{i=1}^{NC} \pi r_i^2 \tau_i (L-2R_i) + \frac{4}{3}\pi R_i^3]/[L A(1 - \alpha)];$$

and for the Dual Tube Vug model,

$$\phi_{i(DTV)} = \frac{\pi rl_i^2 \tau l_i(L - 2R_i) + \pi rs_i^2 \tau s_i(L - 2R_i) + \frac{4}{3}\pi R_i^3 + \frac{\alpha}{1-\alpha}V_{ext}}{L a_i}$$

$$= \frac{\pi rl_i^2 \tau l_i (L - 2R_i) + \pi rs_i^2 \tau s_i (L - 2R_i) + \frac{4}{3}\pi R_i^3}{L a_i (1-\alpha)}$$

$$\phi_{b(DTV)} = \left(\sum_{i=1}^{NC} \phi_i \; a_i\right) / A$$

$$= \sum_{i=1}^{NC} \frac{\pi \; (L - 2R_i) \; (rl_i^2 \; \tau l_i + rs_i^2 \; \tau s_i) \; + \; (4/3) \; \pi \; R_i^3}{L \; A \; (1 - \alpha)} \; .$$

Section 2.2.2 Formation Factor

The resistivity formation factor is the proportionality constant between the resistivity of a 100% water-saturated rock and that of the fluid with which it is saturated. It is apparent that the formation factor is, by definition, always greater than 1.0. This property can be understood as the influence of the pore structure on the resistance of the sample. This property was first defined by Sundberg (1932) as the "resistivity factor", and was calculated for various packings of spherical grains. This concept was later advanced in the form of the "formation resistivity factor" by Archie (1942) and a large number of Gulf Coast sandstones were used to investigate and expound upon the original hypothesis.

Simply stated, the formation factor can be represented by the formula,

$$F = \frac{R_o}{R_w}$$

from which, the equations for the formation factor for the Tube, Tube Vug, and Dual Tube Vug models follow. Additionally, the bulk formation factor for the entire network is given by calculating the conductance of the individual cells acting in parallel:

$$C_i = a_i / (R_o L) = a_i / (F_i R_w L)$$

An additional amount of parallel matrix or fluid conductance can be related to the bulk properties of the network. One such conductive mechanism can consist of additional cells in the network whose displacement pressures have not yet been overcome and are still saturated with the wetting conductive phase. Therefore, the addition of a bulk conductance can represent the sum of the conductances of portions of the pore system where $P_{d_i} > P_{d_{NC}}$. Laboratory capillary pressure experiments support the observation that at extremely high capillary pressures (on the order of 50,000 psi) there remain very fine capillaries into which the non-wetting phase can still be injected. The pressure required to displace water volumes held in residual pendular rings is likewise very great. Other physical mechanisms can include the extra conductivity of the water associated with the Waxman-Smits shaly-sand model, the "clay water" in the Dual-Water model, or surface conductivity from clay minerals lining the pore system. Givens (1987) notes that a small amount of illite can produce a large conductance in addition to that of the water-saturated tubes. Therefore, the bulk conductance can be written as,

$$C_b = \{[\sum_{i=1}^{NC} (a_i / F_i)] / (R_w L)\} + C_{extra}$$

In relation to bulk properties, the conductance of the network is

$$C_b = A / (R_w L F) .$$

Equating the last two equations results in the formula for the bulk formation factor,

$$F_b = A / \sum_{i=1}^{NC} [(a_i / F_i) + R_w L C_{extra}] .$$

The cell and bulk formation factors for the Tube model are thus:

$$F_{i(T)} = \frac{R_w L_e}{\pi r_i^2} / (\frac{R_w L}{a_i}) = \frac{\tau_i a_i}{\pi r_i^2}$$

$$F_{b(T)} = A / [\sum_{i=1}^{NC} (\pi r_i^2 / \tau_i) + R_w L C_{extra}] .$$

For the Tube Vug model, the electrical resistance attributed to the vug is that of the two intersections with the tube. It can be approximated by the electrical resistance of two point electrodes, with each electrode contributing $R_w / (2 \pi r)$,

$$R_{O(TV)} (L/a_i) = \frac{R_w \tau_i (L - 2R_i)}{\pi r_i^2} + (2 \frac{R_w}{2 \pi r_i})$$

$$F_{i(TV)} = \frac{R_w \tau_i (L - 2R_i) + R_w r_i}{\pi r_i^2} / (\frac{R_w L}{a_i})$$

$$= \frac{a_i [r_i + \tau_i (L - 2R_i)]}{\pi r_i^2 L}$$

$$F_{b(TV)} = A \; / \; \{ \sum_{i=1}^{NC} (\pi \, r_i^2 \, L) \; / \; [r_i + \tau_i \, (L - 2R_i)] + R_w \, L \, C_{extra} \}$$

and for the Dual Tube Vug model, the inverse of the resistance of a water-saturated cell is

$$\frac{L}{R_o a_i} = \frac{1}{[\frac{R_w \, \tau l_i (L - 2R_i)}{\pi \, rl_i^2} + 2 \, \frac{R_w}{2 \, \pi \, rl_i}]} + \frac{1}{[\frac{R_w \, \tau s_i (L - 2R_i)}{\pi \, rs_i^2} + 2 \, \frac{R_w}{2 \, \pi \, rs_i}]}$$

$$1/F_{i(DTV)} = \frac{L \, \pi}{a_i} \; [\frac{1}{\frac{\tau l_i \, (L - 2R_i)}{rl_i^2} + \frac{1}{rl_i}} + \frac{1}{\frac{\tau s_i \, (L - 2R_i)}{rs_i^2} + \frac{1}{rs_i}}]$$

$$F_{i(DTV)} = \frac{a_i}{L \;\; \pi} \{ \frac{[\tau l_i \, (L - 2R_i) + rl_i] \, [\tau s_i \, (L - 2R_i) + rs_i]}{rl_i^2 \, [\tau s_i \, (L - 2R_i) + rs_i] + rs_i^2 \, [\tau l_i \, (L - 2R_i) + rl_i]} \}$$

$$F_{b(DTV)} = A \; / \; \sum_{i=1}^{NC} (L \;\; \pi \; / \; F_i)$$

$$= A \; / \{ \sum_{i=1}^{NC} L \pi \frac{rl_i^2 [\tau s_i (L - 2R_i) + rs_i] + rs_i^2 [\tau l_i (L - 2R_i) + rl_i]}{[\tau l_i (L - 2R_i) + rl_i][\tau s_i (L - 2R_i) + rs_i]} + R_w L C_{extra} \}.$$

Section 2.2.3 Absolute Permeability

Absolute permeability is another property of the porous medium and is a measure of the capacity of the medium to transmit a single-phase fluid. In 1856, Darcy introduced an equation relating permeability to bulk quantities of the material and the fluid. He discovered experimentally that the rate of flow through porous media is linearly proportional to the applied pressure gradient. His results, with the addition of the viscosity factor, can essentially be given as

$$Q = \frac{(P_2 - P_1)\ A\ k}{L\ \mu} ,$$

where

Q - Volume rate of flow of fluid in cm^3/sec

$(P_1 - P_2)$ - Pressure differential in atmospheres

A - Cross sectional area in sq cm

k - Permeability in darcies

L - Length in cm

μ - Viscosity of fluid in centipoise.

Alternatively, the fluid conductivity through a capillary tube can be expressed by Poiseuille's Law, which can be put in the form,

$$Q = \frac{(P_2 - P_1)\ \pi\ r^4\ c_1\ c_2}{8\ L_e\ \mu} ,$$

where

Q - Volume rate of flow of fluid in cm^3/sec

$(P_2 - P_1)$ - Pressure differential in dynes/cm^2

r - Radius of the conduit in cm

c_1 - Unit conversion constant equal to 1.0133×10^6 dynes/cm^2 atm

c_2 - Unit conversion constant equal to 100 centipoises/poise

L_e - Effective length along the tube in cm

μ - Vicosity of fluid in poises.

Equating the fluid rate of flow for Darcy's Equation to that of Poiseuille's Law, in a similar manner to Carman (1939), Wyllie and Gardner (1958) and Amyx, Bass, and Whiting (1960), yields a useful equation for the permeability of a unit cell:

$$\frac{\Delta P \ A \ k}{L \ \mu} = \frac{\Delta P \ \pi \ r^4 \ c_1 \ c_2}{8 \ L_e \ \mu}$$

$$k_{i(T)} = \frac{(1.0133 \times 10^8) \ \pi \ r_i^4}{8 \ a_i \ \tau_i} \ ,$$

With the provision of laminar flow, this equation relates k to the tube radius, the cross-sectional area, and the tortuosity, and is independent of the pressure differential, the viscosity, and the flow rate. The two unit conversion constants, c_1 and c_2, have been grouped together into a new constant, C. In deriving the permeability for a network of cells acting in parallel, the flow rate from Darcy's Equation would be

$$Q_b = \frac{\Delta P}{L \ \mu} \sum_{i=1}^{NC} a_i \ k_i \ .$$

With respect to the bulk property of the total network, the flow rate is

$$Q_b = \frac{\Delta P \; A \; k}{L \; \mu} \; .$$

Equating the last two equations leads to the bulk permeability of the network

$$k_{b(T)} = \left(\sum_{i=1}^{NC} a_i \; k_i \right) / \; A \; .$$

The individual cell and bulk permeabilities for the Tube model are the same as those given above.

For the Tube Vug model, the composite permeability of the unit cell is calculated from the permeabilities of the tortuous tube and the vug, acting in series. From Amyx, Bass, and Whiting (1960), Darcy's Equation for elements in series yields,

$$k_{i(TV)} = \frac{L}{\sum_{j=1}^{2} (L_j \; / \; k_j)} = \frac{L}{\frac{(L - 2R_i)}{k_{tube}} + \frac{(2R_i)}{k_{vug}}} \; ;$$

note that the terms L_j in Darcy's Law are straight-line paths between the beginning and the end of the conduit, i.e. tortuosity is not applicable. The effective path length, L_e, is an integral path of Poiseuille's Law only. Since the permeability of the vug is very much greater than that of the tube, the second term in the denominator can be approximated by zero, and we have

$$k_{i(TV)} \approx \frac{L}{\frac{(L - 2R_i)}{k_{tube}}}$$

Substituting k_{tube},

$$k_{i(TV)} = L / \left[\frac{L - 2R_i}{\left(\frac{\pi \; r_i^4 \; C}{8 \; a_i \; \tau_i}\right)} \right] = L / \left[\frac{L - 2R_i}{\left(\frac{\pi \; r_i^4 \; C \; L}{8 \; a_i \; L_e}\right)} \right]$$

$$= L / \left[\frac{L - 2R_i}{\left(\frac{\pi \; r_i^4 \; C \; L}{8 \; a_i \; \tau_i (L - 2R_i)}\right)} \right]$$

$$= \frac{\pi \; r_i^4 \; L^2 \; (1.0133 \times 10^8)}{8 \; a_i \; \tau_i \; (L - 2R_i)^2}$$

$$k_{b(TV)} = \left(\sum_{i=1}^{NC} a_i \; k_i \right) / A$$

$$= \frac{(1.0133 \times 10^8) \; \pi \; L^2}{8} \left\{ \sum_{i=1}^{NC} r_i^4 / [\tau_i \; (L - 2R_i)^2] \right\}$$

The composite permeability of the unit cell of the Dual Tube Vug model is equal to the parallel flow combination of the tube permeabilities, each of which is in series with the vug. Darcy's Law for elements in parallel (Amyx, Bass, and Whiting, 1960), is

$$k_{i(DTV)} = \frac{a_i \; (k_{tube1} + k_{tube2})}{a_i}$$

$$= \frac{\pi \; rl_i^4 \; L^2 \; (1.0133 \times 10^8)}{8 \; a_i \; \tau l_i \; (L - 2R_i)^2} + \frac{\pi \; rs_i^4 \; L^2 \; (1.0133 \times 10^8)}{8 \; a_i \; \tau s_i \; (L - 2R_i)^2}$$

$$= \frac{\pi \ L^2 \ (1.0133 \times 10^8)}{8 \ a_i} \left[\frac{rl_i^4}{\tau l_i \ (L - 2R_i)^2} + \frac{rs_i^4}{\tau s_i \ (L - 2R_i)^2} \right]$$

$$k_{b(DTV)} = \left(\sum_{i=1}^{NC} a_i \ k_i \right) / A$$

$$= \frac{\pi L^2 (1.0133 \times 10^8)}{8} \sum_{i=1}^{NC} \left[\frac{rl_i^4}{\tau l_i (L - 2R_i)^2} + \frac{rs_i^4}{\tau s_i (L - 2R_i)^2} \right]$$

Section 2.2.4 Water Saturation

The water saturation of the network is equal to the ratio of water-saturated porosity to the total porosity, assuming a two-phase condition. The oil saturation is therefore equal to (1 - Sw). The water-saturation, and all saturation-dependent properties, are most convieniently derived and understood as bulk properties, therefore the subscript "b" will be implicit. For the Tube model, the total volume of water will be the volume of water in the water-saturated cells plus the volume of water in the extraneous porosity of the cells that are oil-saturated. The water saturation for the drainage of the network (drainage of the wetting phase) can therefore be described as

$$Sw_{(T)} = \left[\sum_{i=1}^{M} V_{ext} + \sum_{i=M+1}^{NC} (\phi_{i(T)} \ L \ a_i) \right] / \phi_{b(T)}$$

$$= \left[\sum_{i=1}^{M} \left(\frac{\alpha}{1-\alpha} \pi r_i^2 Le_i \right) + \sum_{i=M+1}^{NC} (\phi_{i(T)} a_i) \right] / \phi_{b(T)}$$

The water saturation for the Tube Vug model is then given by

$$Sw_{(TV)} = \left\{ \sum_{i=1}^{M} \left[\frac{\alpha}{1-\alpha} (\pi r_i^2 \tau_i (L - 2R_i) + \frac{4}{3} \pi R_i^3) \right] + \sum_{i=M+1}^{NC} (\phi_{i(TV)} La_i) \right\} / \phi_{b(TV)}$$

In the Dual Tube Vug model, when the displacement pressure of the larger tube in the cell is exceeded, the larger tube and the vug are saturated with the non-wetting fluid; the smaller tube and the extraneous porosity remain water-saturated. The Sw equation for this model is therefore,

$$Sw_{(DTV)} = \frac{\sum_{i=1}^{M} \frac{\alpha}{1-\alpha} \{ \pi (L-2R_i) [(rl_i^2 \tau l_i + rs_i^2 \tau s_i) + rs_i^2 tsi] + \frac{4}{3} \pi R_i^3 \} + \sum_{i=M+1}^{NC} (\phi_{i(DTV)} La_i)}{\phi_{b(DTV)}}$$

At partial saturations for a water-wet medium, the wetting phase will preferentially occupy the pores associated with the smallest throats. Therefore, any residual oil remaining during the imbibition phase will be in the pores that correlate with a low M index. The modification of the Sw equations above for imbibition merely involve subtracting $V_{oil} = \gamma V_p$ from the second term of the denominator, where γ runs from 0.0 to β and increases with decreasing M.

Section 2.2.5 Resistivity Index

The resistivity index, I, is the ratio of the resistivity of the partially saturated rock to that of the water saturated rock,

$$I = \frac{R_t}{R_o} ;$$

or, alternatively, as the ratio of the water saturated conductivity to the partially saturated conductivity. The conductivity of the network decreases as the cells are increasingly filled with the nonconductive fluid and was given above by

$$C_b = \left[\sum_{i=1}^{NC} (a_i / F_i) \right] / (R_w L) .$$

The Tube and Tube Vug models are able to conduct electrical current through all water saturated ($i > M$) cells; an identical situation occurs for the Dual Tube Vug model because the conductive path through the water in the small tubes (for cells of $i < M+1$) is interupted by the nonconductive oil in the vug. Therefore, the resistivity ratios for the Tube, Tube Vug, and Dual Tube Vug models are expressed as

$$I = \frac{\sum_{i=1}^{NC} (a_i / F_i)}{\sum_{i=M+1}^{NC} (a_i / F_i)} .$$

Section 2.2.6 Cementation Exponent

According to the well-established and empirically-derived Archie (1942) relationship, the formation factor and porosity are related by the cementation exponent, m, by

$$F = \phi^{-m} .$$

The F-ϕ relationship for 5 different sandstones (Archie, 1942) show the same linear trend and approximately the same derived values of m; this is shown in Figure 10.This relationship has been researched and verified by many authors, including Owen (1952), Winsauer et al (1952), Wyllie and Spangler (1952), Wyllie and Gregory (1953), Wyllie and Gardner (1958), Atkins (1961), Towle (1962), and Schopper (1966). Values of m typically range from 1.6 to 2.2, although they have been reported as low as 1.3 and as high as 3. Towle (1962) cites the physical significance of m as discussed by previous authors as related to (1) degree of cementation of grains, (2) grain shape, sorting, and packing, (3) type of pore system - intergranular, intercrystalling, vuggy, fracture, etc., (4) tortuosity of pores, and/or (5) compaction of rock by overburden.

In an analysis of the effect of various pore geometries on the F-ϕ relationship (Towle, 1962), systems of square tubes and planar fractures result in values of m that are low (1.13-1.65 for square tubes, 1.07-1.25 for planes). A planar-vug conductance network, with octahedral nodal pores, resulted in m's that were low to approximately 2; a spherical vug network obtained m's that were typically high (2.6 - ∞). A square tube - spherical vug geometry, however, produced values for m (from 1.5 to 2.5) that match

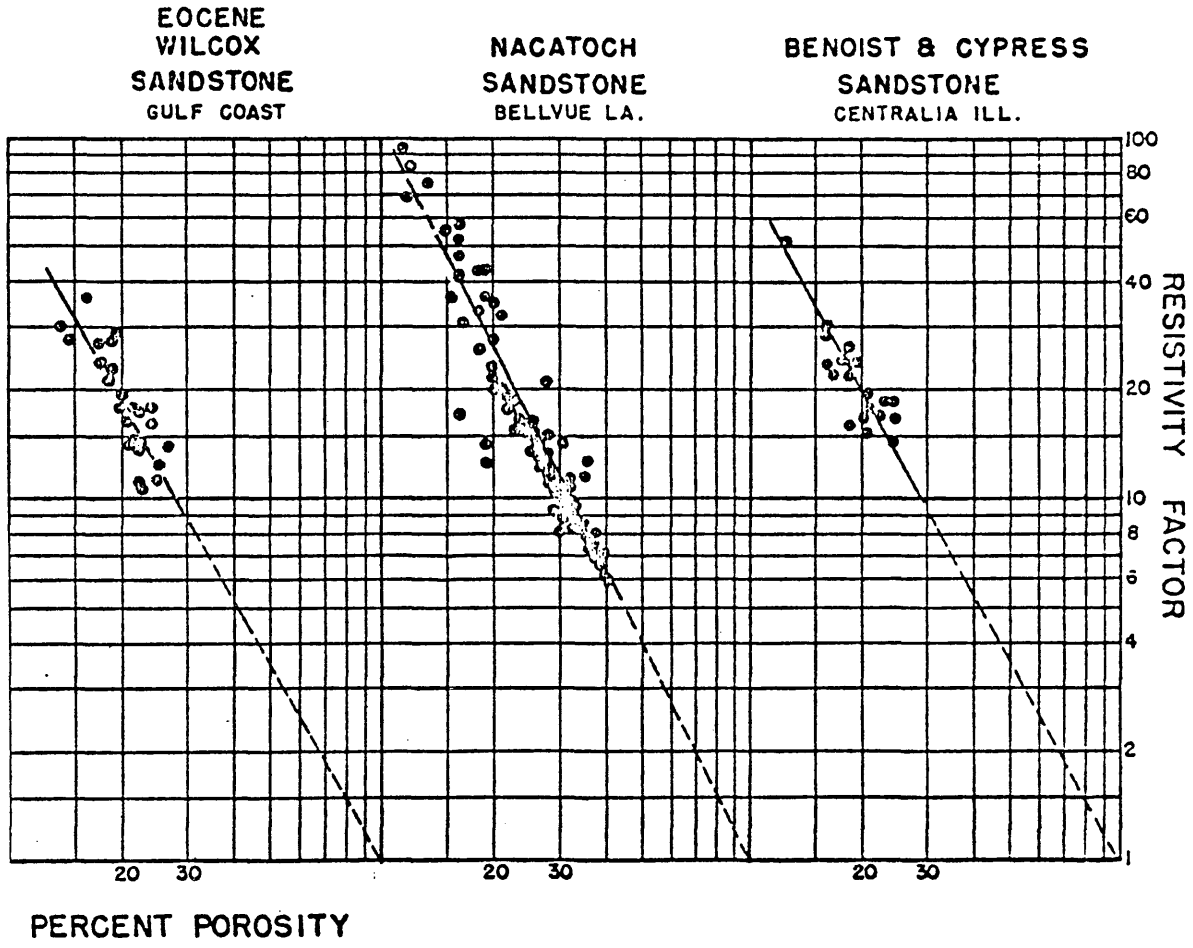

Figure 10. Relation of porosity to formation resistivity factor (Archie, 1942).

those most commonly seen in reservoir rocks. The primary advantage of this network was the ability to get any desired m by selecting tube and vug radii. In summary, rocks with primarily fracture porosity could tend to exhibit low values of m, while vuggy porosity could result in higher values. Rasmus (1987) also substantiated these results by interpretation of the effects of fractures and vugs on F and m. He concluded that fractures within a rock system will tend to decrease m dramatically, while vugs increase it.

Taking the logarithm of both sides of the F-ϕ equation, we arrive at an expression for m for all three models, in terms of F_b and ϕ_b,

$$\log F_b = -m \log \phi_b$$

$$m = -\frac{\log F_b}{\log \phi_b} .$$

Section 2.2.7 Saturation Exponent

Archie (1942) also derived an empirical relationship between the resistivity ratio, I, and the water saturation, Sw, by using resistivity measurements on partially saturated and fully saturated samples (Figure 11). The saturation exponent, n, is the linking factor and is commonly approximated as 2.0. The relationship is given as

$$I = \frac{R_t}{R_o} = Sw^{-n}.$$

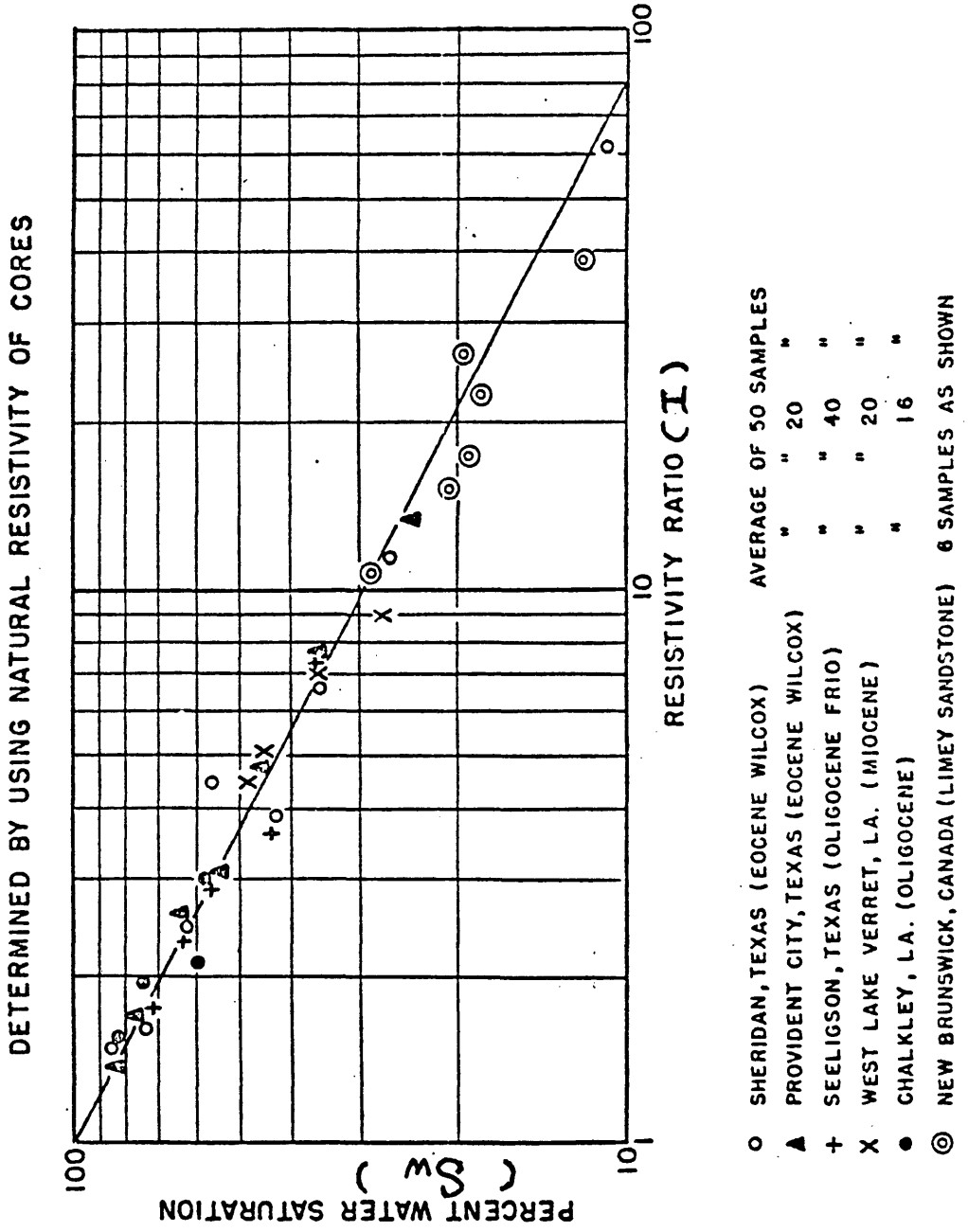

Figure 11. Relation of water saturation to resistivity ratio (Archie, 1942).

The value of the saturation exponent can be affected by the wettabilities of different samples; the water-oil wetness of the mineral surfaces can have an important influence upon n (Higdon, 1963). Whether the system is under drainage or imbibition has little difference on n, as does the lithology of non-shaly samples. A summary of investigated values of n is provided in Table 1.

Taking the logarithm of both sides of the equation solves for n, for all three models,

$$n = - \frac{\log I}{\log Sw} \quad .$$

Section 2.2.8 Relative Permeability

Darcy's Law for flow in porous media requires that the material was entirely saturated with the flowing fluid. When the saturation of that fluid is less than 100%, the ability of the material to conduct the fluid is known as the effective permeability to that fluid. It will range from zero to the value of the permeability at 100% saturation. The relative permeability can then be defined as the ratio of the permeability to the fluid at a given saturation to the permeability of the 100% saturated state (the absolute permeability), i.e.,

$$\text{kr (water)} = \frac{k_w}{k} \qquad \text{kr (oil)} = \frac{k_o}{k} \quad .$$

Since the absolute permeability is a constant for a given material for liquid saturations, the relative permeabilities vary with fluid saturation; they will range from a value of zero at low

Table 1

Values of the saturation exponent, n, from various sources (from Kwon, 1976).

Investigator	Year	n	Measured Sample	Range of Sw(%)
Leverett	1936	1.8 ~ 2.0	Unconsolidated sand pack	15 ~ 100
Wychoff	1936	± 2.0	Various sand	10 ~ 100
Martin	1938	± 2.0	Consolidated sand	10 ~ 100
Archie	1941	± 2.0	Various rock type	10 ~ 100
Dunlap et al	1949	1.17~2.03	Clean, uniform sandstone	
Morgan et al	1951	1.16~1.80		15 ~ 100
Wyllie & Spangler	1952	1.42~2.20	Pennsylvanian, Berea, Turcaloosa sandstone	
Rust	1952	1.75~2.40	Clean sand	
Fatt	1956	2.22~3.10		40 ~ 100

saturations of that fluid to a value of 1.0 at 100% saturation of that fluid.

When the porous volume in the HRP model is saturated with non-wetting fluid, then the tube loses the ability to conduct the wetting fluid, and vise versa. The relative permeabilities for this cell to the wetting and non-wetting phases are 0.0 and 1.0, respectively. The relative permeabilities therefore change as the network progresses from a water-saturated state to an oil-saturated state. The equations for the Tube and Tube Vug models that follow from this paradigm are similar to those of the resistivity index:

$$kr_w = \frac{\sum_{i=M+1}^{NC} (a_i\, k_i)}{\sum_{i=1}^{NC} (a_i\, k_i)}$$

$$kr_{nw} = \frac{\sum_{i=1}^{M} (a_i\, k_i)}{\sum_{i=1}^{NC} (a_i\, k_i)} \quad .$$

For the Dual Tube Vug model, the expression for K_{rw} is identical to that given above, since both tubes still have full conductivity in water-staurated cells. Relative permeability to the non-wetting phase arises from the argument that when the larger tube becomes filled with oil, this prohibits any conductivity of the water trapped in the smaller tube. The numerator for the parameter Kr_{nw} therefore includes only the contribution of the larger tube:

$$kr_{nw} = \frac{\sum_{i=1}^{M} \frac{\pi\ C\ L\ rl_i^4}{8\ \tau l_i\ (L - 2R_i)}}{NC} \Bigg/ \sum_{i=1} \frac{\pi\ C\ L}{8\ (L - 2R_i)} \left(\frac{rl_i^4}{\tau l_i} + \frac{rs_i^4}{\tau s_i}\right) .$$

The parametric equations for kr and drainage Sw can define the drainage kr curves; likewise, the imbibition Sw equations can be implemented to calculate kr during the imbibition phase.

Section 2.2.9 Capillary Pressure

It is essential in petrophysical modelling that a pore structure network should generate capillary pressure curves that approximate their empirical counterparts. The curves provide qualitative information on pore structure, fluid permeability, and reservoir producibility (see Figure 12). Fatt (1956) was one of the first reasearchers to realize that the tube radius distribution is a primary control on the P_c curves. If there is a greater proportion of smaller pores to larger pores, the plateau of the Pc curve is steeper, which is indicative of lower permeability. The shape and slope of the plateau can therefore be controlled by modifying input radii to the model. Figure 13 exhibits the hysteresis effect during the imbibition phase that was discussed in Section 2.1.

The pressure at which the non-wetting phase enters the tube of the cell and displaces the

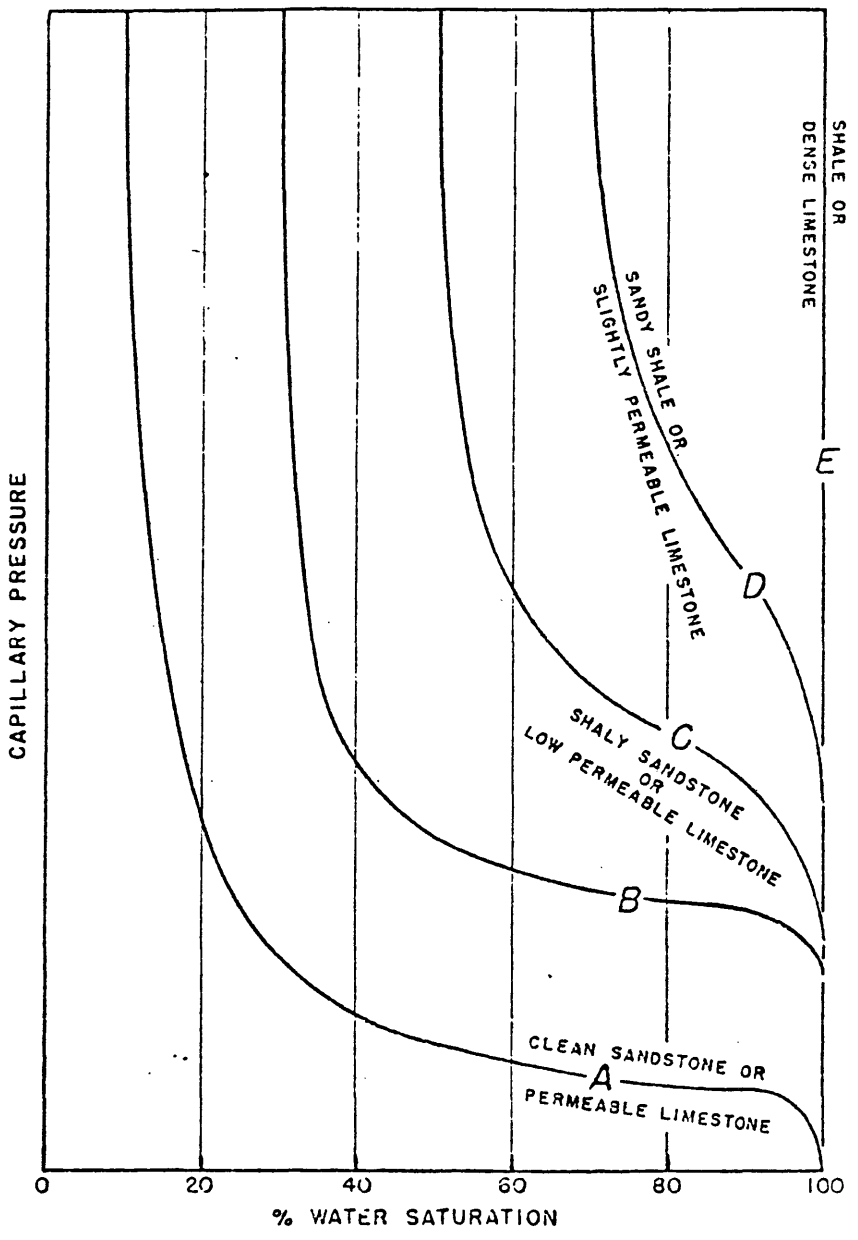

Figure 12. General relation of capillary pressure curves for different types of formations (from Archie).

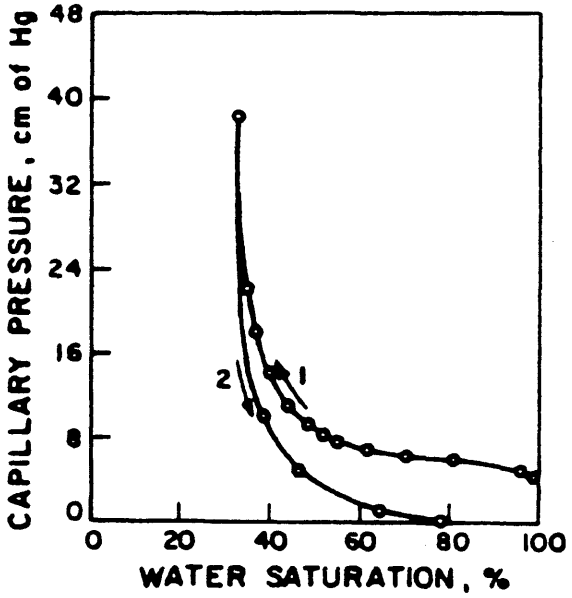

Figure 13. Capillary pressure characteristics with imbibition, strongly water-wet rock (Killins et al., 1953).

wetting phase is known as the displacement pressure, P_d. It is described by Plateau's equation:

$$P_{d_i} = T\ [1/66510\ psi/(dyne/cm^2)]\ \left(\frac{1}{R_1} + \frac{1}{R_2}\right) \cos\theta,$$

where

P_{d_i} - Displacement capillary pressure for cell in psig

T - Surface tension (interfacial tension) between two immiscible fluids in dyne/cm

R - Principal radii of curvature of the interfacial surface

θ - The contact angle in degrees.

If the fluid interface is spherical and the contact angle is assumed to be 0°, this equation for the Tube and Tube Vug models reduces to

$$P_{d_i} = \frac{2\ T\ [1/66510\ psi/(dyne/cm^2)]}{r_i} ,$$

while that of the Dual Tube Vug model substitutes the term rl_i in the denominator. Note that the observation that the pressure required to empty a pore is inversely proportional to the radius also satisfies Laplace's Equation (Harris, 1965). The drainage capillary pressure curve for the network can now be calculated from the parametic equations for P_d and drainage Sw. Use of the imbibition Sw equations will yield the imbibition capillary pressure curve.

Section 2.2.10 Bulk Density

The bulk density of the network is governed by the volume-weighted averaging equation,

$$\rho_b = \phi\ Sw\ \rho_w + \phi\ (1 - Sw)\ \rho_o + (1 - \phi)\ \rho_m.$$

For the Tube model, the density is therefore given by

$$\rho_{b(T)} = \phi_{b(T)}\ [\ Sw\ \rho_w + (1 - Sw)\ \rho_o] + (1 - \phi_{b(T)})\ \rho_m\ ;$$

for the Tube Vug model,

$$\rho_{b(TV)} = \phi_{b(TV)} [Sw \rho_w + (1 - Sw) \rho_o] + (1 - \phi_{b(TV)}) \rho_m ;$$

and for the Dual Tube Vug model;

$$\rho_{b(DTV)} = \phi_{b(DTV)} [Sw \rho_w + (1 - Sw) \rho_o] + (1 - \phi_{b(DTV)}) \rho_m .$$

Section 2.2.11 Surface Area per Unit Volume

The surface area per unit volume, S_v, is a useful property in permeability determination and shaly-sand analysis. The Kozeny Equation (1927), which was later modified by P. C. Carman, has been widely used in relating measurable rock properties with permeability:

$$k = \frac{\phi^3}{5 \, S_v^2 \, (1 - \phi)^2} ,$$

in which S_v is the surface area of the grains exposed to the fluid per unit volume of material. Since S_v is a ratio of area and volume, the resultant dimensionality is 1/Length; therefore, a decrease in grain size produces an increase in S_v. The Kozeny-Carman equation then explains why a fine-grained sand has a smaller permeability than a coarse-grained one of the same porosity; the equation shows that as grain size decreases, S_v increases, and consequently, resistance to flow increases. Dodds and Lloyd (1971), while

modelling spherical packing models, incorporated the specific surface area into their network equations.

The Kozeny-Carman expression was developed from flow equations in capillary tubes. The application is commonly extrapolated to well-sorted spherical packs; it does a poorer job with nonspherical grains (in particular, clays), or ones that are poorly sorted or nonuniformly packed. Currently, research on shaly sands includes empirical determination of S_V. Clays have the largest values for S_V of any group of minerals. Therefore, the introduction of clay into sands leads to a slight reduction in the porosity, but it may cause a decrease in the permeability by as much as several orders of magnitude.

The surface area per unit volume of the three models are derived purely from geometric relationships. For the Tube model,

$$S_{v(T)} = \sum_{i=1}^{NC} \frac{2 \pi r_i L_e}{a_i L} = \sum_{i=1}^{NC} \frac{2 \pi r_i \tau_i}{a_i} ;$$

for the Tube Vug model,

$$S_{v(TV)} = \sum_{i=1}^{NC} \frac{2 \pi r_i \tau_i (L - 2R_i) + 4 \pi R_i^2 - 2 \pi r_i^2}{a_i L}$$

$$= \sum_{i=1}^{NC} \frac{2 \pi [r_i \tau_i (L - 2R_i) + 2R_i^2 - r_i^2]}{a_i L} ;$$

and for the Dual Tube Vug model,

$$S_{v(DTV)} = \sum_{i=1}^{NC} \frac{2\pi(L - 2R_i)(rl_i\ \tau l_i + rs_i\ \tau s_i) + 4\pi R_i^2 - 2\pi rl_i^2 - 2\pi rs_i^2}{a_i\ L}$$

$$= \sum_{i=1}^{NC} \frac{2\pi[(L - 2R_i)(rl_i\ \tau l_i - rs_i\ \tau s_i) + 2R_i^2 - rl_i^2 - rs_i^2]}{a_i\ L} \quad .$$

CHAPTER 3. MONTE CARLO SIMULATION

Section 3.1 Monte Carlo Theory

This modelling technique can be implemented in a great number of ways to yield an even greater array of results. The uses vary from petroleum exploration to economic forecasting to dispersion and flow rate phenomena. Dodds and Kiel (1959) utilized Monte Carlo methods in the petrophysical realm to study fluid displacement and wettabilities. The method involves specifying probability distributions for all variables in the model and the mathematical and logical relationships defining them. Repetitive passes through the model, with the aid of random number generators, will reveal the distribution of possible outcomes.

Section 3.1.1 Generalized Procedure

The model can be made as simple or as complex as desired and can be altered quite readily to incorporate new data and variables. Whatever the use, and however complex the model, the design of the Monte Carlo simulation follows six general steps (modified from Newendorp, 1975):

Step 1: **Define the variables.** In this step, we wish to define the variable of interest (whether it be pore dimensions, recoverable hydrocarbons, net present value, or rate of return). This variable, in

turn, may be dependent upon other variables. Examples of this include the dependency of the amount of metal produced per day upon ore grade, and the reliance of recoverable reserves upon porosity and water saturation. Note that dependency is not absolute. The decision of whether a variable is dependent can be made on the basis of available data or the complexity of the model.

Step 2: **Define relationship(s) between the variables**. This step involves modelling a complex real world system by specifying one equation or a set of equations. These relationships may be either mathematical of logical. An example of a mathematical relationship would be an equation for the net present value of a hydrocarbon prospect, in which we would compute recoverable reserves, use the price and discount rate to convert to discounted revenues, and finally subtract the exploration-development-operating expenses. A logical relationship could be the dependence upon first having a discovery. These relationships will now form a framework for the simulation program.

Step 3: **Sort the independent variables into two groups, deterministic and stochastic**. The deterministic category includes all variables whose exact values are known. The stochastic variables, on the other hand, are those for which we do not know the exact value. Unfortunately, in petroleum exploration problems, most of the variables

will fall into the second group. We may know the range of possible values, the most probable value, or the average value, but not the exact value of the variable. Examples of variables that will most likely fall into the stochastic category are all variables relating to the size of the prospect, future prices and costs, production curves, and recovery factors.

Step 4: **Define probability distributions for all stochastic variables**. This is the step where professional expertise and judgement are necessary. Fortunately, Newendorp states, the judgement of an experienced engineer or geologist can provide acceptable definitions of the probability distributions for the physical and economic parameters required. These distributions do not have to be specified by a single person; they can be made by the person most knowledgeable and familiar with each parameter. They can be inferred from data nearby, they can be based on physical restraints, or they can be established using purely subjective estimates.

These distributions can have any shape and are not constrained to any particular range. Dependency of one variable on another can be dealt with by either of two methods (Newendorp, 1975): a two-step process, where the determinant is generated according to its probability distribution and then used to generate the dependent variable with its own particular distribution; or by creating a probability distribution crossplot of the two variables and incorporating this into the program.

Step 5: **Perform the simulation**. During this step, a random number generator is used to provide one value for each of the stochastic parameters. These numbers should occur according to the frequency distributions set forth during the previous step. This can be accomplished by either converting the relative frequency distributions to cumulative distributions and applying the random numbers to this curve (Newendorp, 1975 and Inciarte, 1981), or scaling and adding constants to arrive at the appropriate distributions.

The stochastic and deterministic parameters are then inserted into the model equations derived in Step 2 to produce a value for the final output (such as net present value or rate of return). This step is repeated many times (on the order of 50 - 1000). Each pass through this simulation results in one possibility for the outcome of the model.

Step 6: **Compute relative or cumulative frequency diagram for desired output variable**. For example, let us say that we have just computed 1000 results of the net present value of drilling a particular oil well. We can then construct either a histogram or a frequency diagram to give a probability distribution of profitability. An example of this is shown in Figure 10. These frequencies are then representative of the probabilities of occurrence of the various levels of profit, assuming a sufficient number of passes have been made. The most probable value on the relative frequency graph is equal to the Expected Value of the alternative, which can then be used in decision tree analysis.

Section 3.1.2 Advantages of Monte Carlo Simulation

The Monte Carlo approach has several unique advantages over other simulation techniques, as described in Megill (1971), Newendorp (1975), and Inciarte (1981):

- Simulation is completely general and can be applied to any problem involving uncertainty and random variables;

- The number of variables used in the problem can be as large or as small as the explorationist desires;

- The uncertainty is described as a range and distribution of each possible factor;

- It is not necessary that the distributions for each variable be a specific form, such as normal, lognormal, uniform, etc;

- The distributions can be based on data from a variety of sources such as nearby fields (analogy), subjective judgement, or physical constraints;

- The model can be as simple or as complex as desired. It can be readily adapted to meet ever-changing situations;

- The judgements of the probability distributions can come from the person or data source most knowledgeable about that particular parameter;

- It is possible to subdivide the problem to deal with the risk and uncertainty of several different stages (such as exploration, development, and production);

- Simulation models usually require less computer time;

- Sensitivity analyses can be performed to determine the effect of changing the distributions of one or more input parameters on the the resulting output.

Section 3.2 Application to HRP Model

The first two steps in developing a Monte Carlo simulation are (1) To define the variables of interest, and (2) To establish the relationships between the variables. The principal cell parameters that will determine the models' response are the tube radius, r_i, rl_i, rs_i, or R_i; the tortuosity of the tube, τ_i, τl_i, or τs_i; and the cross-sectional area, a_i, of the unit cell.

It can be postulated that the effect of an increase in the values for tube radii can not be distinguished from a proportionate decrease in the cross-sectional areas; therefore, we only need study the effects of τ and either r or a. That is, a rescaling of the unit cells and thus the entire model network would yield the same rock property response.

To vary the scale of the model, the ratio of tube area to cell area should be kept constant. For square cell areas, this requires that the ratio r/L be constant (i.e., an increase of 25% in r would necessitate an increase in L by the same). The expression for porosity has an r^2 in the numerator and an $A=L^2$ in the denominator; a change in scale would yield

the same porosity. Like reasoning holds true for formation factor. Permeability, however, holds an r^4 dependence and therefore a change in scale produces an exponential variation in calculated permeabilities. This is one reason why scale changes cannot readily be made, and that all three variables are necessary in defining the model.

The second step in Monte carlo simulation is a crucial one. The interdependence of the cell parameters is apparent from their allowable values:

Tortuosity:	$1 \leq \tau < \infty$	
Tube Radius:	$0 \leq r \leq L/2$	cubic-celled model
	$0 \leq r \leq \sqrt{a}/2$	
	$0 \leq r \leq R$	cylindrical-celled model
	$0 \leq r \leq \sqrt{a/\pi}$	
Cross-sectional Area:	$4r^2 \leq a < \infty$	cubic cells
	$\pi r^2 \leq a < \infty$	cylindrical cells

For the cubic-celled model, the maximum porosity would be $\phi = \pi/4 \approx 79\%$, whereas the model of cylindrical cells can have $\phi = 100\%$. These conditions observed, the cells can have any dimensions desired; they can be on the order of millimeters to model microscopic rock phenomena, or have measurements in the hundreds of meters as in reservoir simulation and hydrology studies.

Attempts at modeling in the past have focused on such deterministic frameworks as spherical packs and networks of capillary tubes. However, the deposition of sedimentary material is a stochastic process and the resulting rocks have a full statistical variation in their geometric parameters. The three parameters r, τ, and a will be modeled as continous stochastic variables and will therefore be described by their probability distributions. The following density functions will be used in this thesis to compute the model parameters: single-valued, uniform, Gaussian (or normal), lognormal, and Beta distributions. The definitions and characteristics of these are given in Appendix B.

The empirical determination of pore radii and tortuosities is an area that can afford much future research. The simultaneous measurement of all parameters for a statistically relevant number of samples takes much effort. Finding adequate distributions is crucial in modeling research, since variables such as r influence every attribute (F, ϕ, k, S_{wirr}, P_c, k_r, etc.) of the rock. The topic of scale also merits consideration. Porous materials can appear homogeneous at large scales, only to exhibit full statistical variation at smaller scales. Fortunately, the modelling procedures of these "embedded networks" (see Madden, 1976) can be incorporated into the heterogeneous rock properties model. The determination of stochastic distributions for the three central parameters r, τ, and a, based upon empirical research, is addressed in the following sections.

Section 3.2.1 Cross-sectional Area

Since this thesis will involve applying the heterogeneous rock properties model at the scale of the individual pores, it is reasonable to suggest equating the cross-sectional area with sedimentary grain sizes. These sizes, which can be expressed by diameter or area, are

a fundamental attribute of siliciclastic rocks. They can be important in the descriptive sense, but may also have genetic significance.

The distribution of particle sizes in nature forms a continuum; it has, however, been divided into a number of size classes by various researchers. The most universal grain size classification used today is the Wentworth scale (Figure 14, reprinted from Boggs [1987]), a geometric scale in which boundary values differ by a factor of 2. It ranges from 0.06 mm to over 4 meters and is subdivided into four major size categories - clay, silt, sand, and gravel.

The distributions of grain sizes can be symmetrical or skewed. If the data set has an excess "tail" of fine particles, it is said to be positively skewed, right skewed, or fine skewed. The opposite is true for the presence of excess coarse particles. The sorting of the population finds mathematical expression in the standard deviation. This statistical parameter can give indication of the range of grain sizes present and the magnitude of the deviation about the mean particle size.

The size and the sorting may reflect sedimentary environments and depositional mechanisms. Facies contrasts often manifest themselves in contrasts of mean grain size. Boggs (1987) lists three factors in the size distribution of the grains: (1) availability of grain sizes at the source, (2) transport and depositional processes, and (3) postdepositional diagenetic changes. The mean and maximum grain sizes commonly indicate the energy of the depositional environment (Boggs [1987] and Dapples [1975]). postdepositional diagenetic changes. The mean and maximum grain sizes commonly indicate the energy of the depositional environment (Boggs [1987] and Dapples [1975]). For instance, fluvial sediments are usually coarser than their beach or dune counterparts. They are also more likely to be poorly sorted because they do not undergo extensive

		U.S. Standard sieve mesh	Millimeters		Phi (ϕ) units	Wentworth size class
GRAVEL			4096		−12	
			1024		−10	Boulder
			256	256	− 8	
			64	64	− 6	Cobble
			16		− 4	Pebble
		5	4	4	− 2	
SAND		6	3.36		− 1.75	
		7	2.83		− 1.5	Granule
		8	2.38		− 1.25	
		10	2.00	2	− 1.0	
		12	1.68		− 0.75	
		14	1.41		− 0.5	Very coarse sand
		16	1.19		− 0.25	
		18	1.00	1	0.0	
		20	0.84		0.25	
		25	0.71		0.5	Coarse sand
		30	0.59		0.75	
		35	0.50	½	1.0	
		40	0.42		1.25	
		45	0.35		1.5	Medium sand
		50	0.30		1.75	
		60	0.25	¼	2.0	
		70	0.210		2.25	
		80	0.177		2.5	Fine sand
		100	0.149		2.75	
		120	0.125	⅛	3.0	
		140	0.105		3.25	
		170	0.088		3.5	Very fine sand
		200	0.074		3.75	
		230	0.0625	1/16	4.0	
MUD	SILT	270	0.053		4.25	
		325	0.044		4.5	Coarse silt
			0.037		4.75	
			0.031	1/32	5.0	
			0.0156	1/64	6.0	Medium silt
			0.0078	1/128	7.0	Fine silt
			0.0039	1/256	8.0	Very fine silt
	CLAY		0.0020		9.0	
			0.00098		10.0	Clay
			0.00049		11.0	
			0.00024		12.0	
			0.00012		13.0	
			0.00006		14.0	

Figure 14. Grain size scale for sediments showing Wentworth size classes and equivalent phi (ϕ) units (Boggs, 1987).

reworking. Poorly sorted sediments can also be deposited by gravity flows, glaciers, or storms. Fluvial and eolian sediments tend toward positive skewness, whereas littoral sands tend to be negatively skewed (Figure 15). These generalizations may prove useful in refining the cross-sectional area distributions.

Grain size distributions can be chosen as input for the model; assuming spherical grains, these yield five cross sectional area distributions (Table 2). The mean grain sizes (in phi units: 10.5ϕ, 6.5ϕ, 3.5ϕ, 2.5ϕ, 1.5ϕ, 0.5ϕ) of these Gaussian distributions are the midpoints of the following classifications: clay, fine-medium silt, very fine sand, fine sand, medium sand, and coarse sand. Although the clastic classification was used, these same distributions can be used to model carbonate lithologies.

Table 2. Comparison of Wentworth Grain Size Classes and Cross-sectional Areas, a_i

Size Class [μm]	Mean Diameter [μm]	ϕ Units	Area [(μm)^2]
Clay	1	10.5ϕ	1
Silt	10	6.5ϕ	78
VF Sand	90	3.5ϕ	6,400
F Sand	180	2.5ϕ	25,400
M Sand	360	1.5ϕ	102,000
C Sand	720	0.5ϕ	407,000

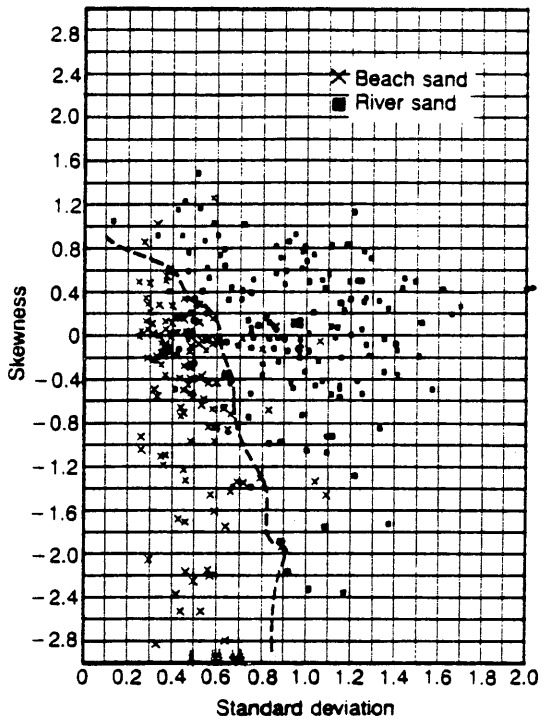

Figure 15. Bivariate plot of skewness vs. standard deviation. Beach sands and dune sands are separated by this plot into two moderately well-defined fields (from Boggs, 1987).

Section 3.2.2 Tube and Vug Pore Radii

The first attempt to address the modeling of tube radius distributions within rocks was done by Fatt (1956c) and applied to a 2-D simple tube model. Poiseuille's Law was utilized to calculate permeabilities, but the method was hindered due to inadequate empirical knowledge about pore space geometry. Another topic of consideration was the determination of the coordination number, the number of pore channels intersecting a

central node. The generalized Kozeny-Carman Equation follows from Poiseuille's Law in the derivation of a complex capillary tube probability model (Wyllie and Gardner, 1958ab). This model employed the mean hydraulic radius, in triple conjunction with a capillary "shape factor" and the tortuosity, which was defined as a reflection of pore radius areal variation. It was concluded that the deviation of pore sizes for unconsolidated media for application of the Kozeny Equation was approximately -10% to +10% about the central mean. However, due to the wide distributions of permeability (the dominant parameter of which is the tube radius) and the results from sphere pack models, this range is probably too confining.

Limited substantial research on pore radii was accomplished prior to 1974, the most notable being tube radii distributions from tetrahedral packing of unequal spheres (Dodds and Lloyd, 1971) and the distributions from displacement phenomena (Simon and Kelsey, 1971). The main problems of these network models were also due to insufficient information on pore structure.

A significant advance was achieved in correlating model parameters with geometric dimensions in real rocks by the research of Dullien et al (1972, 1974, 1975, 1976). Their investigations focused upon the characterization of pore structure by photomicrography and mercury porosimetry. Technological advances in the areas of optical data processing, image analysis of pore geometries, and application of Fourier transforms provided the capability and the impetus. The results are based upon the theory of quantitative stereology, or the extrapolation of 2-dimensional sections to the determination of 3-dimensional space. As such, the critical assumption of this body of work is that given a statistically significant number of features, valid results may be obtained through

geometrical probability. Assuming this hypothesis to be true, then 3-dimensional space can be represented by 2-dimensional abstractions (compare Figures 6 and 16).

Dullien began by stating that every method of pore size determination defines a "pore size" in terms of a pore model which is best suited to the quantity measured in the particular experiment. He therefore cautioned against using the mean hydraulic diameter, which is not derived from the actual geometry of the pore space. The photomicrographs of polished sections of Berea BE-1 sandstone showed justification that the pore space can be divided into large nodal pores connected by smaller pore throats or tubes. The diameters of the large pores are abbreviated D, and those of the controlling necks, De, for pore of entry diameter. Figure 13 shows the distributions of pore diameters with increasing capillary

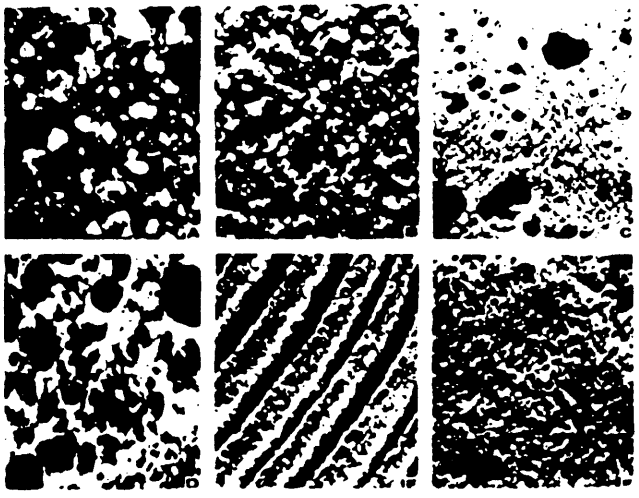

Figure 16. Examples of natural porous materials (x10): (A) beach sand; (B) sandstone; (C) limestone; (D) rye bread; (E) wood; (F) human lung, (Collins, 1961).

pressures. The mean diameter D is seen to be between 50 and 80 μm, with entry diameters from 4 to 22 μm. The additional penetration at 44.7 psia not only increased the number of saturated small pores, but filled many larger pores which were blocked by the smallest pores. This shielding effect was also recognized by Wardlaw (1976) and Morrow and Heller (1985).

Research of pore diameters of Bartlesville and Berea sandstones (Dullien and Dhawan, 1975) yielded values for D that extend to 90-120 μm, whereas De does not exceed 40 μm. In most sandstones, the ratio D/De averages near 10, but no correlation between De and D was apparent. Figure 14 shows the bivariate distribution of pore diameters that supports the Tube Vug model. The vugs modeled after this distribution should have a mean diameter of 30-50 μm, with the tube diameters having a much narrower distribution, with a mean of approx. 10 μm. This determination of the pore volume composed of the pore necks and vugs has a critical part in determining equilibrium properties such as capillary pressure, capillary hysteresis, displacement, and absolute and relative permeabilities, and as such, represents a marked improvement over sphere pack analysis.

Transformation of a Sw vs. depth, or capillary pressure, profile (Raymer and Freeman, 1984) yielded pore size distributions with mean effective pore radii of 5.0 μm for sample L, 6.5 μm for sample M, and 9.0 μm for sample H. It was also concluded that vertical variations in pore size distributions can be quantified. However, as Ehrlich and Davies (1989) point out, the routinely-derived capillary pressure curves do not carry information about the spatial distribution of the pores and throats, or the size or shape of pore bodies. This spatial referencing would have direct impact upon permeabilities for instance. In addition, their image analysis revealed the presense of an unusually large

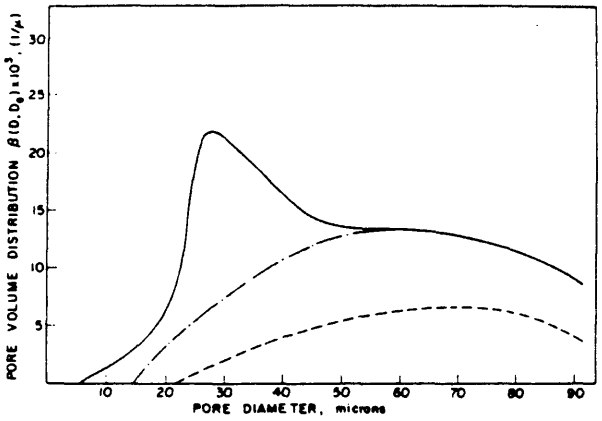

	P (psia)	D_t (μm)	Symbol
13	44.7	4.8	
20	14.7	14.4	
3	9.6	22.0	

Figure 17. Photomicrograph pore size distributions of penetrated portions of Berea BE-1 sandstone at various injection pressures of Wood's metal (Dhawan, 1972).

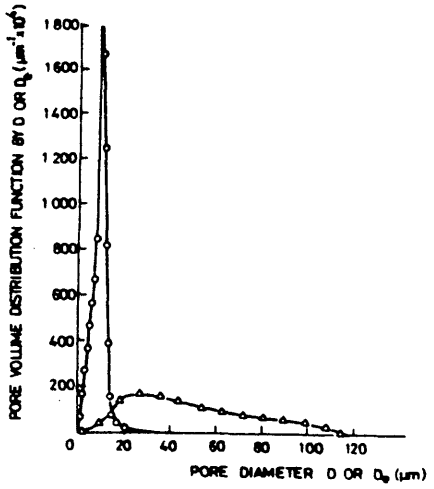

Figure 18. Relative frequencies of pore entry diameter De (o) and complete pore size distribution D (Δ), (Dullien, 1975).

number of very small pore throats (< 0.4 microns) due to dissolution that could not be identified with past pore determination methods.

Section 3.2.3 Tortousity

Tortuosity has been defined in many ways by previous researchers and is probably the least understood of the three rock parameters. It was introduced by Carman in 1937 as the square of the ratio of the effective path length to the length of the sample:

$$\tau = \left(\frac{L_e}{L}\right)^2 \qquad \text{(Carman, 1937).}$$

It was used initially as a correction factor in order to agree with experimental permeability values; it can theoretically range from 1 to infinity.

Tortuosities (which, for the remainder of this thesis, will be defined as simply Le/L) between 5 and 72 were obtained by Wyllie and Spangler (1952) from investigation of the Carman-Kozeny equation and the Archie F-ϕ relationship. They also pointed out that the higher tortuosities for consolidated rocks is the principal difference between consolidated and unconsolidated media. Particle shape and sorting highly influence the tortuosities obtained from unconsolidated rocks (Wyllie and Gregory, 1953). Winsauer et al. (1952) were correct to realize that values of τ are, at best, statistical averages due to pore space geometrical factors. Their research concluded that Le/L should be between 1 and 5;

for indurated sandstones, the obtained τ's ranged from 1.5 to 3.3. Owen (1952) also agreed that correct F-ϕ ratios could be obtained without the tortuosities of 5 - 72.

Tortuosity has also been viewed as the expression of areal effects (Wyllie and Gardner, 1958a), rather than the sinuosity around individual grains; as a statistically-based impedance factor, representing the probability of pore interconnections (Wyllie and Gardner, 1958b); as a product of statistical distributions of channel parameters; as a shape or constriction factor (Haring and Greenkorn, 1970); as a probability of pore "clustering" (Kirkpatrick, 1973); and as a tensor describing the deviation from macroscopic fluid flow direction at every point (Bear and Bachmat, 1966, 1967). Additional data derived from a definition similar to Le/L include $\tau \approx 3$ (Johnson and Stewart, 1965) and $\tau \approx \sqrt{3} \approx 1.73$ (various authors, cited by Dullien et al. 1976). Although differences between hydraulic and electrical tortuosity have been theorized since 1952, empirical confirmation has not yet been established.

Section 3.3 Design of the Monte Carlo HRP Simulation Program

Three versions of a Monte Carlo simulation program were developed to run on the VAX8600a at CSM. Each version employs a particular applied cellular model - the Tube Model, the Tube Vug Model, or the Dual Tube Vug Model. The Dual Tube Vug version is included as Appendix A. The computer algorithm developed for this study is written in Fortran 77 language. The random number generators used in the sampling process are multiplicative pseudorandom type generators from the IMSL software library. The generated random numbers were assigned to individual cells using an array addressing

system. A review of basic probability theory as it relates to the studied statistical distributions and the call statements for the subroutines is included in Appendix B. The calculation time required for executing a 50-iteration, 1000-cell model simulation, with both drainage and imbibition, is approximately 3-4 minutes on the VAX8600.

A particular rock formation can and will yield different values of porosity, formation factor, permeability, and cementation exponent, among other properties, when examined by core analysis techniques. This can be due to the natural volumetric heterogeneity of the formation, or even sample, of the rock, or to the measurement process / quality control involved. In view of this, the program was designed to yield a histogram of MC results, where MC is the number of Monte Carlo iterations, that represent the empirical spread of F, ϕ, k, and m values. This can express qualitatively the magnitude and nature of the uncertainty in the solution. Therefore, statistical distributions of model parameters, in conjunction with several Monte Carlo simulations, will yield empirical distributions of the desired petrophysical properties. The algorithm is outlined as follows:

Step 1. Prompt user for number of iterations, MC; number of cells, NC.

Step 2. Prompt user for upper and lower acceptable limits on F, ϕ, k.

Step 3. Prompt for type of area, a_i, distribution and parameters.

Step 4. Prompt for type of radius, r_i, rl_i, rs_i, R_i, distributions and parameters.

Step 5. Prompt for type of tortuosity, τ_i, τl_i, τs_i, distributions and parameters.

Step 6. Prompt for singular-value cell length L, α, and β.

Step 7. Retrieve NC values of a_i and check for values of $a_i < 0.0$.

Step 8. Retrieve NC values of r_i, rl_i, rs_i, R_i and check for values of $r_i < 0.0$ or $> 0.5(a_i)^{1/2}$.

Step 9. Retrieve NC values of τ_i and check for values of $\tau_i < 1.0$.

Step 10. Calculate bulk F, ϕ, k, m.

Step 11. Repeat Steps 7-10 for MC iterations.

Step 12. Check for F, ϕ, k outside rejection limits.

Step 13. Calculate minimum, mean, and maximum F, ϕ, k.

Step 14. Recall $\{a,r,\tau\}$ array suite for most representative iteration, that with F,ϕ,k closest to mean values.

Step 15. Calculate S_V.

Step 16. Sort tube radii, find minimum and maximum displacement pressures.

Step 17. Drainage loop: Repeat Steps 18-19 for P_c from 0.0 to maximum displacement pressure by incremental capillary pressure.

Step 18. If $P_c > P_{d_i}$, then cell saturates with oil and M=M+1.

Step 19. Calculate Sw, I, ρ_b, Kr_w, Kr_{nw}, P_c.

Step 20. Imbibition loop: Repeat Steps 21-22 for P_c from maximum P_d to 0.0 by incremental displacement pressure.

Step 21. If $P_c < P_{d_i}$, then cell resaturates with water minus residual oil satuation and M=M-1.

Step 22. Calculate Sw, Kr_w, Kr_{nw}, P_c.

This program exhibits many of the benefits of Monte Carlo simulation outlined in Section 3.1.2, namely flexibility, generality, expandability, interpretability, and statistical stability. If this program were run twice with the same input data, the results would be slightly different, because the random number arrays generated are different each time the

program is run. However, the results are statistically equal, thereby contributing to the effectiveness of the program.

CHAPTER 4. MODELLING RESULTS AND ANALYSIS

A principal reservoir in the western Central Graben area of the North Sea is the Upper Jurassic Fulmar Sandstone. As exploration activity for Middle Jurassic sands reduced in the mid-1970's, the sands of the Fulmar Formation offered new opportunities. The trapping mechanism was primarily small structures with stratigraphic components. Most are located above the elongate trend where the source rocks of the Upper Jurassic Kimmeridge Clay are thermally mature.

Generation and migration of hydrocarbons in this area began during Cretaceous time and has continued to the present. These hydrocarbons have commonly accumulated in stratigraphic facies changes between Upper Jurassic sands and Triassic Smith Bank shale pods. Future discoveries will continue to be increasingly stratigraphic in nature and will require detailed analysis of the seismic expression and petrophysical facies.

The Fulmar was deposited as a transgressive systems tract during a rapid rise in sea level. This Kimmeridgian unit onlaps unconformably onto Middle Jurassic strata as the Jurassic sea transgressed the basin margin. The marginal marine environment led to the deposition, largely sourced from the Triassic Skagerrak Formation, of a laterally continuous sheet sand. The thickest accumulations of sandstone appear to be located in rim synclines around Permian Zechstein salt diapirs; this highlights the correlation between salt movment and Upper Jurassic reservoir deposition and preservation.

The Fulmar is seen in cores to consist of bioturbated VF to F sands, with relatively few primary depositional features. Facies classification within the Fulmar has been done primarily on the basis of grain size, burrow types, and clay content. The main reservoir

facies has porosities from 12-32% and permeabilities from 1-3000 mD at Kittiwake Field (Boland, 1990); and ϕ = 18-24%, k = 100-1000 mD (Facies 2.3) and ϕ = 20-30%, k = 500-4000 mD (Facies 2.2) at Fulmar Field (Millson, 1987). The reservoir quality is primarily controlled by grain size and sorting. Current work on the Fulmar involves discerning large scale areal trends in reservoir quality from petrophysical data.

A 1990 study by Shell UK Exploration & Production focused on developing provisional development plans, with primary emphasis on re-examining petrophysical data on the Fulmar Sandstone in the Kittiwake and Fulmar fields. The following petrophysical objectives were planned for the study:

(1) To gather petrophysical data required for a new reservoir model;
(2) To interpret new core data that had become available;
(3) To derive a porosity - permeability transform;
(4) To examine consistency of saturation to height profiles and compare them to capillary pressure curves;
(5) To create a petrophysical model for evaluating development wells;
(6) To establish need for further data gathering in development wells.

Six wells were cored over the Fulmar and upper part of the Middle Jurassic Skagerrak formations. Recovery was generally good (90-100%), which resulted in approximately 800 ft of Fulmar core. The wells were logged by Dresser Atlas in salt-saturated water based mud. The logs run include the induction/acoustic/gamma ray, density/neutron, dipmeter, and formation pressure tester. In addition, the dual

laterolog/microlateralog were run in three of the wells and the spectral gamma ray in one well at Kittiwake field.

Porosity values reported in this thesis are a mix of those from conventional core analysis and those derived from logs. The porosity was calculated from the density log using fixed matrix and fluid parameters from the equation,

$$\phi_{log} = (\rho_m - \rho_b) / (\rho_m - \rho_f) ,$$

where ρ_m = 2.665 g/cc, ρ_f = 0.73 g/cc (oil bearing drilled with water based mud), and ρ_f = 1.056 g/cc (water bearing drilled with water based mud). The sonic was not chosen for porosity determinations due to its poorer vertical resolution.

Log porosity, converted to atmospheric conditions, and porosity from conventional core analysis over the same layers were compared to estimate the accuracy of the porosity calculation parameters. The differences between the two porosities on a per unit basis were summed to determine the net effect of underestimating log porosity to core porosity, on the average, of 0.15.

Sixty-seven capillary pressure curves were obtained in this study. Of these, 42 were mercury-air drainage curves and 25 were oil-water drainage curves. Imbibition curves were not available. An interfacial tension of the oil-water system was estimated at at Kittiwake Field to be 35 dynes/cm (Boland, 1990), which is the value used in the Monte Carlo simulation program.

On the basis of core and log data, the reservoir rock has been divided into three major units, Facies 1, Facies 2, and Facies 3; Facies 2 has been further subdivided into five subunits, which are referred to as Facies 2.1 - 2.5.

The application of the HRP model to simulation of empirical data from the Fulmar Sandstone will be of two parts: the first will be simulation and analysis of nonreservoir silty units within the Fulmar, in particular those of Facies 1; and the second, of productive reservoir units, represented by Facies 2.3. This petrological classification will be useful in contrasting the geological and petrophysical characteristics and in revealing the strengths and weaknesses inherent in the modelling process.

There have been few pore space-matrix models that have been rigorously compared with empirical data. Most past models have simply reproduced general characteristics and trends in the data. Although this is certainly the first step of petrophysical modelling, much more information about pore space controls on petrophysical properties and the applicability of the model can be determined from exact comparison with experimental results.

Over 350 preliminary simulations were run over Fulmar Facies 1 and Facies 2.3 in order to 1) test the effects of varying pore parameters on the modelled properties, i.e. forward modelling; 2) determine the most appropriate cell structure (Tube, Tube Vug, Dual Tube Vug) for the modelling process; and 3) invert the experimental petrophysical data to yield information about the pore space. The parameter distributions obtained would be non-unique since a distribution has, in principle, an infinite number of parameter components. Since many simulations were run with different pore parameter distributions until the model data was similar to the the experimental data, the modelling was only pseudo-inverse. A generalized Marquardt-style inversion process, due to the large number of parameters and mix of data forms, would have required extraordinary amounts of computer run time and disk space.

For each of the simulations, 50 Monte Carlo iterations were run, yielding 50 values of F, ϕ, k, and m. This provided enough data points to determine interrelationships between these variables and corresponded with the average number of points on such crossplots of Fulmar empirical data. Various network sizes were investigated; generally those with less than 100 cells gave subsequent simulations that were statistically inconsistant and P_c, I, and Kr curves that were not smooth. Therefore, most of the simulations were done with 1000-cell networks, which had a very reasonable average run time of 3-4 minutes each.

The simulation of experimental data for both the nonreservoir and reservoir facies involved the following steps:

1.) Determine the inflection points and average capillary displacement pressure of the plateau of the P_c curve and calculate equivalent tube radii. The calculated plateau radius can serve as an initial guess, with the inflection radii serving as minimum and maximum allowable values.

2.) Use cross-sectional area of average particle size, if available, for a_i initial guess (see Table 2); use τ_i initial guess of 2.50.

3.) Construct a homogeneous network from singular-valued distributions of r_i, τ_i, and a_i. Use apparent Sw_{irr} from P_c and Kr_w curves as α, and apparent So_{res} from Pc imbibition curve and Kr_{nw} curve as β.

4.) Since formation factor data for the Fulmar is not differentiated by facies units, adjust singular-value distributions in subsequent simulations to improve the match on the k-ϕ crossplot.

5.) Adjust calculated values of m till it lies between 1.5 and 2.5; from the equations for F and ϕ, an increase in a_i or decrease in τ_i will result in lower values of m.

6.) Expand into uniform heterogeneous distributions, using the a_i, r_i, and τ_i values from the best-fit homogeneous network as midpoints. Determine optimum range of uniform distributions to match k-ϕ data spread and Pc curve.

7.) Add extra conductance of network, C_{extra}, to further adjust average m to desired value; adjust average n by modifying α.

8.) If possible, further refine shape of P_c curve with distributions of varying shape. Final check of effects upon other properties.

Although there were other processes of matching the model to the experimental data with this computer program, this procedure proved the most efficient and reliable. The Tube Model succeeded in matching F, ϕ, k, m, n, I, P_c, and ρ_b data as completely as the Tube Vug and the Dual Tube Vug Models, without the added complication of the extra parameters in the later two models. The Tube Vug and Dual Tube Vug Models performed

better in producing reasonable Sv results, and the Dual Tube Model provided limited improvement in the Kr curves. The results of the best simulations for Facies 1 and Facies 2.3 are detailed in the following sections.

Section 4.1 Fulmar Sandstone - Nonreservoir Facies

Subsequent simulations yielded improved matches between the model data and the data obtained from logs and cores. Table 3 lists the input distribution parameters of the simulation that produced the best match.

TABLE 3

Facies 1: Input Distribution Parameters for Best-fit Simulation

Model Cell Style: Tube Model

Input Variable	Distribution Type	Distribution Parameters
a_i (sq. μm)	Uniform	min = 0.0, max = 240.0
r_i (μm)	Uniform	min = 0.0, max = 1.8
τ_i	Beta	α=2,β=5,min=1.0,max=6.4
α	Singular	α = 0.45
β	Singular	β = 0.25
C_{extra} (mhos)	Singular	C_{extra} = 0.0076

The group of simulations was begun with an initial a_i of 7000 sq μm, which corresponds to that of very fine grained sandstone (see Table 2). The model started to converge on the proper F, ϕ, k values when an a_i = 120 sq μm was approached, corresponding to silt-sized grains. Tube radii, likewise, are extraordinarily fine, beyond the resolution of either mercury porosimetry or photomicrography. Determined tortuosities are within the 1 - 5 range recommended by many authors. Table 4 provides a summary of the important properties simulated by this run.

A crossplot of permeability and porosity (Boland, 1990) shows the differentiation of Fulmar Facies 1, 2, and 3 (Figure 19); Facies 1 and 2 are very well defined, with Facies 1 exhibiting lower porosities, and permeabilities of 3 orders of magnitude lower. A linear regression through the points of Facies 2 would show permeabilities lower for Facies 1 than would be expected of a rock of a given porosity. Figure 20 shows the correlation between k-ϕ data from the model and the laboratory. While the porosity range of the model data (7.6 - 19.5 %) is excellent, the permeabilities display less heterogeneity than is seen in the real rock. However, the average values of the permeabilities are close. With permeabilities of real rocks ranging over eight orders of magnitude, this result is very promising. Extra heterogeneity in the real samples can be attributed to the presence of clays, fluid turbulence, two or more fluids, or the increased natural complexity of the pore space.

The flow rate, Q, and consequently the permeability is proportional to the fourth power of the radius. The permeability is therefore dominated by the flow capacity of the larger pores. An increase in r_i distribution width in the direction of increasing r will increase k by a much greater amount than expanding about the midpoint of the distribution. Hence, k is most sensitive to changes in standard deviation in networks with larger pore

TABLE 4

Facies 1: Comparison between Experimental and Calculated Properties

	Experimental	**Calculated**
Porosity, ϕ	7.9 - 22.9%	7.6-19.5%
Formation Factor, F	15 - 150	42-61
Permeability, k	.096 - 11 md	.88 - 2.6 md
Cement. Expon., m	1.91	1.90
Satur. Expon., n	2.02	2.05
Plateau Pd	9.8±2.5 psi	7.1 psi
Sw_{irr}	45%	60%
So_{res}	25%	25%
Average ρ_b	Not available	2.43 g/cc
Average Sv	Not available	0.174 m^2/cm^3
Net/gross ratio	0.34	-
Average So	40%	-
ρ_m	2.655 g/cc	-
ρ_w	1.056 g/cc	-
ρ_o	0.730 g/cc	

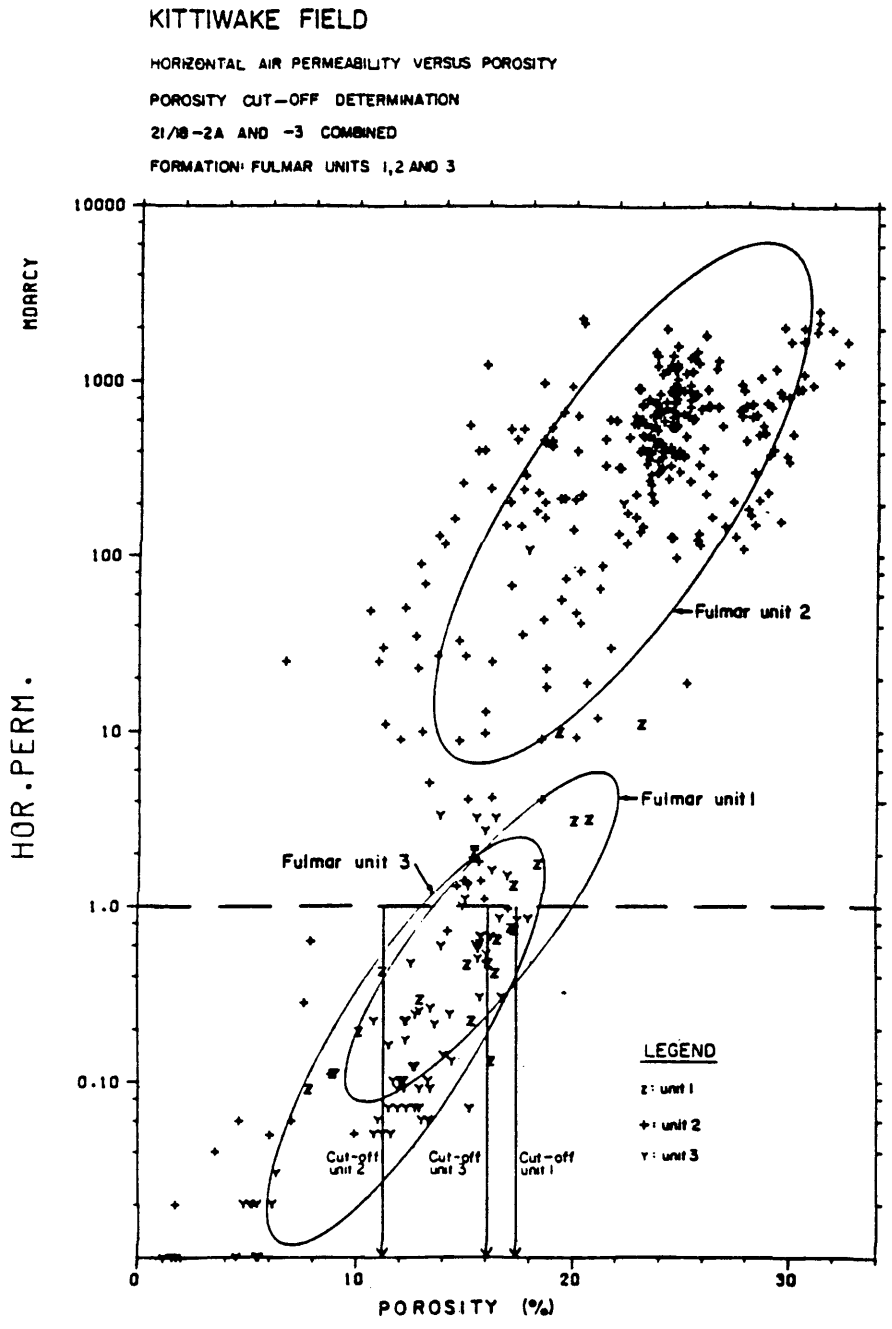

Figure 19. Porosity - permeability crossplot for Fulmar Facies 1,2,3 (Boland, 1990).

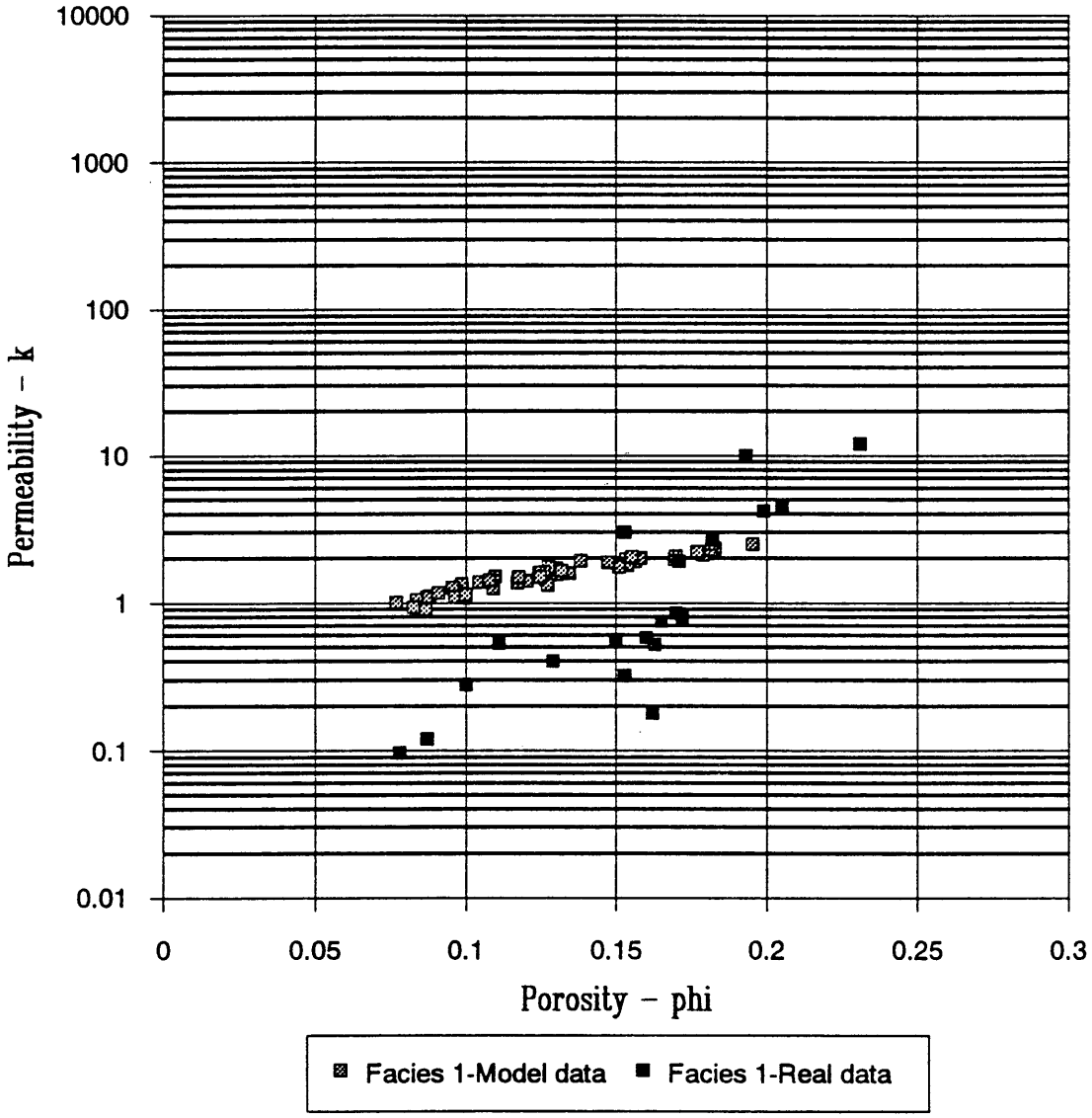

Figure 20. Fulmar Facies 1: Porosity - permeability crossplot.

tube sizes. However, the observation that poorer sorting of grain sizes (wider a_i and r_i distributions) decreases permeability (Masch and Denny, 1966) is not exhibited by the model. An increase in the width increases the heterogeneity of the results, but does not effect the median result. Since porosity is only dependent on the second power of r, it is significantly less effected by variations in the tube radius than the permeability.

Calculated formation factors also fall within the empirical range with a value of C_{extra} = 0.0076 mhos. A value of 0.0 mhos resulted in formation factors that are too high by a factor of 2. Since the inherent water-saturated conductance of the network is approximately 0.0053 mhos, the conductivity of the network has essentially been doubled. This is reasonable due to the silty nature (mean a_i = 120.0 sq. μm) which can introduce extra conductivity from extremely fine pores with very high P_c, or from the presence of clays as Facies 1 grades vertically into the Kimmeridge Clay Formation. The empirical values of F reported in Table 4 were available only general values for the Fulmar (all units) seen in Kittiwake Field.

Trials with the Tube Vug Model showed a relationship between the percent volume in the nodal pores and the cementation exponent. In general, a high proportion of vug porosity to total porosity effected to increase m (see Table 5). This was also concluded by the research of Towle (1962) and Rasmus (1987); Yale (1984) agreed by identifying m as a measure of the decoupling between [total] pore volume and conductivity pore volume. The difference between these two volumes is attributed to the vug. Crossplotting F and ϕ (Figure 21), values of m can be determined for each of the 50 Monte Carlo iterations by determining the slope of the line through the point and (1,1). Cementation exponents from 1.62 - 2.31 were simulated; Figure 22 shows that the mean m of 1.90 makes an excellent comparison with the reported value of 1.91.

TABLE 5

Relationship between Percent Volume in Vugs and Cementation Exponent, m

Cell Type	Pore Volume in Vugs	m
Tube	0%	2.09
Tube Vug	37%	2.19
Tube Vug	62%	3.18
Tube Vug	74%	3.62
Dual Tube Vug	25%	1.96
Dual Tube Vug	61%	2.87
Dual Tube Vug	70%	3.23

Note: Remaining pore volume resides in tubes and extraneous porosity. $C_{extra} = 0.0$, $m = -(\log F / \log \phi)$.

Values for the resistivity ratio, I, were calculated as nonwetting fluid saturation increased with increasing capillary pressure. The resistance of the network, R_t, is seen to be dependent upon the resistance of each pore and the ratio of wetting fluid to nonwetting fluid saturations. As seen from Ohm's Law, $R = R_W (L / A)$, the electrical properties of this network are directly related to the nature and geometries of the electrical paths through the pore system. Therefore, as the current paths through the network change with varying

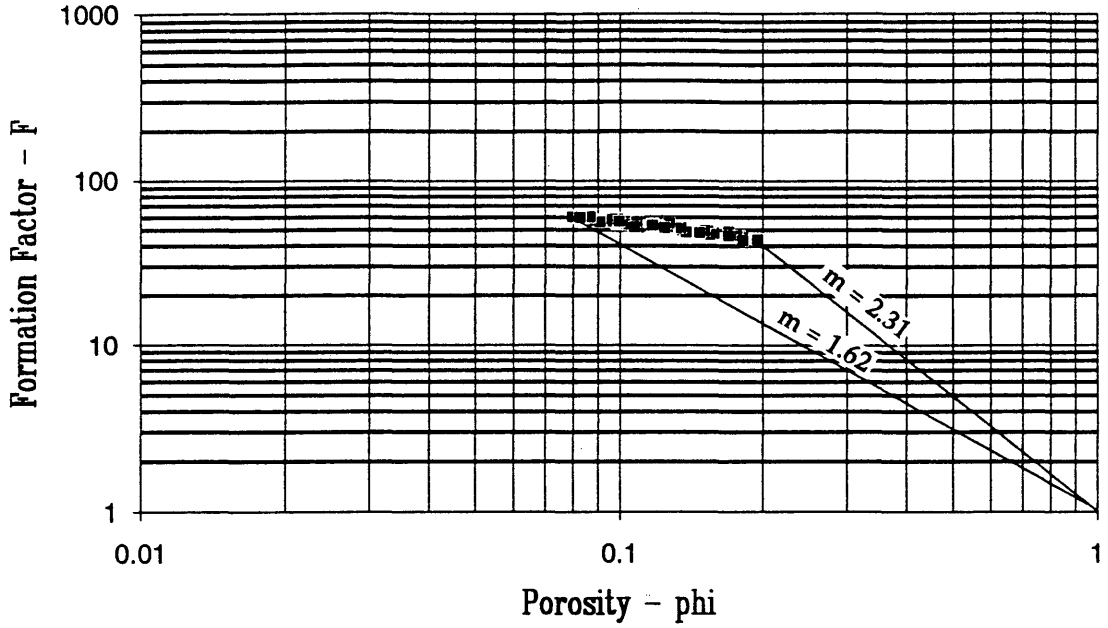

Figure 21. Facies 1: Porosity - F crossplot. Note range of m from 1.62 to 2.31.

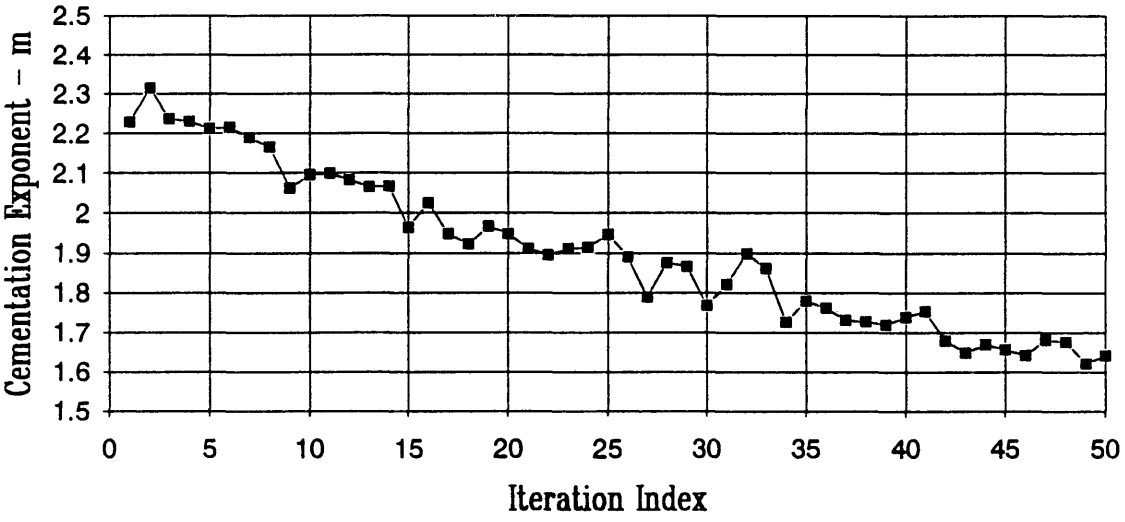

Figure 22. Calculated cementation exponents.

saturation, a relation between I and Sw becomes apparent.

This simulation correctly predicts a relation of the form $R_t = Sw^{-n} R_o$, where R_t is the resistivity of the partially saturated network, Sw is the saturation of the wetting phase, and n is the saturation exponent, seen from Table 1 to typically be between 1.5 and 2.5. Figure 23 shows I for increasing Pc and decreasing Sw. It is seen that the slope of the relation is nearly 2 for most of the range. This gives an excellent match between the average value of modelled n (2.05) and that reported for the Fulmar in the literature (2.02). As the irreducible water saturation of 60% is approached, the relation deviates from simply exponential. This variation of n over the range of observed saturations was observed by Ehrlich and Davies (1989) in samples of Benoist sandstone (Figure 24) and in studies of water-wet cores by Keller (1953). Higdon (1963) notes that the water-oil wetness of the rock is an important factor in n. Both exhibit higher resistivity indices than would be expected for a given water saturation as Sw_{irr} is approached. This might be due to globules of oil blocking the smallest pores, thereby interrupting hydraulic and electrical continuity. It is then essential to determine whether measured porosity is the same quantity that controls electrical conduction.

Calculated values of n for the simulation are shown in Figure 25 and show this increase in n, from disporportionate increases in I, as Sw is lowered. Wide variability in n is observed as the largest pores become oil-saturated and lose their electrical conductivity. Pirson (1948) reported data from partially saturated unconsolidated sands where n was a function of Sw for $70\% < Sw < 100\%$. Further observations from Wyllie and Rose (1950) also concur with this phenomenon. The irreducible water saturation level is also an additional factor in determining the magnitude of this effect, as seen in Figure 26. The higher Sw_{irr} input into the model, the greater values for n will be calculated.

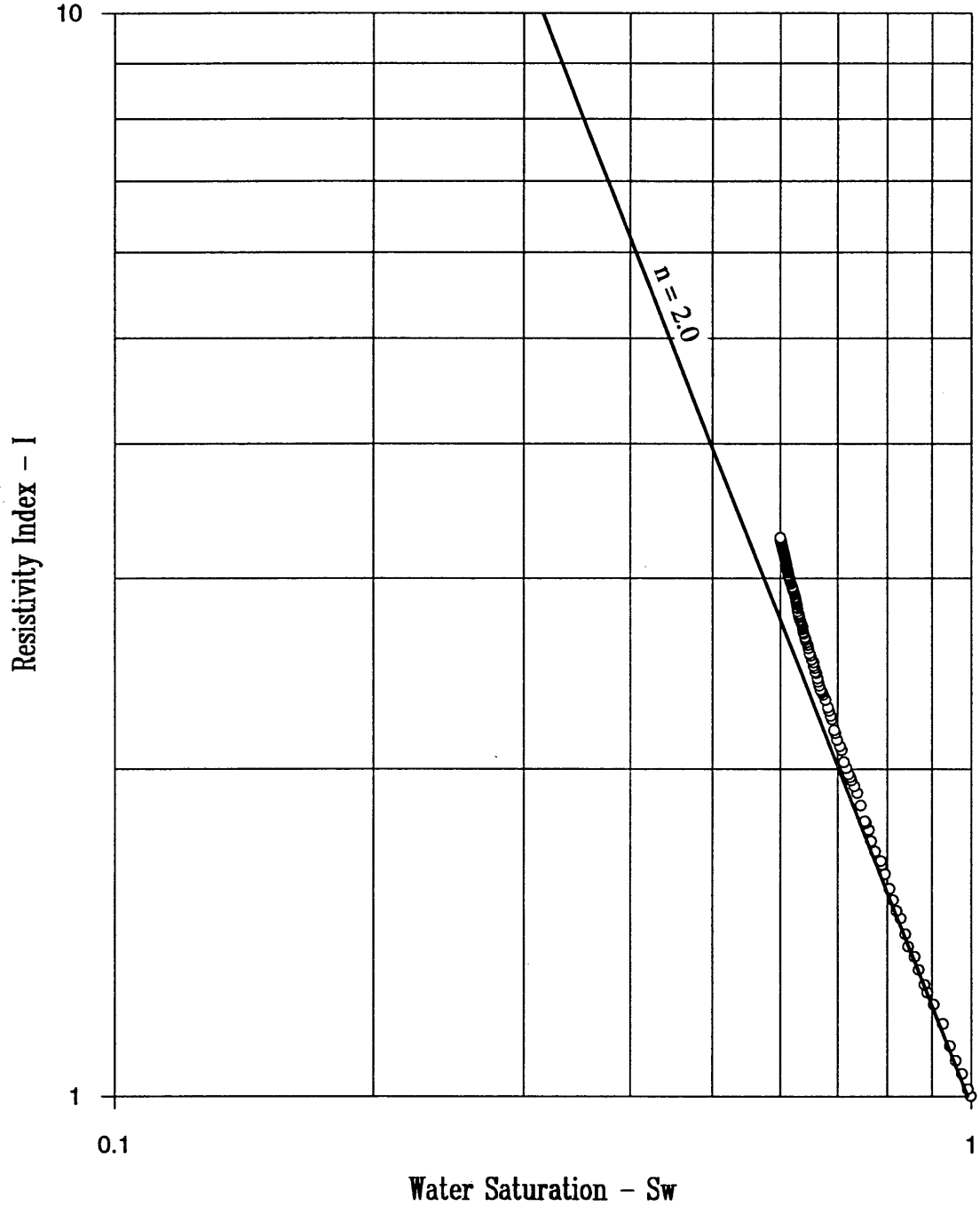

Figure 23. Fulmar Facies 1: Resistivity Index - Sw crossplot.

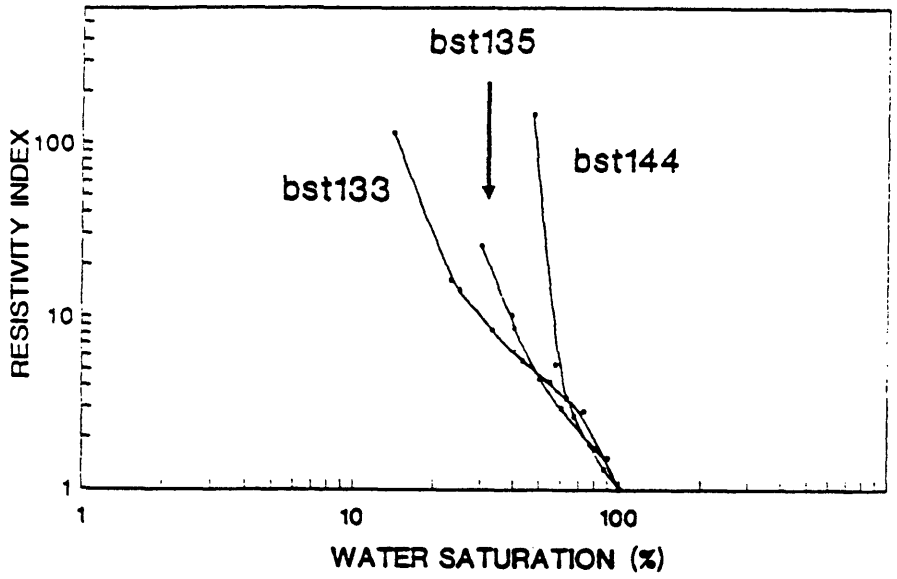

Figure 24. Resistivity indices for three samples of Benoist sandstone (Ehrlich and Davies, 1989).

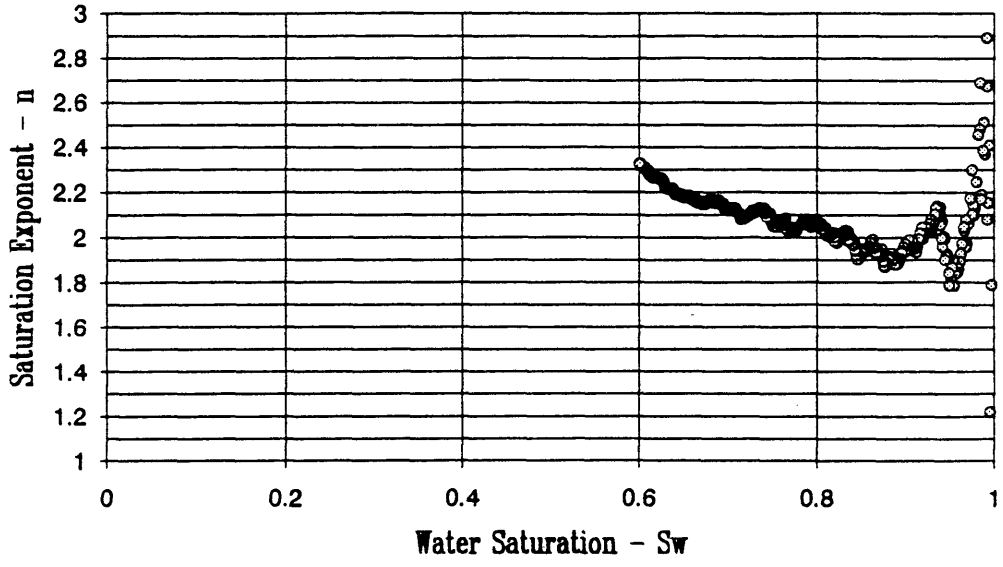

Figure 25. Fulmar Facies 1: Saturation exponent as function of Sw, $\alpha = .60$, $C_{extra} = 0.0076$.

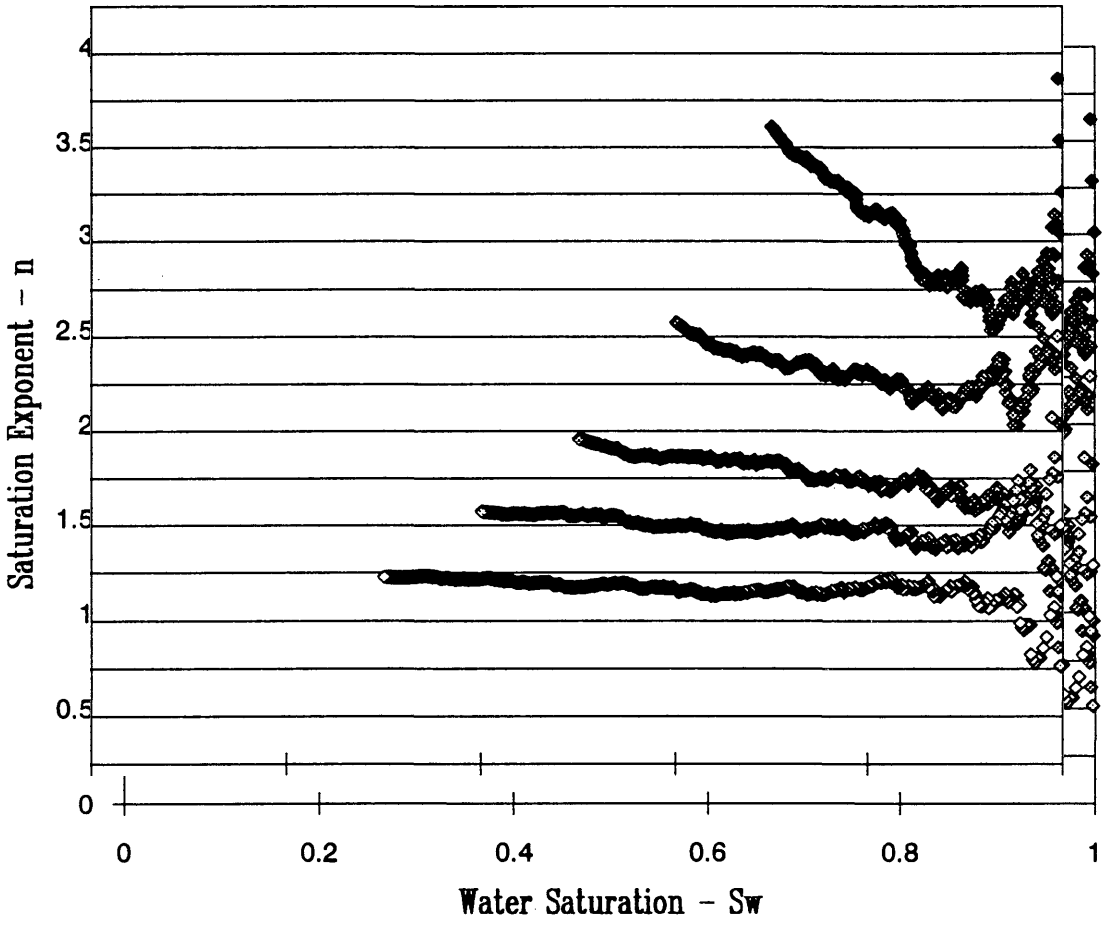

Figure 26. Fulmar Facies 1: Effect of varying α = .30, .40, .50, .60, .70.
Note $\alpha = Sw_{irr}$ = 60% provides best values for n.

The capillary pressures calculated by the model are shown as increasing functions of nonwetting phase saturation. It can be divided into three segments: an initial vertical part where little or no oil is injected for relatively large increase in pressure; a flatter section, or plateau, where a maximum number of cells are saturated with oil over a small pressure increase; and an asymptotic section that approaches irreducible water saturation as capillary pressure increases. Calculated drainage P_c curves for increasingly wider r_i distributions from Table 6, with $\alpha = Sw_{irr} = 45\%$, are shown in Figure 27. The curves are only shown to 25 psi to clearly identify the curves. At $P_c = 70$ psi, Sw_{irr} of the real rock approaches 45%. The high irreducible water saturation is correctly modelled. These fluids may be trapped as pendular rings or in clusters of extremely fine pores when these pores lose their hydraulic continuity.

The real data are characterized by a relatively gently sloping curve with very little plateau, that the uniform distributions are not able to capture. The average displacement pressures for the model curves range from 5.9 to 12.5 psi, but the displacement pressure values for the real data are much more variable. The wider the range of pore sizes, the higher the slope on the plateau. Narrower ranges represent rock samples with a greater degree of sorting. Data series 9, which is a uniform distribution with minimum $r_i = 0.0$ and midpoint r_i = mean r_i for homogeneous network, represents the maximum heterogeneity that can be obtained. Figure 28 show the drainage P_c curves of the final two series and two additional series, with $Sw_{irr} = 0.60$. Series 12 changes the shape of the $\{a_i, r_i, \tau_i\}$ distributions to Beta with $\alpha = 2$, $\beta = 5$. Series 11 then doubles the range of the Beta distributions. All four curves make a satisfactory match to the real data, with that of series 11 providing the optimal match. The largest deviation of the two curves occurs below 10 psi, where the real data curve was extrapolated from 9 psi to the point (1,0).

TABLE 6

Facies 1: Distribution Parameters for Capillary Pressure Curves

Model Cell Style: Tube Model

Uniform distributions defined by maximum and minimum values

Series	Cross-sectional Area	Tube Radius	Tortuosity	α	β
1	115, 125	0.85, 0.95	3.5, 3.7	.45	.25
2	110, 130	0.80, 1.0	3.2, 4.2	.45	.25
3	100, 140	0.70, 1.1	2.7, 4.7	.45	.25
4	90, 150	0.60, 1.2	2.2, 5.2	.45	.25
5	75, 165	0.5, 1.3	1.7, 5.7	.45	.25
6	60, 180	0.4, 1.4	1.2, 6.2	.45	.25
7	30, 210	0.2, 1.6	1.1, 6.3	.45	.25
8	15, 225	0.1, 1.7	1.0, 6.35	.45	.25
9	0, 240	0.0, 1.8	1.0, 6.4	.45	.25

Note: Best-fit homogeneous network had a_i = 120 sq μm, r_i = 0.9 μm, τ_i = 3.7.

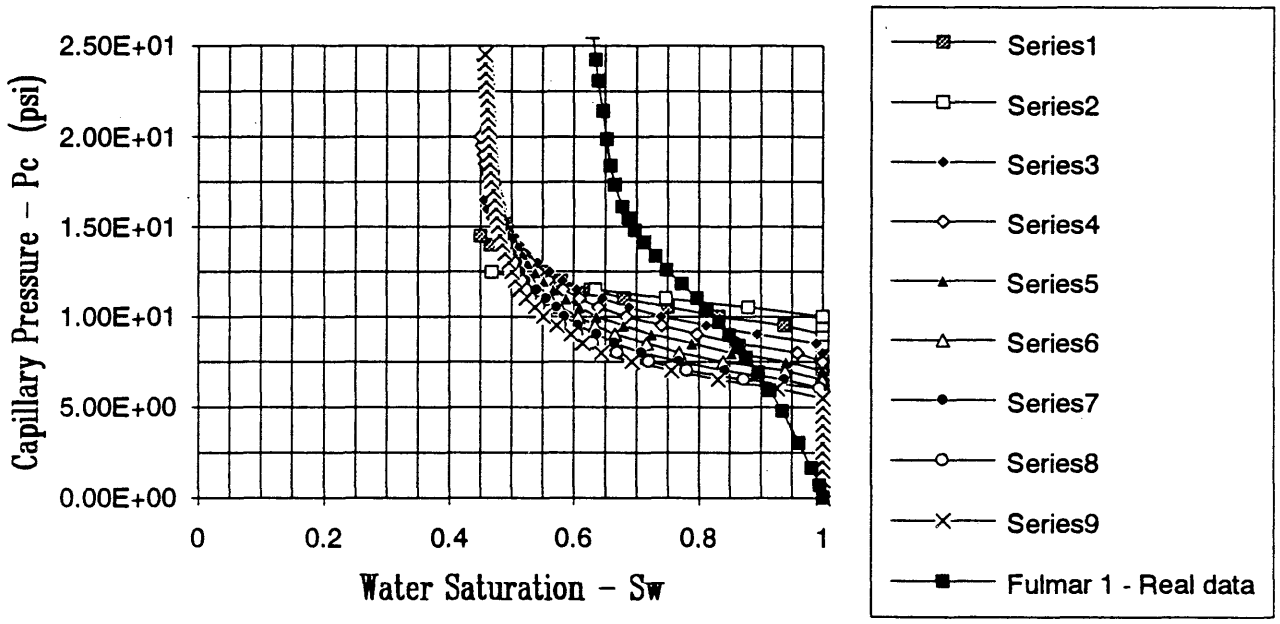

Figure 27. Fulmar Facies 1: Effect of width of uniform $\{a_i, r_i, \tau_i\}$ distributions on P_c curve, $Sw_{irr} = 45\%$.

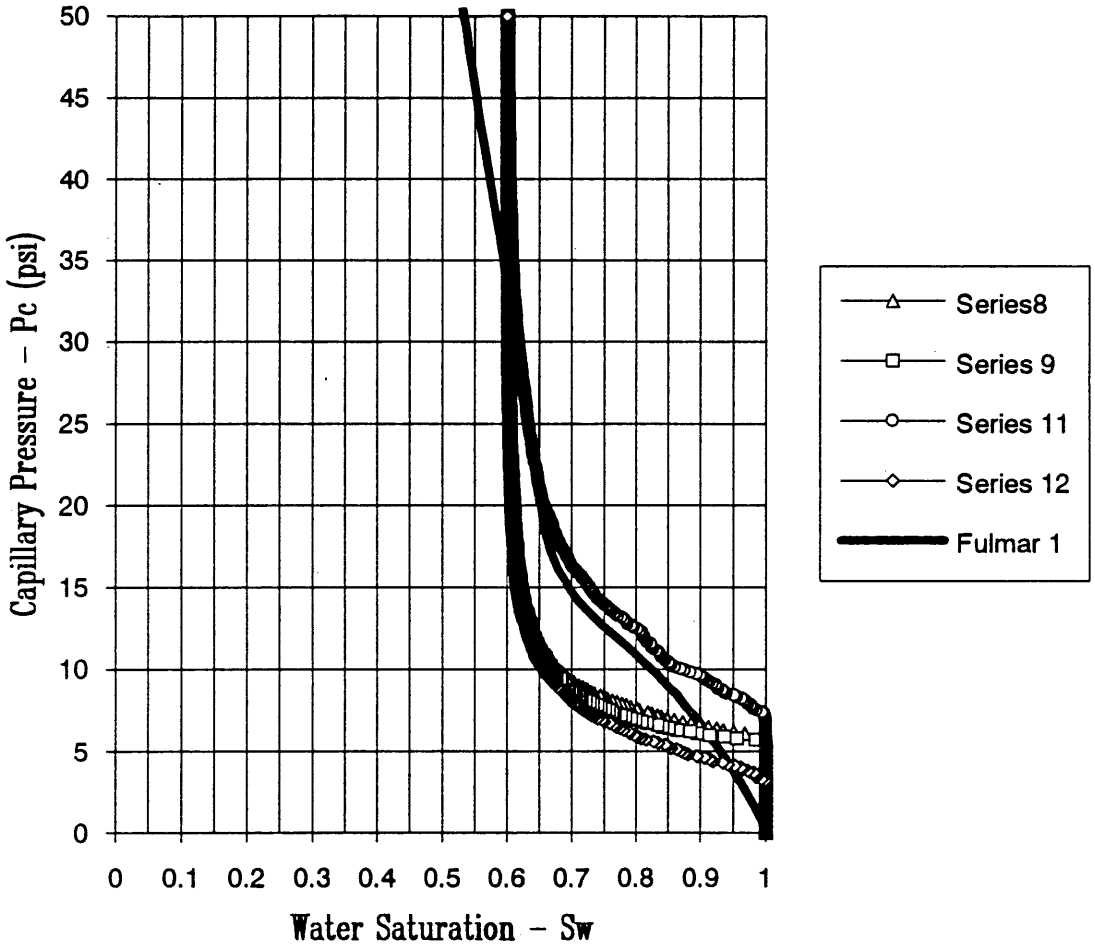

Figure 28. Fulmar Facies 1: Capillary pressure curves with $Sw_{irr} = 60\%$.

From the simulations, it can be concluded that the tube radius distribution uniquely controls the capillary pressure curves. The smaller the pore throats, the lower the permeability and conductance, and the greater the Sw for a given P_c. If smaller pores are preferentially more abundant than larger ones, than the plateau of the P_c curve is steeper. Neither the magnitude nor the range of r_i effect the observed Sw_{irr} on the model curves; it is determined by the parameter α alone.

The relationship between P_c and Sw is not unique but depends upon the saturation history of the system. When the pressure differential across the network is reduced, most of the non-wetting fluid flows back out of the pore system. The presence of this residual oil saturation forms a hysteresis effect during the imbibition process. Figure 29 shows this correctly modelled hysteresis for the series 11 drainage curve. There was no imbibition data available for comparison. The difference between the drainage and imbibition curves (the amount of residual oil as a percentage of the pore space) increases as the pressure decreases. This increases to yield a residual oil saturation at 0.0 psi of 25% and indicates that the larger pores are retaining a greater portion of the oil. This high residual nonwetting phase saturation, and therefore low recovery efficiency, commonly indicates low porosity rocks with low degrees of pore interconnectivity.

Relative permeability curves for Facies 1 is shown in Figure 30, along with those of Facies 2.1-2.5. The wetting phase curves are those that are concave to the left.It is observed that the ability of a porous medium to conduct a fluid decreases if the material is desaturated of that fluid. Curves for Facies 1, for the nine distributions in Table 6, were constructed with the modelling program (Figure 31) with $\alpha = 60\%$. The width of the distributions did not have a significant impact on the Kr curves.

The shape of the curves imply a slower increase in Kr_w as the oil is initially

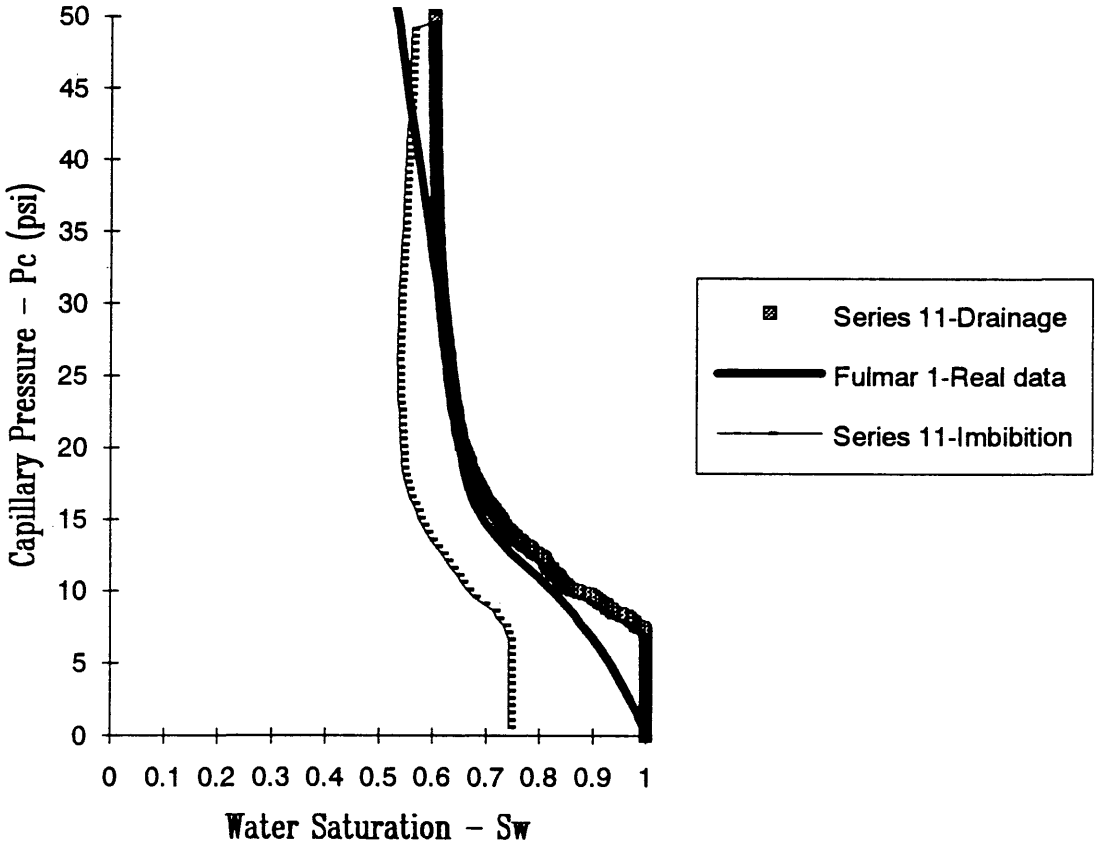

Figure 29. Fulmar Facies 1: Drainage and imbibition curves with r_i = Beta ($\alpha = 2$, $\beta = 5$, min = 0.0, max = 480.0).

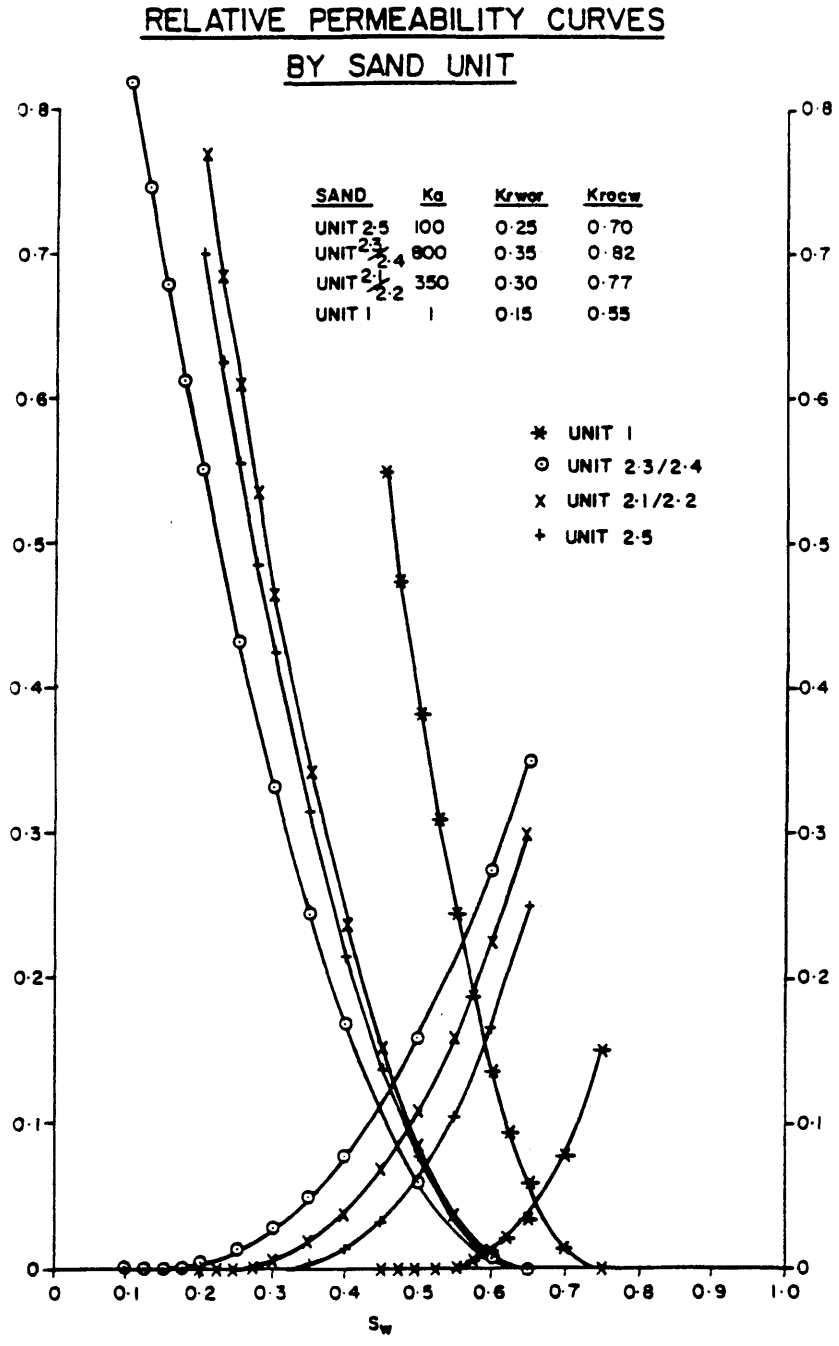

Figure 30. Relative permeability curves for wetting and nonwetting phases, Units 1, 2.1-2.5 (Boland, 1990).

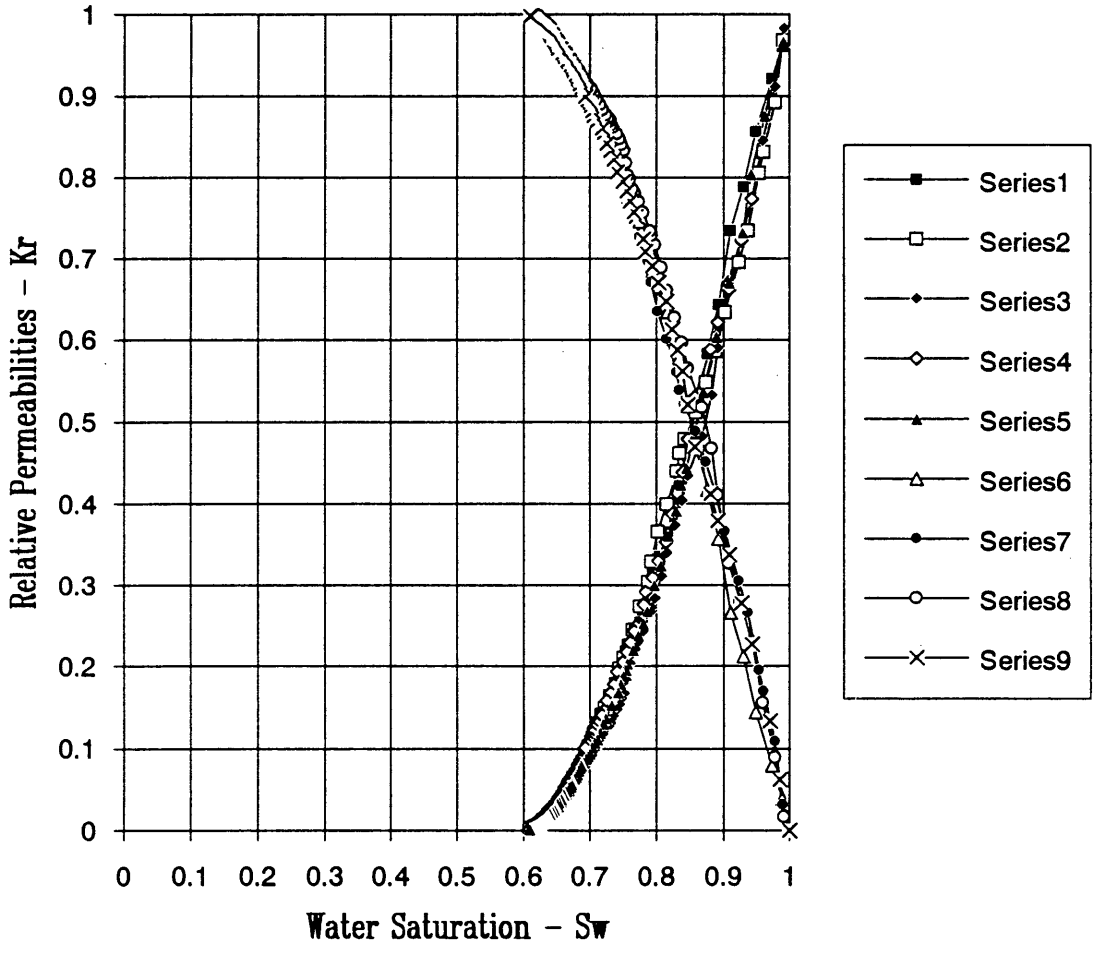

Figure 31. Fulmar Facies 1: Tube Model relative permeability curves from distributions in Table 6 for wetting and nonwetting phases.

produced, with the rate increasing as the reservoir is drained. This can be attributed to the high oil-water ratio at early stages of production; at later stages, water is driven into the more desirable, central portions of the pore space vacated by the oil. The Kr_{nw} curve shows an inverse geometry, due to the same effect; as the oil phase becomes more discontinuous during production, the relative permeability starts to decrease at a greater rate. The wetting phase curve shows relative permeabilities of 1.0 at Sw = 100% and 0.0 at Sw_{irr}, and is concave to the left. This agrees with characteristics seen in real Kr_w curves. The nonwetting phase curve runs smoothly from 1.0 at Sw_{irr} to 0.0 at Sw = 100%. Although it is common to observe Kr_{nw} = 1.0 at wetting phase saturations greater than 1.0, it is usually not observed at Sw = 60%. Furthermore, the Tube Model shows that the sum of the relative permeabilities is equal to 1.0, which is generally not observed.

As an improvement in these two areas, the Dual Tube Vug Model was used to model both drainage and imbibition over the same saturation range (Figure 32). At Sw_{irr}, Kr_{nw} is less than one, which implies the existence of water-saturated cells whose permeability has been interrupted by nonwetting phase. The curves also intersect between 0.4 and 0.5, which correctly models the effect the fluid interference effect seen in real rocks. The intersection point is greater than Sw = 50%, revealing a water wet character in model data. The imbibition curves for this example are very steep, with a predetermined So_{res} of 25%, as seen on the observed data. These curves show a decreased water saturation for a given Kr, where the amount increases with decreasing P_c. Similar to the imbibition capillary pressure curves, the Kr curves show that a greater portion of residual oil is contained in the larger pore spaces.

Although the model curves do not match the observed curves, the model curves show characteristics from physical effects between the rock-fluid system that are more

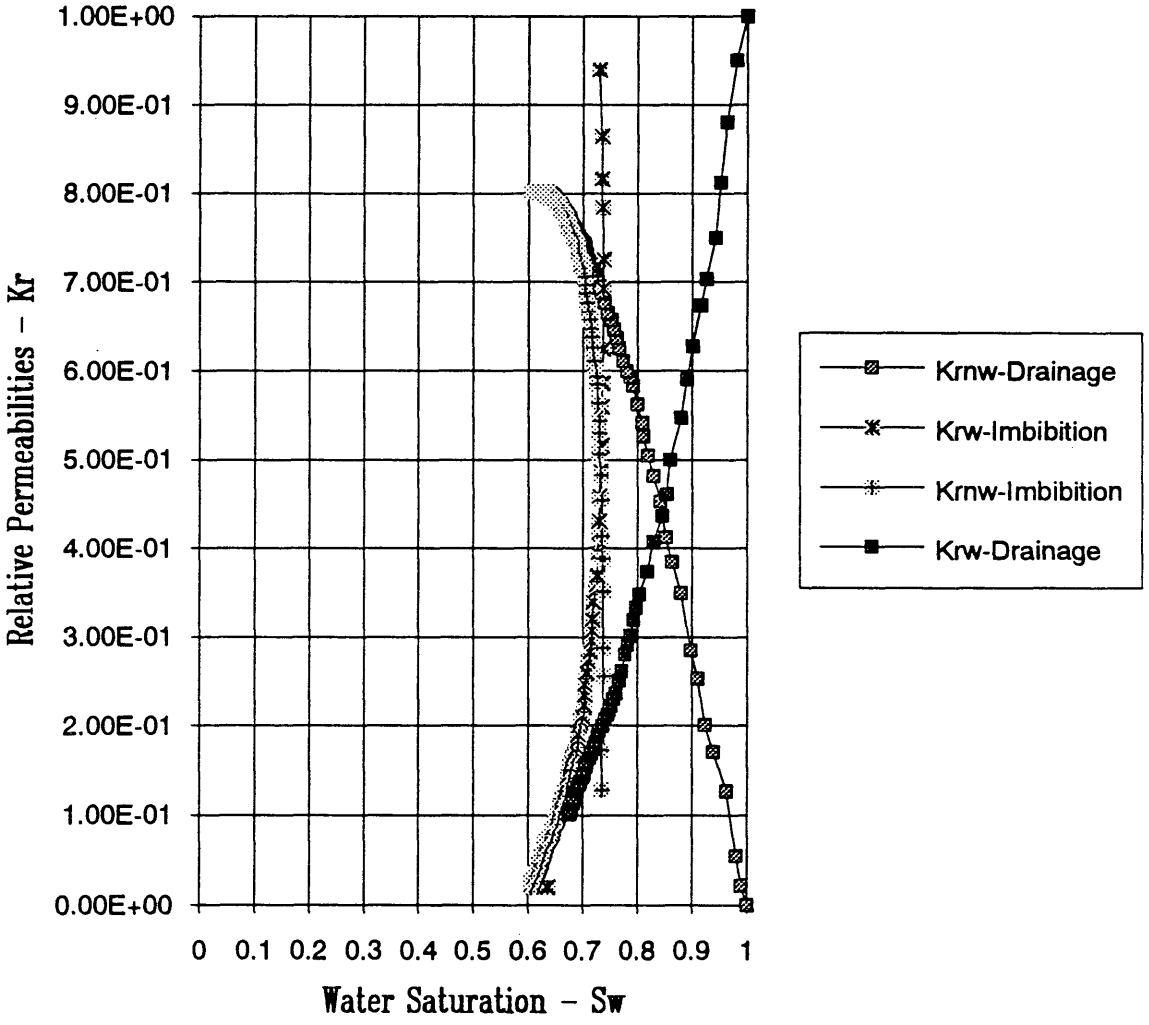

Figure 32. Fulmar Facies 1: Dual Tube Vug Model with drainage and imbibition curves for wetting and nonwetting phases.

reasonable than those of the real data. In particular, it is very unlikely that the rock would lose virtually all of its conductivity at Sw = 65%. Additionally, since Kr curves can be measured during both drainage and imbibition, and the saturation history of the laboratory samples is unknown, these curves may be 1st, 2nd, or 3rd generation drainage or imbibition curves. Therefore, an exact match may require many iterations with several unfounded assumptions.

Athough no empirical data was available for either bulk density or surface area per unit volume, the calculated values are reasonable. A bulk density for a 60% water saturated sandstone of 2.43 g/cm^3 agrees with those of other formations observed from logs and core analysis. Likewise, an S_V of 0.174 m^2/cm^3 is within a factor of 10 to those seen in the Upper and Middle Wilcox and the Catahoula Sandstones. The model did not account for the added S_V due to clays, which would increase the calculated values much higher. Application of the Tube Vug or Dual Tube Vug Models would give a greater degree of influence over S_V, since it is dependent upon the third power of R, rather than r^2 in the Tube Model. Finally, comparison of the individual contributions of the cells toward S_V showed that S_V is dominated by the large surface-to-volume ratio of the smaller pores.

Section 4.2 Fulmar Sandstone - Reservoir Facies

A comparative analysis between the nonreservoir and reservoir units of the Fulmar can be begun by studying Tables 7 and 8. The input parameters for the best-fit simulation, shown in Table 7, show the an initial guess of a_i = 7000 sq μm was very close to the inverted average grain size of 6000 sq μm, which corresponds to that of fine-grained sandstone. Average tube radii (r_i = 11.5 μm) are ten times larger than those of Facies 1. Tortuosities centered around 2.9 are within reasonable bounds.

TABLE 7

Fulmar Facies 2.3: Input Distribution Parameters for Best-fit Simulation

Model Cell Style: Tube Model

Input Variable	Distribution Type	Distribution Parameters
a_i (sq μm)	Uniform	min=2000, max=10000
r_i (μm)	Uniform	min=2.5, max=20.5
τ_i	Gaussian	μ=2.9, σ=0.9
α	Singular	α = 0.10
β	Singular	β = 0.35
C_{extra} (mhos)	Singular	C_{extra} = 0.11966

TABLE 8

Fulmar Facies 2.3: Comparison between Experimental and Calculated Properties

	Experimental	**Calculated**
Porosity, ϕ	20.0-24.8%	23.7-27.1%
Formation Factor, F	15 - 150	16 - 19
Permeability, k	140 - 835 md	679 - 844 md
Cement. Expon., m	1.91	2.08
Satur. Expon., n	2.02	1.25 - 2.25
Plateau Pd	0.6±0.3 psi	0.6 psi
Sw_{irr}	10%	10%
So_{res}	35%	35%
Average ρ_b	Not Available	2.18 g/cc
Average S_v	Not Available	0.0349 m^2/cm^3
Net/gross Ratio	1.0	
Average So	91%	-
ρ_m	2.655 g/cc	-
ρ_w	1.056 g/cc	-
ρ_o	0.730 g/cc	

A further differentiation of the five Unit 2 subfacies is shown on the porosity - permeability crossplot of Figure 33 (Boland, 1990). Unit 2.3 is seen to have the highest permeabilities (140 - 835 md) of any of the other units, combined with high porosities from 20 - 25%. The correlation between k-ϕ model data for the best simulation and to that from the plot in Figure 33 is given by Figure 34. The porosities have approximately the same range and are within 2% of the real data. Calculated permeabilities display an average value of about 750 md, which exceeds the empirical average of 450 md. This result is satisfactory, being within one order of magnitude. Although these permeabilities are greater than those of Facies 1 by factors of 100-10000, they also display less heterogeneity than that of the real data.

Using an extra conductance of 0.11966 mhos produced formation factors that lie within the low end of the range of expected values. Since formation factors were only reported for all the Fulmar units combined, Facies 2.3 with its higher porosities could indeed occupy the lower part of the range. An F-ϕ crossplot (Figure 35) illustrates cementation exponents from a relatively narrow range, 1.98 - 2.15 (Figure 36). Again, this makes a good comparison to the established value of 1.91.

The crossplot of I and Sw shows that the slope of the line with respect to the point (1, 1) is much more dependent on the value of Sw (Figure 37). With a decrease in water saturation, the network experiences a greater-than-exponential increase in I. This curve also exhibits a curvature that is concave to the left, similar to that of Facies 1 and the results of Keller (1953) and Ehrlich and Davies (1989). Calculated values for n (Figure 38) show exponents that are between 1.25 and 2.25 for most of the range. As the level of irreducible water saturation is a factor in the calculated value for n, the low Sw_{irr} is the probable reason for low average values for n. As the saturation exponents are probably

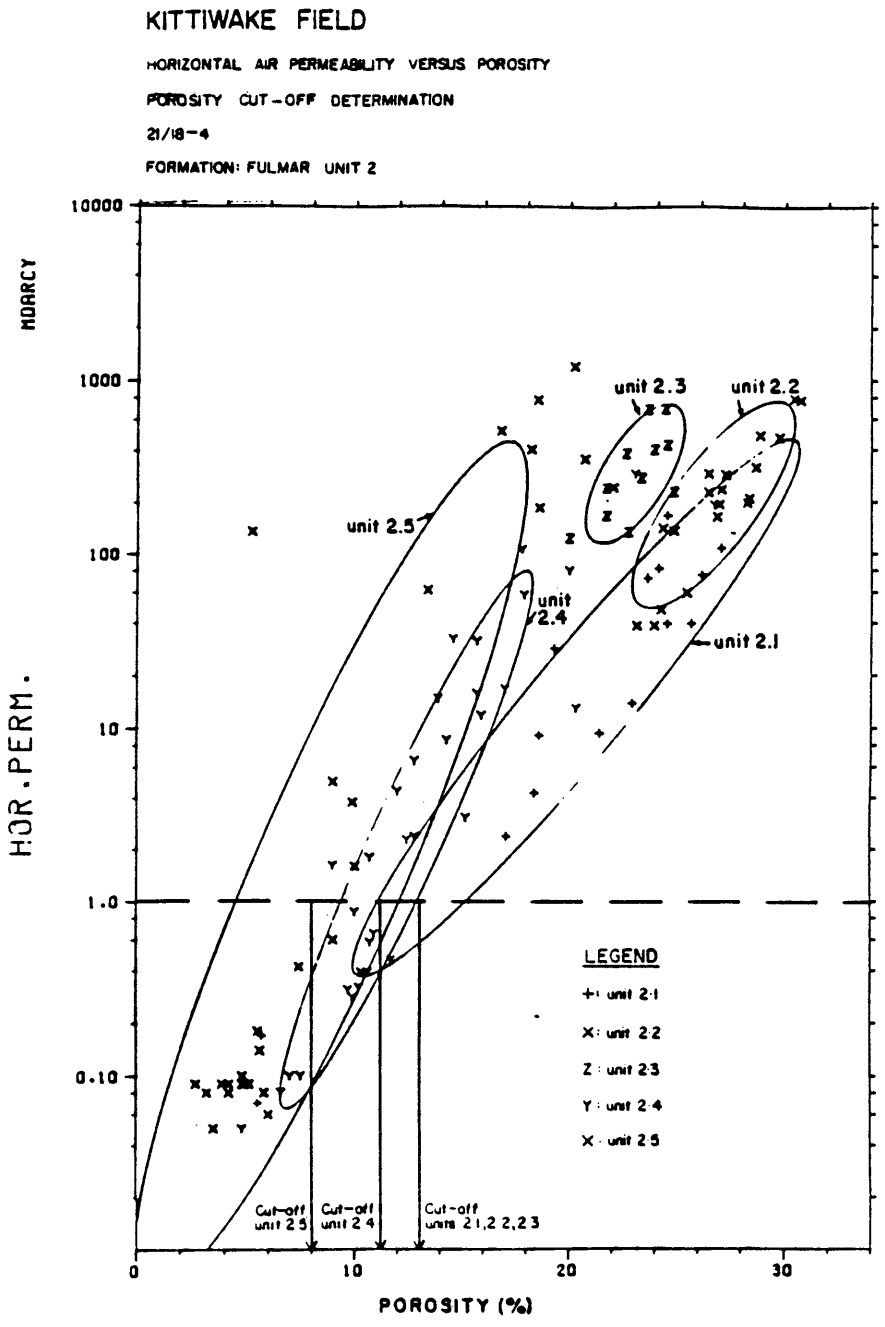

Figure 33. Porosity - permeability crossplot for Fulmar Facies 2.1-2.5 (Boland, 1990).

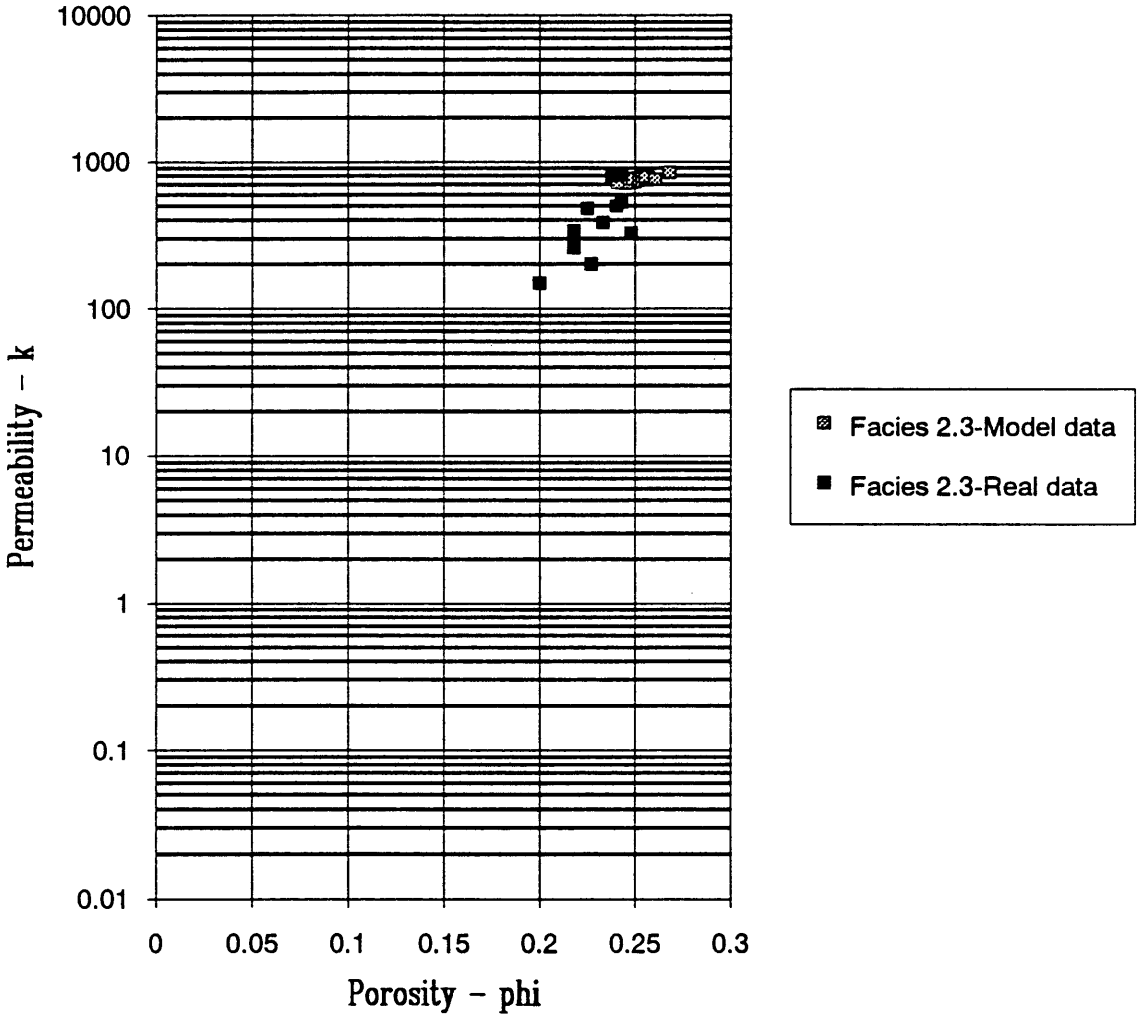

Figure 34. Fulmar Facies 2.3: Porosity - permeability crossplot.

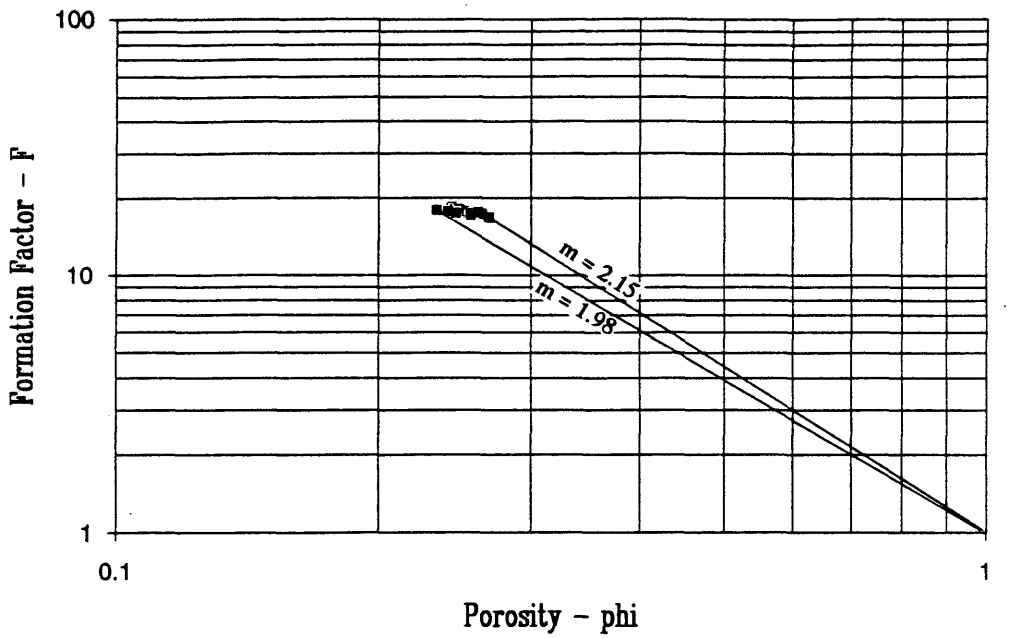

Figure 35. Fulmar Facies 2.3: Porosity - formation factor crossplot. Note range of m from 1.98 to 2.15.

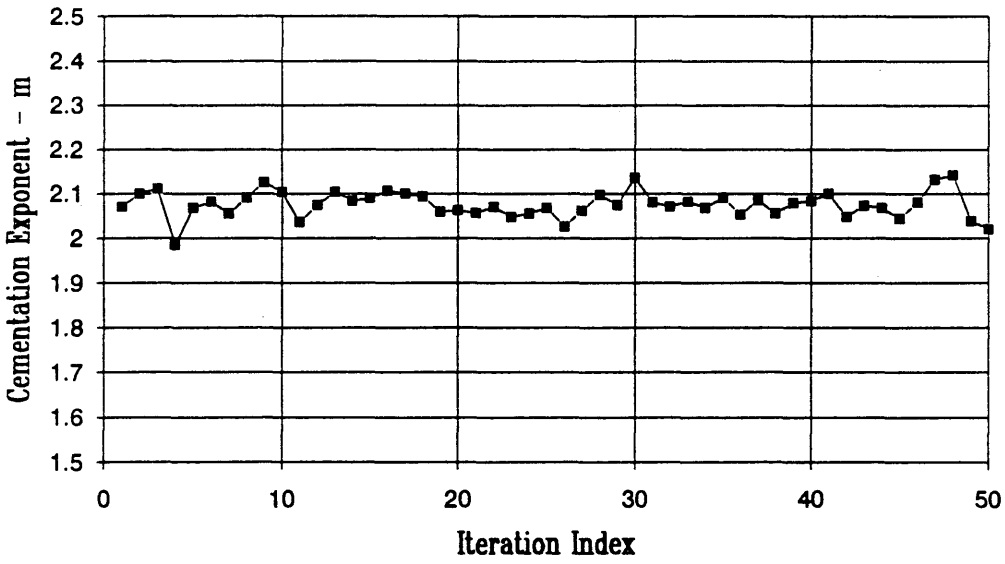

Figure 36. Fulmar Facies 2.3: Calculated cementation exponents.

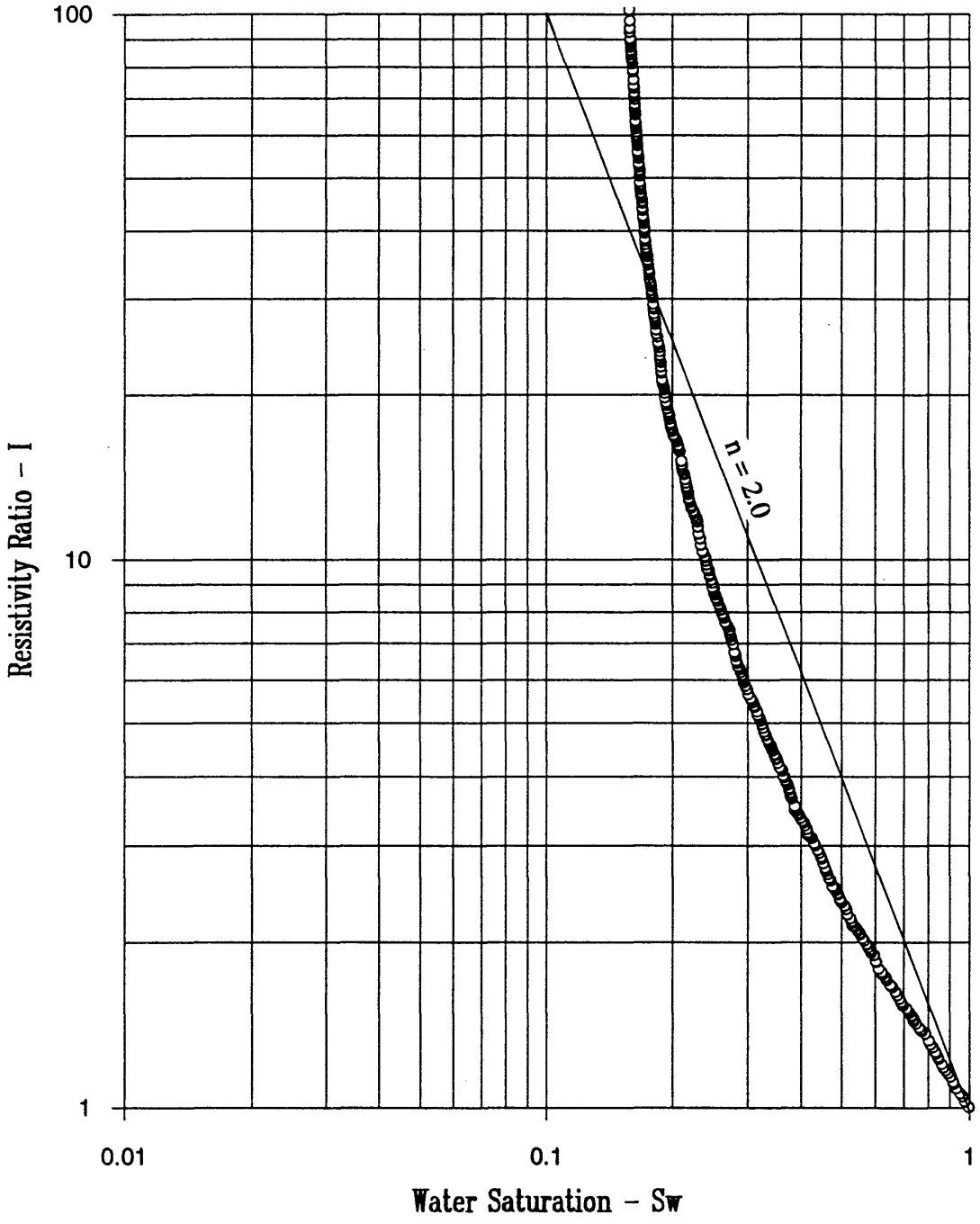

Figure 37. Fulmar Facies 2.3: Resistivity Index - Sw crossplot.

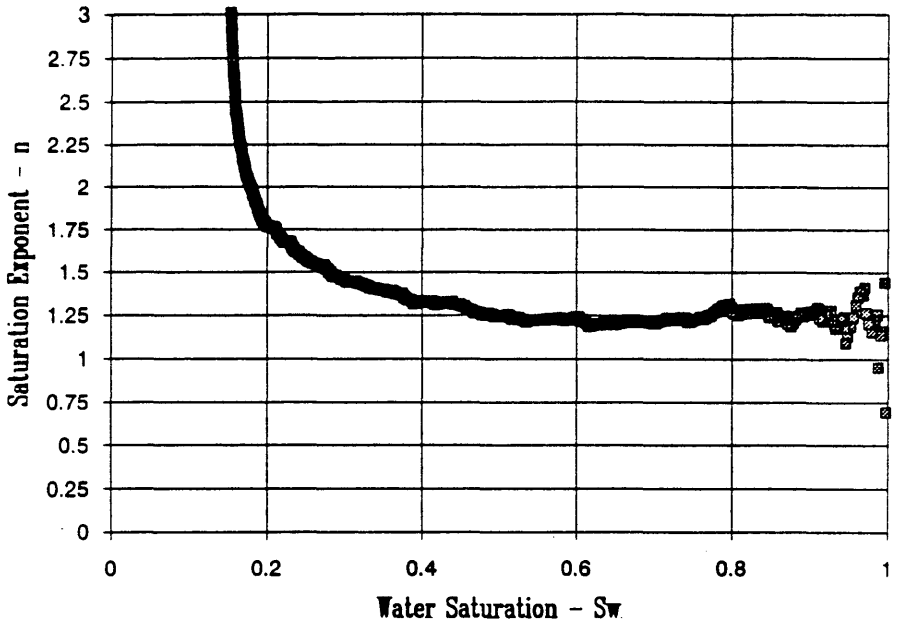

Figure 38. Fulmar Facies 2.3: Saturation exponent as function of Sw; $\alpha = 0.10$, $C_{extra} = 0.11966$.

calculated in the lab from resistivity measurements of oil-saturated core (Sw = 10 - 20%, note the average So is 9%), n values in this saturation range (1.75+) are more reasonable.

The best-fit capillary pressure curve, with an irreducible water saturation of 10% is compared to the core analysis curve in Figure 39. The model curve has a similar steeply-sloping, flat plateau shape and very low displacement pressures to the real curve. The narrow size range indicates good sorting of the grain sizes, which is generally an indicator of high permeability. The gentler slope on the experimental curve indicates a relatively greater proportion of smaller tube radii, which the standard distributions were not able to exactly emulate. The imbibition curve, since it was generally indistinguishable from the

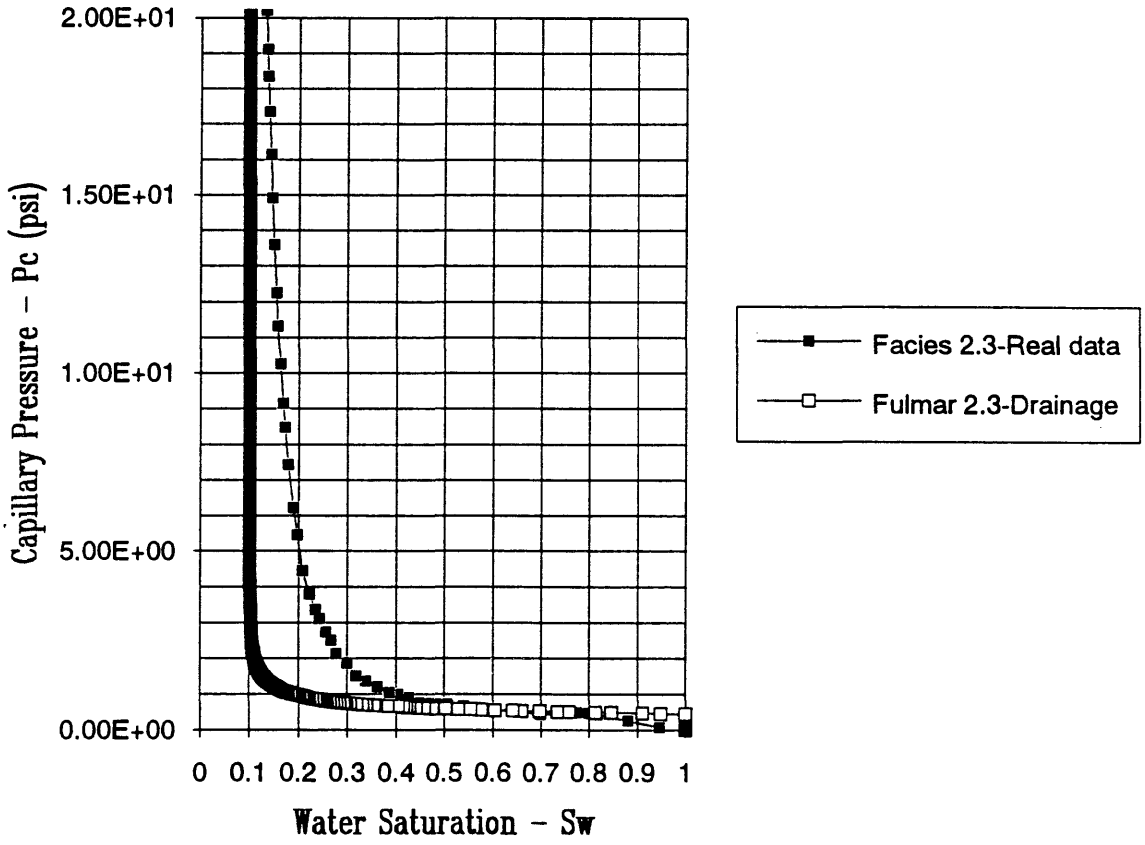

Figure 39. Fulmar Facies 2.3: Capillary pressure curve with Sw_{irr} = 10%.

drainage curve, was not shown. The close association of the drainage and imbibition curves is a direct manifestation of low Sw_{irr} and few deadend pore spaces.

Figure 40 includes relative permeability curves for both drainage and imbibition for the wetting and nonwetting phases. The process of draining the wetting phase by injection of oil is seen to continue to Sw_{irr} = 10%, then the pressure is incrementally dropped, with the network approaching So_{res} = 30 - 35%. Both the drainage and the imbibition curves are similar in shape to those of Facies 1, which correctly model the microscopic fluid properties during production of the reservoir.

No data for surface area per unit volume or bulk density were available for Facies 2.3. However, calculated values of ρ_b = 2.18 g/cc for a 91% oil saturated network and an S_V = 0.0349 m^2/cm^3 lie within expected ranges. The lower S_V of this network, compared to that of Facies 1, can be attributed to the decreased surface-to-volume ratio of the larger pores in this network.

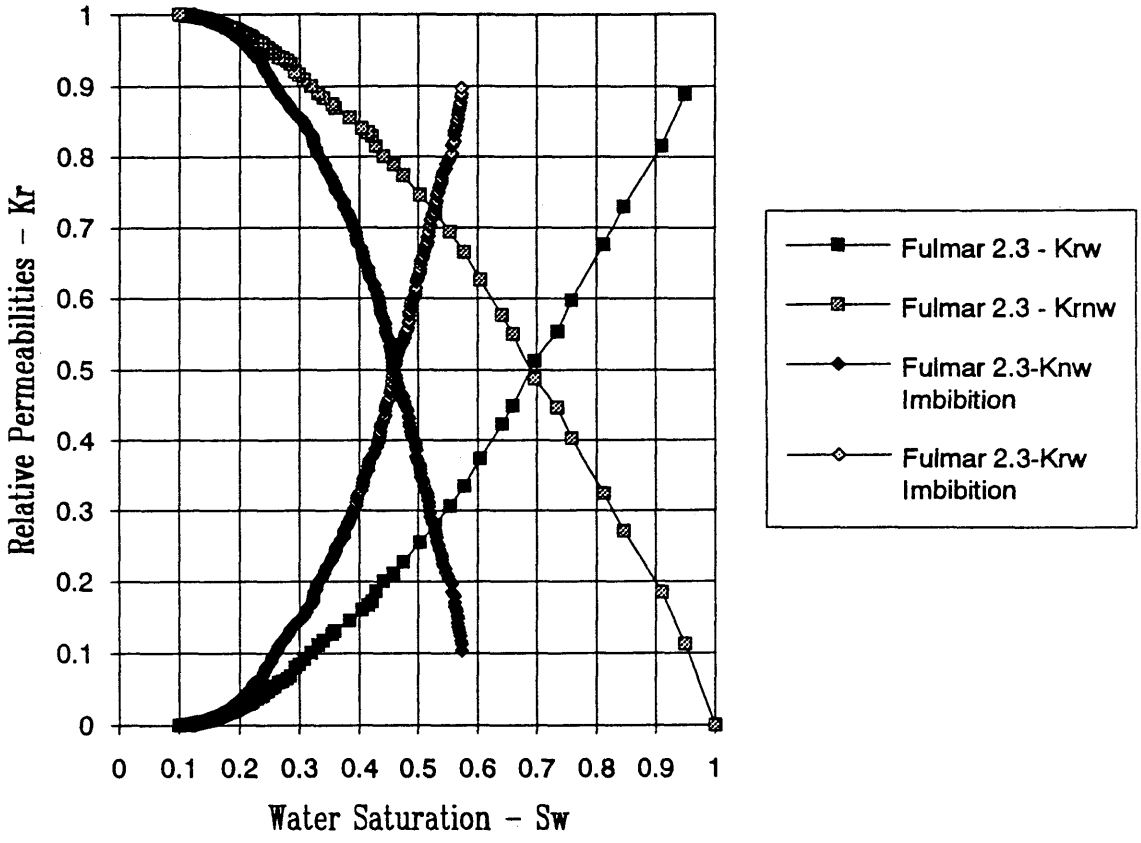

Figure 40. Fulmar Facies 2.3: Relative permeability drainage and imbibition curves for wetting and nonwetting phases.

CONCLUSIONS

The HRP model proved in general to behave similarly to real pore systems. The equations defining the transformation from input pore space parameters to petrophysical properties provided a clear understanding of the physical aspects of the rock and fluid. Throughout the development of the modelling framework, satisfactory simulations of one property provided improved simulations of other properties. The interdependence of these characteristics of reservoir and nonreservoir rock follow from their mutual dependence on the same input parameters.

The model provided data which exhibit similar qualitative relationships to the real Fulmar data between F and ϕ, I and Sw, and Pc and Sw. Simulated formation factors, porosities, and permeabilities compared favorably to those observed in the laboratory. Ranges of Sw_{irr} and So_{res} match those manifested in capillary pressure and relative permeability curves. Porosity, cementation exponent, and S_V were seen to be strongly dependent on vuggy pore space, while permeability was proportional to the fourth power of the tube radius. The average pore size, the range of pore size, and to a lesser extent the shape of the pore size distribution uniquely determined the shape of the capillary pressure curves. Assymptotic limits on the P_c and Kr curves were established by judicious choice of the parameters α and β.

Based upon over 350 preliminary simulations, the Tube Model proved to be the most intuitive and the most effective in simulating the desired properties. The effect of varying the input parameter distributions was quickly seen by reference to the equations. The Tube Model succeeded in matching F, ϕ, k, m, n, I, P_c, and ρ_b as accurately as the

Tube Vug Model and the Dual Tube Vug Model. For the latter two models, convergence towards the solution was less efficient; the additional input variables typically produced convergence towards one property and divergence away from others. The Dual Tube Vug Model provided limited improvement in the Kr curves by reducing Kr_w and Kr_{nw} to a sum less than 1.0. The HRP model was seen to generally provide excellent fits of F, ϕ, k, m, and ρ_b data; good matches to P_c, I, n, and S_v; and fair simulations of Kr curves.

Comparison of network simulations of nonreservoir Fulmar Sandstone Facies 1 and reservoir Facies 2.3 provided the following specific conclusions.

Facies 1, the nonreservoir unit of the Fulmar Sandstone, was typified by moderate to high porosities (8 - 23%), low permeabilities (0.096 - 11 md), highly variable pore throat sizes, high irreducible water saturations (45 - 60%) and higher values for S_v (0.174 m^2/cm^3). The large range of pore sizes produces highly variable displacement pressures (7.3 - 12.3 psi) that lead to gently sloping capillary pressure curves with steep plateaus.

The principal reservoir unit of the formation, represented by Facies 2.3, exhibited high porosities (20 - 25%), high permeabilities (140 - 835 md), a narrower range of pore throat sizes, very low irreducible water saturations (10%), and lower S_v (0.0349 m^2/cm^3). A homogeneity of pore throat sizes produces a narrow range of displacement pressures (0.3 - 0.9 psi) and steeply sloping capillary pressure curves. Flat plateaus are observed, correctly simulating good grain sorting, homogeneous pore sizes, and a high degree of pore interconnectivity.

It can be postulated that these different petrofacies may have had identical depositional characteristics, and exhibit entirely different petrophysical attributes solely from diagenetic alteration. However, the pseudo-inversion of the data revealed silt-sized grains (a_i = 0 - 240 sq μm), extremely fine pore throat sizes (r_i = 0 - 1.8 μm), and shaly

conductance for Facies 1, which can be now interpreted as a low-energy marine shaly siltstone; similarly, Facies 2.3 can be interpreted as a VF - F grained moderate-energy marginal marine argilliceous sandstone from its sand-sized grains (a_i = 2000 - 10000 sq μm), larger pore sizes (r_i = 2.5 - 20.5 μm), and extra shaly conductance.

The HRP model can serve as a "stand-alone" framework for petrophysical modelling or perhaps, with increases in computer power, serve as an integral component of a reservoir modelling package. Detailed reservoir characterization of the reservoir - nonreservoir rock and fluid system can be substantially improved with microscopic attention to the cellular network. Bulk model networks might be then combined in series and parallel combinations to simulate megascopic rock unit geometries.

The process of evaluating the predictive power of the model was dependent on the limited set of experimental observations. The type and amount of data required for fully comprehensive petrophysical description is diverse. Further empirical investigation into pore space geometries, in conjunction with theoretical inquiry, will greatly improve petrophysical evaluation and differentiation of reservoir and nonreservoir rock.

Future work on the HRP modelling framework can involve the comparison of simulated data to a more comprehensive suite of petrophysical data over a wide range of lithologies; the investigation of ϕ-k relationships for particular rock types; the study of pressure effects on the model response; incremental analysis of the interrelationships between properties via parametric equations, with Sw or M as the independent variable; or the extension to elastic, gravimetric, or nuclear phenomena.

REFERENCES CITED

Amyx, J., D. Bass, R. Whiting, Petroleum Reservoir Engineering: Physical Properties, New York: McGraw-Hill Book Company, 1960.

Archie, G. E., The Electrical Resistivity Log as an Aid in Determinining Some Reservoir Characteristics, Transactions of AIME, 1942, Page 54.

Boggs, S., Principles of Sedimentology and Stratigraphy, Columbus, Ohio: Merrill Publishing Company, 1987.

Boland, M., Petrophysical Review of Kittiwake, Shell U.K. Expro UEDC/44, Note No. UEDC/44.90.003, October 1990.

Carman, P. C., Journal Soc. Chem. Ind., Volumes 57 and 58, 1939.

Chatzis, I. and F. A. L. Dullien, Modelling Pore Structure by 2-D and 3-D Networks with Application to Sandstones, Journal of Canadian Petroleum Technology, Vol. 16, 1977, Page 97.

Dodd, C. G. and O. G. Kiel, Evaluation of Monte Carlo Methods in Studying Fluid-Fluid Displacement and Wettability in Porous Rocks, Journal of Physical Chemistry, Vol. 63, 1959, Page 1646.

Dodds, J. A. and P. S. Lloyd, A Model for the Void Structure in Multi-component Sphere Packs Applied to Capillary Pressure Curves, Powder Technology, Vol. 5, 1971/72, Page 69.

Dullien, F. A. L., New Network Permeability Model of Porous Media, AIChE Journal, Vol. 21, 1975a, Page 299.

Dullien, F. A. L., I. Chatzis and M. S. El-Sayed, Modelling Transport Phenomena in Porous Media by Networks Consisting of Non-Uniform Capillaries, SPE paper #6191, 1976.

Dullien, F. A. L. and G. K. Dhawan, Characterization of Pore Structure by a Combination of Qualitative Photomicrography and Mercury Porosimetry, Journal of Coll. Interfac. Science, Vol 47, 1974, Page 337.

Dullien, F. A. L. and G. K. Dhawan, Bivariate Pore-Size Distributions of Some Sandstones, Journal of Coll. Interfac. Science, Vol. 52, 1975, Page 129.

Ehrlich, R. and D. K. Davies, Image Analysis of Pore Geometry: Relationship to Reservoir Engineering and Modelling, SPE Preprint #19054, 1989.

Etris, E. L., D. S. Brumfield, R. Ehrlich, and S. J. Crabtree, Relations between Pores, Throats, and Permeability: A Petrographic/Physical Analysis of Some Carbonate Grainstones and Packstones, Carbonates and Evaporites, Vol. 3, No. 1, 1988, Page 17.

Fatt, I., The Network Model of Porous Media: I. Capillary Pressure Characteristics, Transactions of the AIME, Vol. 207, 1956a, Page 144.

Fatt, I., The Network Model of Porous Media: II. Dynamic Properties of Single Size Tube Network, Transactions of the AIME, Vol. 207, 1956b, Page 160.

Greenberg, R. J., and W. F. Brace, Archie's Law for Rocks Modelled by Simple Networks, Journal of Geophysical Research, Vol. 74, 1969, Page 2099.

Haring, R. E. and R. A. Greenkorn, A Statistical Model of a Porous Medium with Nonuniform Pores, AIChE Journal, Vol. 16, 1970, Page 477.

Harris, C. C., Latin Square as a Network Model of Random Packing, Nature, Vol. 205, 1965, Page 353.

Iczkowski, R. P., Electrical Conductivity of Partially Saturated Porous Solids, Ind. Eng. Chem. Fundam., Vol. 9, 1970, Page 674.

Kirkpatrick, S., Percolation and Conduction, Reviews of Modern Physics, Vol. 45, 1973, Page 574.

Kwon, B.S., A Mathematical Pore Structure Model and Pore Structure Interrelationships, Colorado School of Mines PhD dissertation, 1976.

Larson, R. G., L. E. Scriven and H. T. Davies, Percolation Theory of Residual Phases in Porous Media, Nature, Vol. 268, 1977, Page 409.

Madden, T. R., Random Networks and Mixing Laws, Geophysics, Vol. 41, 1976, Page 1104.

Millson, J. A., A Sedimentological Review of Middle and Early Upper Jurassic Sandstone Reservoirs in the Central Graben, Shell U.K. Expro UEE/33, Exploration Note: EN87008CNS, July 1987.

Nicholson, D. and J. H. Petropoulos, Capillary Models for Porous Media: III. Two-phase Flow in a Three-dimensional Network with Gaussian Radius Distribution, Journal Phys. D: Applied Physics, Vol. 4, 1971, Page 181.

Owen, J. E., The Resistivity of a Fluid-filled Porous Body, Transactions of the AIME, Vol. 195, 1952, Page 169.

Preston, F. W. and J. C. Davis, Sedimentary Porous Materials as a Realization of a Stochastic Process, Random Processes in Geology, New York: Springer-Verlag, 1976, Page 63.

Raymer, L. L. and P. M. Freeman, In-Situ Determination of Capillary Pressure, Pore Throat Size and Distribution, and Permeability from Wireline Data, SPWLA 25th Annual Logging Symposium, Paper CCC, 1984.

Rink, M. and J. R. Schopper, Computations of Network Models of Porous Media, Geophysical Prospecting, Vol. 16, 1968, Page 277.

Shante, V. K. S. and S. Kirkpatrick, An Introduction to Percolation Theory, Advances in Physics, Vol. 20, 1971, Page 325.

Simon, R. and F. J. Kelsey, The Use of Capillary Tube Networks in Reservoir Performance Studies: I. Equal Viscosity Miscible Displacements, Society Petroleum Engineers Journal, Vol. 11, 1971, Page 99.

Simon, R. and F. J. Kelsey, The Use of Capillary Tube Networks in Reservoir Performance Studies: II. Effect of Heterogeneity and Mobility on Miscible Displacement Efficiency, Society of Petroleum Engineers Journal, Vol. 12, 1972, Page 345.

Somerton, C., and P. Wood, Effect of Walls in Modelling Flow through Porous Media, Journal of Hydraulic Engineering, Vol. 114, Number 12, 1988, Page 1431.

Towle, G. H., An Analysis of the Formation Factor - Porosity Relationships for Some Assumed Pore Geometries, SPWLA Third Annual Symposium, 1962.

Winsauer, W. O., H. M. Shearin, P. H. Masson, and M. Williams, Resistivity of Brine-saturated Sands in Relation to Pore Geometry, Bulletin of the AAPG, February 1952, Page 253.

Wyllie, M. R. J., and G. H. F. Gardner, The Generalized Kozeny-Carman Equation, Parts I and II, World Oil, March and April 1958.

Wyllie, M. R. J., and A. R. Gregory, Formation Factors of Unconsolidated Porous Media: Influence of Particle Shape and Effect of Cementation, Petroleum Transactions of the AIME, Vol. 198, 1953, Page 103.

Wyllie, M. R. J., and M. B. Spangler, Application of Electrical Resistivity Measurements to Problem of Fluid Flow in Porous Media, Bulletin of the American Association of Petroleum Geologists, February 1952, Page 359.

Yale, D. P., Network Modelling of Flow, Storage, and Deformation in Porous Rocks, Stanford University PhD dissertation, 1984.

APPENDIX A

Monte Carlo HRP Model Simulation Program

```
*--  PROGRAM MONTE
*--
*--
*--  This program will determine F, PHI, and K distributions based
*--  on a user-specified number of Monte Carlo simulations of a given
*--  rock type; will calculate Pc, I, and Kr curves as a function of
*--  water saturation for imbibition and drainage phases; will calculate
*--  cementation and saturation exponents, Sv, and bulk density;
*--  will output data for F-PHI and K-PHI relationships.
*_   Dual tube vug version, with tortuosity, Swirr, Sores, and Cextra.
*--
*--  Programmed by:  Rob Elliott (3-5-92)
*--
*-------------------------------------------------------------------------
*--
*--  INPUT:  Interactive.
*--
*--  OUTPUT:  AHIST.DAT  -  Contains the random values/1000 for the
*--                         cross-sectional area for the first of
*--                         the Monte Carlo iterations.
*--
*--           RHIST.DAT  -  Contains the random values for the tube
*--                         radius for the first of the Monte Carlo
*--                         iterations.
*--
*--           THIST.DAT  -  Contains the random values for the
*--                          tortuosity for the first of the
*--                          Monte Carlo iterations.
*--
*--           PHI.DAT - Set of MC values of calculated porosity.
*--
*--           F.DAT - Set of MC values of calculated formation factor.
*--
*--           K.DAT - Set of MC values of calculated permeability.
*--
*--           SW.DAT - M, Sw for drainage phase.
*--
*--           PC.DAT - M, Sw, Pc for drainage.
*--
*--           I.DAT - M, Sw, I for drainage.
*--
*--           M.DAT - Iteration index, cementation exponent.
*--
```

```
*--         N.DAT - Water saturation, saturation exponent.
*--
*--         RHOB.DAT - Water saturation, bulk density.
*--
*--         KRW.DAT - M, Sw, Krw for drainage.
*--
*--         KRNW.DAT - M, Sw, Krnw for drainage.
*--
*--         SWIMB.DAT - M, Sw for imbibition phase.
*--
*--         PCIMB.DAT - M, Sw, Pc for imbibition.
*--
*--         KRWIMB.DAT - M, Sw, Krw for imbibition.
*--
*--         KRNWIMB.DAT - M, Sw, Krnw for imbibition.
*--
*--         RESULTS.DAT - All decriptive information on run
*--                 parameters and calculated values.
*--
*-----------------------------------------------------------------------
* Variables
*
      REAL  PI, PHILOW, PHIHI, FLOW, FHI, KLOW, KHI, MIN, MAX, SIGMA
      REAL  MEAN, ALPHA, BETA, SV, RLIMIT, DIST(2000), A(1000), L
      REAL  R(2000), TAUL(1000), BADR(1000), REPLACE(100), K(50)
      REAL  BULKAREA, PHIBULK, FBULK, KBULK, FMIN, KW, KNW, TMP(1000)
      REAL  FMAX, PHIMIN, PHIMAX, KMIN, KMAX, FSUM, PHISUM, KSUM, C
      REAL  FMEAN, PHIMEAN, KMEAN, D, CLOSE, FACIALT, RMIN, RVUG(1000)
      REAL  TOP, TEMP, IUPPER, ILOWER, KWUPPER,KNWUPPER,KLOWER, ARCHIEI
      REAL  RMAX, PDMIN, PDMAX, PD, SW, VP, F(50), PHI(50), PC, MBAR
      REAL  AMAT(50,1000), RLMAT(50,1000), TAULMAT(50,1000), MSUM
      REAL  RVUGMAT(50,1000), RL(1000), RS(1000), TAUS(1000)
      REAL  RSMAT(50,1000), TAUSMAT(50,1000), MMAX, PCMAX
      INTEGER  MC, NC, I, J, M, N,LIMFLAG, DISTFLAG, BADSUM, ARBADSUM
      INTEGER  BADPHI, BADF, BADK, AFLAG, RFLAG, TFLAG, ICLOSE
      INTEGER  BWARRAY(300), RTYPE, TTYPE, NR

      PI = 3.1415926535
      C = 101330000.0
      FACIALT = 35.0
      RHOM = 2.655
      RHOO = 0.730
      RHOW = 1.056

*-----------------------------------------------------------------------
* Output data files
*
      OPEN(UNIT=10,FILE='A.DAT',STATUS='NEW')
      OPEN(UNIT=11,FILE='R.DAT',STATUS='NEW')
      OPEN(UNIT=12,FILE='TL.DAT',STATUS='NEW')
      OPEN(UNIT=13,FILE='PHI.DAT',STATUS='NEW')
      OPEN(UNIT=14,FILE='F.DAT',STATUS='NEW')
```

```
      OPEN(UNIT=15,FILE='K.DAT',STATUS='NEW')
      OPEN(UNIT=16,FILE='M.DAT',STATUS='NEW')
      OPEN(UNIT=17,FILE='PHIF.DAT',STATUS='NEW')
      OPEN(UNIT=18,FILE='PHIK.DAT',STATUS='NEW')
      OPEN(UNIT=20,FILE='SW.DAT',STATUS='NEW')
      OPEN(UNIT=21,FILE='PC.DAT',STATUS='NEW')
      OPEN(UNIT=29,FILE='RESULTS.DAT',STATUS='NEW')
      OPEN(UNIT=30,FILE='RVUG.DAT',STATUS='NEW')
      OPEN(UNIT=31,FILE='L.DAT',STATUS='NEW')
      OPEN(UNIT=32,FILE='RL.DAT',STATUS='NEW')
      OPEN(UNIT=33,FILE='RS.DAT',STATUS='NEW')
      OPEN(UNIT=34,FILE='TS.DAT',STATUS='NEW')

*-----------------------------------------------------------------------
* Prompt for program parameters
*
      WRITE(*,*) ' '
1     WRITE(*,*) 'This program will determine porosity, formation
     + factor, and permeability distributions based upon a user-
     + specified number of Monte Carlo simulations.  It will also
     + calculate Pc, I, and Kr curves as a function of Sw, bulk density,
     + cementation and saturation exponents.'
      WRITE(*,*) ' '
      WRITE(*,*) '************************************************'

      WRITE(*,*) 'Enter the number of Monte Carlo iterations desired.'
      READ(*,*)  MC
      WRITE(29,*)  'Number of Monte Carlo iterations = ', MC
      WRITE(*,*) 'Enter the number of cells in the network.'
      READ(*,*)  NC
      WRITE(*,*) ' '
      WRITE(29,*) 'Number of cells = ', NC
      WRITE(*,*) '************************************************'
      WRITE(*,*) ' '
      WRITE(*,*) 'Select lower and upper limits on F, PHI, and K.'
      WRITE(*,*) 'If 10%+ of values lie below the lower limit or above
     + the upper limit, the distributions will be rejected and the
     + program will prompt for new R, A, and TAU distributions.'
      WRITE(*,*) ' '
      WRITE(*,*) 'Option (1):  PHI  --  2% - 45%'
      WRITE(*,*) '             F    --  1 - 10,000'
      WRITE(*,*) '             K    --  .001 - 15,000 mD'
      WRITE(*,*) ' '
      WRITE(*,*) 'Option (2):  PHI  --  5% - 40%'
      WRITE(*,*) '             F    --  3 - 5000'
      WRITE(*,*) '             K    --  .001 - 10,000 mD'
      WRITE(*,*) ' '
      WRITE(*,*) 'Option (3):  User specified limits.'
      WRITE(*,*) ' '
      WRITE(*,*) 'Enter option number.'
      WRITE(*,*) ' '
      READ(*,*)  LIMFLAG
```

```
      IF (LIMFLAG .EQ. 1) THEN
        PHILOW = 0.02
        PHIHI = 0.45
        FLOW = 1.0
        FHI = 10000.0
        KLOW = 0.001
        KHI = 15000.0
      ELSEIF (LIMFLAG .EQ. 2) THEN
        PHILOW = 0.05
        PHIHI = 0.40
        FLOW = 3.0
        FHI = 5000.0
        KLOW = 0.001
        KHI = 10000.0
      ELSE
        WRITE(*,*) 'Enter PHI lower limit, upper limit.'
        READ(*,*)  PHILOW, PHIHI
        WRITE(*,*) 'Enter F lower limit, upper limit.'
        READ(*,*)  FLOW, FHI
        WRITE(*,*) 'Enter K lower limit, upper limit.'
        READ(*,*)  KLOW, KHI
      ENDIF
      DO  60  j = 1, MC, 1
*-----------------------------------------------------------------------
* Prompt for and calculate A distribution, apply restrictions.
*
      IF (j .EQ. 1) THEN
5       WRITE(*,*) 'Choose the type of distribution for the cross-
     + sectional area (A).'
        WRITE(29,*) 'Choose the type of distribution for the cross-
     + sectional area (A).'
      ENDIF
      IF (j .EQ. 1) THEN
        CALL DISTRIB (NC,j,DISTFLAG,SV,MIN,MAX,MEAN,ALPHA,BETA,
     +   SIGMA,DIST)
        AFLAG = DISTFLAG
        ASV = SV
        AMIN  = MIN
        AMAX = MAX
        AMEAN = MEAN
        AALPHA = ALPHA
        ABETA = BETA
        ASIGMA = SIGMA
      ELSE
        CALL DISTRIB (NC,J,AFLAG,ASV,AMIN,AMAX,AMEAN,AALPHA,
     +   ABETA,ASIGMA,DIST)
      ENDIF
      BADSUM = 0
      DO 10 i = 1, NC, 1
        IF (DIST(i) .LT. 0.000) THEN
          DIST(i) = 0.0 - DIST(i)
          BADSUM = BADSUM + 1
```

```
      ENDIF
10   CONTINUE
     IF (BADSUM .GT. NC/10) THEN
       WRITE(*,*) 'Distribution Error:  A(i) negative.'
       WRITE(29,*) 'Greater than 10% A(i) negative.'
       GOTO 5
     ENDIF
     DO 11 I = 1, NC, 1
       A(i) = DIST(i)
       IF (j .EQ. 1) THEN
         WRITE(10,*)  A(i)
       ENDIF
11   CONTINUE
     RTYPE = 1

*-----------------------------------------------------------------------
* Prompt for and calculate r distribution, apply restrictions.
*
     DO 37 ik = 1, 3
     IF (j .EQ. 1 .AND. RTYPE .EQ. 1) THEN
15       WRITE(*,*) 'Choose the type of distribution for the radius
    + of the larger tubes.'
       WRITE(29,*) 'Choose the type of distribution for the tube
    + radius (large).'
     ELSEIF (j .EQ. 1 .AND. RTYPE .EQ. 2) THEN
       WRITE(*,*) 'Choose the type of distribution for the radius
    + of the smaller tubes.'
       WRITE(29,*) 'Choose the type of distribution for the tube
    + radius (small).'
     ELSEIF (j .EQ. 1 .AND. RTYPE .EQ. 3) THEN
       WRITE(*,*) 'Choose the type of distribution for the radius
    + of vug.'
       WRITE(29,*) 'Choose the type of distribution for the tube
    + radius.'
     ENDIF
     IF (j .EQ. 1) THEN
       IF (RTYPE .EQ. 1) THEN
         CALL DISTRIB (NC,j,DISTFLAG,SV,MIN,MAX,MEAN,ALPHA,
    +      BETA,SIGMA,DIST)
         RFLAG = DISTFLAG
         RSV = SV
         RMIN = MIN
         RMAX = MAX
         RMEAN = MEAN
         RALPHA = ALPHA
         RBETA = BETA
         RSIGMA = SIGMA
       ELSEIF (RTYPE .EQ. 2) THEN
         CALL DISTRIB (NC,j,DISTFLAG2,SV2,MIN2,MAX2,MEAN2,ALPHA2,
    +      BETA2,SIGMA2,DIST)
         R2FLAG = DISTFLAG2
         R2SV = SV2
```

```
            R2MIN = MIN2
            R2MAX = MAX2
            R2MEAN = MEAN2
            R2ALPHA = ALPHA2
            R2BETA = BETA2
            R2SIGMA = SIGMA2
          ELSE
            CALL DISTRIB (NC,j,DISTFLAG3,SV3,MIN3,MAX3,MEAN3,
     +       ALPHA3,BETA3,SIGMA3,DIST)
            R3FLAG = DISTFLAG3
            R3SV = SV3
            R3MIN = MIN3
            R3MAX = MAX3
            R3MEAN = MEAN3
            R3ALPHA = ALPHA3
            R3BETA = BETA3
            R3SIGMA = SIGMA3
          ENDIF
        ELSEIF (RTYPE .EQ. 1) THEN
          CALL DISTRIB (NC,j,RFLAG,RSV,RMIN,RMAX,RMEAN,
     +    RALPHA,RBETA,RSIGMA,DIST)
        ELSEIF (RTYPE .EQ. 2) THEN
            CALL DISTRIB (NC,j,DISTFLAG2,SV2,MIN2,MAX2,MEAN2,
     +       ALPHA2,BETA2,SIGMA2,DIST)
        ELSEIF (RTYPE .EQ. 3) THEN
            CALL DISTRIB (NC,j,DISTFLAG3,SV3,MIN3,MAX3,MEAN3,
     +       ALPHA3,BETA3,SIGMA3,DIST)
        ENDIF
        BADSUM = 0
        ARBADSUM = 0
        DO 20 i = 1, NC, 1
          IF (DIST(i) .LT. 0.00) THEN
            DIST(i) = 0.0 - DIST(i)
            BADSUM = BADSUM + 1
          ENDIF
          RLIMIT = 999999999.
          IF (DIST(i) .GT. RLIMIT) THEN
            BADR(i) = DIST(i)
            ARBADSUM = ARBADSUM + 1
          ENDIF
20      CONTINUE
        IF (BADSUM .GT. NR/10) THEN
          WRITE(*,*) 'Distribution Error:  r(i) negative.'
          WRITE(29,*) 'More than 10% r(i) negative.'
*         GOTO 15
        ENDIF
        IF (ARBADSUM .GT. 0 .AND. ARBADSUM .LT. NR/10) THEN
          IF (DISTFLAG .EQ. 1) THEN
            WRITE(*,*) 'Distribution Error:  More than 10% of R(i)
     + are too large to fit in cell.  Reselect R distribution.'
            WRITE(29,*) 'Distribution Error:  More than 10% of R(i)
     + are too large to fit in cell.  Reselect R distribution.'
```

```
          GOTO 15
        ELSEIF (DISTFLAG .EQ. 2) THEN
          CALL RNUN(ARBADSUM, REPLACE)
          DO 21 i = 1, ARBADSUM, 1
            IF (j .EQ. 1) THEN
              REPLACE(i) = (REPLACE(i)*(MAX-MIN))+MIN
            ELSE
              REPLACE(i) = (REPLACE(i)*(RMAX-RMIN))+RMIN
            ENDIF
21         CONTINUE
          DO  22 i = 1, NR, 1
            IF (REPLACE(i) .GT. RLIMIT) THEN
              REPLACE(i) = RLIMIT
            ENDIF
            IF (BADR(i) .GT. 0.0000) THEN
              DIST(i) = REPLACE(i)
            ENDIF
22         CONTINUE
        ELSEIF (DISTFLAG .EQ. 3) THEN
          CALL RNNOA(ARBADSUM, REPLACE)
          DO  23  i = 1, ARBADSUM, 1
            IF (j .EQ. 1) THEN
              REPLACE(i) = (REPLACE(i)*SIGMA) + MEAN
            ELSE
              REPLACE(i) = (REPLACE(i)*RSIGMA)+RMEAN
            ENDIF
23         CONTINUE
          DO  24 i = 1, NR, 1
            IF (REPLACE(i) .GT. RLIMIT) THEN
              REPLACE(i) = RLIMIT
            ENDIF
            IF (BADR(i) .GT. 0.0000) THEN
              DIST(i) = REPLACE(i)
            ENDIF
24         CONTINUE
        ELSEIF (DISTFLAG .EQ. 4) THEN
          IF (j .EQ. 1) THEN
            CALL RNBET(ARBADSUM, ALPHA, BETA, REPLACE)
          ELSE
            CALL RNBET(ARBADSUM, RALPHA, RBETA, REPLACE)
          ENDIF
          DO  25  i = 1, ARBADSUM, 1
            IF (j .EQ. 1) THEN
              REPLACE(i) = (REPLACE(i)*(MAX-MIN)) + MIN
            ELSE
              REPLACE(i) = (REPLACE(i)*(RMAX-RMIN))+RMIN
            ENDIF
25         CONTINUE
          DO  27  i = 1, NR, 1
            IF (REPLACE(i) .GT. RLIMIT) THEN
              REPLACE(i) = RLIMIT
            ENDIF
```

```
            IF (BADR(i) .GT. 0.0000) THEN
              DIST(i) = REPLACE(i)
            ENDIF
27          CONTINUE
          ELSEIF (DISTFLAG .EQ. 5) THEN
            IF (j .EQ. 1) THEN
              CALL RNLNL(ARBADSUM, MEAN, SIGMA, REPLACE)
            ELSE
              CALL RNLNL(ARBADSUM, RMEAN, RSIGMA, REPLACE)
            ENDIF
            DO 32 i = 1, ARBADSUM, 1
              IF (j .EQ. 1) THEN
                REPLACE(i) = (REPLACE(i)*(MAX-MIN)/10.)+MIN
              ELSE
                REPLACE(i) = (REPLACE(i)*(RMAX-RMIN)/10.)+RMIN
              ENDIF
32          CONTINUE
            DO 35 i = 1, NR, 1
              IF (REPLACE(i) .GT. RLIMIT) THEN
                REPLACE(i) = RLIMIT
              ENDIF
              IF (BADR(i) .GT. 0.0000) THEN
                DIST(i) = REPLACE(i)
              ENDIF
35          CONTINUE
          ENDIF
        ELSEIF (ARBAD .GT. NR/10) THEN
          WRITE(*,*) 'Distribution Error:  More than 10% of
       + R(i) are too large to fit in cell, please reselect distri
       + bution.'
          WRITE(29,*) 'Distribution Error:  More than 10% of
       + R(i) are too large to fit in cell, please reselect distri
       + bution.'
          GOTO 15
        ENDIF
        IF (RTYPE .EQ. 1) THEN
          DO 320 i = 1, NC
            RL(i) = DIST(i)
            IF (j .EQ. 2) THEN
              WRITE(32,*) RL(i)
            ENDIF
320       CONTINUE
        ELSEIF (RTYPE .EQ. 2) THEN
          DO 321 i = 1, NC
            RS(i) = DIST(i)
            IF (j .EQ. 2) THEN
              WRITE(33,*) RS(i)
            ENDIF
321       CONTINUE
        ELSEIF (RTYPE .EQ. 3) THEN
          DO 322 i = 1, NC
            RVUG(i) = DIST(i)
```

```
          IF (j .EQ. 2) THEN
            WRITE(30,*)  RVUG(i)
          ENDIF
322       CONTINUE
      ENDIF
      RTYPE = RTYPE + 1
37    CONTINUE
      TTYPE = 1
*-----------------------------------------------------------------------
* Prompt for and calculate tau distribution, apply restriction.
      DO  302 ij = 1, 2
      IF (j .EQ. 1 .AND. TTYPE .EQ. 1) THEN
29       WRITE(*,*) 'Choose the type of distribution for the
     + tortuosity of the larger tubes.'
         WRITE(29,*) 'Choose the type of distribution for the
     + tortuosity (larger tubes).'
      ELSEIF (j .EQ. 1) THEN
         WRITE(*,*) 'Choose the type of distribution for the
     + tortuosity of the smaller tubes.'
         WRITE(29,*) 'Choose the type of distribution for the
     + tortuosity (smaller tubes).'
      ENDIF
      IF (j .EQ. 1) THEN
        IF (TTYPE .EQ. 1) THEN
          CALL DISTRIB (NC,j,DISTFLAG,SV,MIN,MAX,MEAN,ALPHA,
     +       BETA,SIGMA,DIST)
          TFLAG = DISTFLAG
          TSV = SV
          TMIN = MIN
          TMAX = MAX
          TMEAN = MEAN
          TALPHA = ALPHA
          TBETA = BETA
          TSIGMA = SIGMA
        ELSE
          CALL DISTRIB (NC,j,DISTFLAGT2,SVT2,MINT2,MAXT2,MEANT2,
     +       ALPHAT2,BETAT2,SIGMAT2,DIST)
          T2FLAG = DISTFLAGT2
          T2SV = SVT2
          T2MIN = MINT2
          T2MAX = MAXT2
          T2MEAN = MEANT2
          T2ALPHA = ALPHAT2
          T2BETA = BETAT2
          T2SIGMA = SIGMAT2
        ENDIF
      ELSEIF (TTYPE .EQ. 1) THEN
        CALL DISTRIB (NC,j,TFLAG,TSV,TMIN,TMAX,TMEAN,
     +    TALPHA,TBETA,TSIGMA,DIST)
      ELSEIF (TTYPE .EQ. 2) THEN
        CALL DISTRIB (NC,j,DISTFLAGT2,SVT2,MINT2,MAXT2,MEANT2,
     +    ALPHAT2,BETAT2,SIGMAT2,DIST)
```

```
      ENDIF
      BADSUM = 0
      DO 30 i = 1, NC, 1
        IF (DIST(i) .LT. 1.000) THEN
          DIST(i) = 1.000
          BADSUM = BADSUM + 1
        ENDIF
30    CONTINUE
      IF (BADSUM .GT. NC/10) THEN
        WRITE(*,*) 'Distribution Error:  >10% Tau(i) less than 1.0'
        WRITE(29,*) 'Distribution Error:  >10% Tau(i) less than 1.0'
        GOTO 29
      ENDIF
      DO  31  i = 1, NC, 1
        IF (TTYPE .EQ. 1) THEN
          TAUL(i) = DIST(i)
          IF (j .EQ. 2) THEN
            WRITE(12,*)  TAUL(i)
          ENDIF
        ELSE
          TAUS(i) = DIST(i)
          IF (j .EQ. 2) THEN
            WRITE(34,*)  TAUS(i)
          ENDIF
        ENDIF
31    CONTINUE
      TTYPE = 2
302   CONTINUE

*-----------------------------------------------------------------------
* Prompt for cell length L.
      IF (j .EQ. 1) THEN
        WRITE(*,*)  'Enter deterministic value for L in micrometers.'
        READ(*,*)  L
        WRITE(31,*)  L
      ENDIF

*-----------------------------------------------------------------------
* Calculate bulk porosity, formation factor, and permeability.
      IF (j .EQ. 1) THEN
        WRITE(*,*) 'Enter alpha = Vext/Vporetotal.'
        READ(*,*)  ALP
        WRITE(*,*) 'Enter beta = Voil/Vporetotal.'
        READ(*,*)  BET
      ENDIF
      BULKAREA = 0.0
      DO  40  i = 1, NC, 1
        AMAT(j,i) = A(i)
        RLMAT(j,i) = RL(i)
        RSMAT(j,i) = RS(i)
        RVUGMAT(j,i) = RVUG(i)
        TAULMAT(j,i) = TAUL(i)
```

```
      TAUSMAT(j,i) = TAUS(i)
      BULKAREA = BULKAREA + A(i)
40    CONTINUE
      OPEN(UNIT=19,FILE='RHOB.DAT',STATUS='NEW')


      PHIBULK = 0.0
      FBULK = 0.0
      KBULK = 0.0
      DO  50  i = 1, NC, 1
        PHIBULK = PHIBULK + (4./3.)*pi*RVUG(i)**3 + pi*(L-2.*RVUG(i))
     +   *(RL(i)**2*TAUL(i) + RS(i)**2*TAUS(i))
        FBULK = FBULK + ((RS(i)**2*(TAUL(i)*(L-2.*RVUG(i))+RL(i)))+
     +   (RL(i)**2*(TAUS(i)*(L-2.*RVUG(i))+RS(i))))/((TAUL(i)*
     +   (L-2.*RVUG(i))+RL(i))*(TAUS(i)*(L-2.*RVUG(i))+RS(i)))
        KBULK = KBULK + (((RL(i)/10000.)**4/TAUL(i)) +
     +   ((RS(i)/10000.)**4/TAUS(i)))
     +   /((L/10000.-2.*RVUG(i)/10000.)**2)
50    CONTINUE
      PHI(j) = (PHIBULK*(1.+(ALP/(1.-ALP)))) /(L * BULKAREA)
      F(j) = (BULKAREA/ FBULK)/(L*pi)
      K(j) = 1000.0*(KBULK * pi *((L/10000.)**2)* C/8.0) / (BULKAREA
     + /100000000.)
      WRITE(13,*) PHI(j) *100.0
      WRITE(14,*) F(j)
      WRITE(15,*) K(j)
      ARCHIEM = -LOG(F(j))/LOG(PHI(j))
      MSUM = MSUM + ARCHIEM
      WRITE(16,*)  j, ARCHIEM
      WRITE(29,*) 'Iteration ',j,',  m = ',ARCHIEM
      WRITE(17,*)  PHI(j), F(j)
      WRITE(18,*)  PHI(j), K(j)
      IF (j .EQ. 1) THEN
        WRITE(*,*) 'Number of Monte Carlo simulations = ',MC,'.'
      ENDIF
      WRITE(*,*) 'Simulation ', j, ' complete.'

60    CONTINUE

      MBAR = MSUM / REAL(MC)
      WRITE(29,*) 'Average m =', MBAR
      BADPHI = 0
      BADK = 0
      BADF = 0
      DO  70  i = 1, MC, 1
        IF (PHI(i) .LT. PHILOW .OR. PHI(i) .GT. PHIHI) THEN
          BADPHI = BADPHI + 1
        ENDIF
        IF (F(i) .LT. FLOW .OR. F(i) .GT. FHI) THEN
          BADF = BADF + 1
        ENDIF
        IF (K(i) .LT. KLOW .OR. K(i) .GT. KHI) THEN
```

```
          BADK = BADK + 1
        ENDIF
70    CONTINUE
*     IF (BADPHI .GT. MC/10) THEN
*        WRITE(*,*) 'Calculated porosities out of bounds;
*    + try different distributions.'
*        WRITE(29,*) 'Calculated porosities out of bounds;
*    + try different distributions.'
*        GOTO 1
*     ENDIF
*     IF (BADF .GT. MC/10) THEN
*        WRITE(*,*) 'Calculated formation factors out of
*    + bounds; try different distributions.'
*        WRITE(29,*) 'Calculated formation factors out of
*    + bounds; try different distributions.'
*        GOTO 1
*     ENDIF
*     IF (BADK .GT. MC/10) THEN
*        WRITE(*,*) 'Calculated permeabilities out of
*    + bounds; try different distributions.'
*        WRITE(29,*) 'Calculated permeabilities out of
*    + bounds; try different distributions.'
*        GOTO 1
*     ENDIF

*-----------------------------------------------------------------
* Calculate min, mean, and max for PHI, F, and K.
      FSUM = 0.0
      PHISUM = 0.0
      KSUM = 0.0
      FMIN = 99999.9
      FMAX = 0.0
      PHIMIN = 99999.9
      PHIMAX = 0.0
      KMIN = 99999.9
      KMAX = 0.0
      DO  80  i = 1, MC, 1
        IF (F(i) .GT. FMAX) THEN
          FMAX = F(i)
        ELSEIF (F(i) .LT. FMIN) THEN
          FMIN = F(i)
        ENDIF
        FSUM = FSUM + F(i)
        IF (PHI(i) .GT. PHIMAX) THEN
          PHIMAX = PHI(i)
        ELSEIF (PHI(i) .LT. PHIMIN) THEN
          PHIMIN = PHI(i)
        ENDIF
        PHISUM = PHISUM + PHI(i)
        IF (K(i) .GT. KMAX) THEN
          KMAX = K(i)
        ELSEIF (K(i) .LT. KMIN) THEN
```

```
          KMIN = K(i)
        ENDIF
        KSUM = KSUM + K(i)
80    CONTINUE
      CLOSE(12)
      FMEAN = FSUM / REAL(MC)
      PHIMEAN = PHISUM / REAL(MC)
      KMEAN = KSUM / REAL(MC)
      WRITE(*,*) 'Minimum calculated PHI is ', PHIMIN,'.'
      WRITE(29,*) 'Minimum calculated PHI is ', PHIMIN,'.'
      WRITE(*,*) 'Mean PHI is ', PHIMEAN, '.'
      WRITE(29,*) 'Mean PHI is ', PHIMEAN, '.'
      WRITE(*,*) 'Maximum calculated PHI is ', PHIMAX,'.'
      WRITE(29,*) 'Maximum calculated PHI is ', PHIMAX,'.'
      WRITE(*,*) '   '
      WRITE(29,*) '   '
      WRITE(*,*) 'Minimum calculated F is ', FMIN,'.'
      WRITE(29,*) 'Minimum calculated F is ', FMIN,'.'
      WRITE(*,*) 'Mean F is ', FMEAN, '.'
      WRITE(29,*) 'Mean F is ', FMEAN, '.'
      WRITE(*,*) 'Maximum calculated F is ', FMAX, '.'
      WRITE(29,*) 'Maximum calculated F is ', FMAX, '.'
      WRITE(*,*) '   '
      WRITE(29,*) '   '
      WRITE(*,*) 'Minimum calculated K is ', KMIN, '.'
      WRITE(29,*) 'Minimum calculated K is ', KMIN, '.'
      WRITE(*,*) 'Mean K is ', KMEAN, ' millidarcies.'
      WRITE(29,*) 'Mean K is ', KMEAN, '.'
      WRITE(*,*) 'Maximum calculated K is ', KMAX, '.'
      WRITE(29,*) 'Maximum calculated K is ', KMAX, '.'
      WRITE(*,*) '   '
      WRITE(29,*) '   '
      WRITE(*,*) 'Mean m is ', MBAR, '.'
      WRITE(29,*) 'Mean m is ', MBAR, '.'

*-----------------------------------------------------------------
* Find {A,r,tau} suite most representative of mean F, PHI, K.
      CLOSE = 99999.9
      DO  90  i = 1, MC, 1
        D = (F(i)**2) + (PHI(i)**2) + (K(i)**2)
        IF (D .LT. CLOSE) THEN
          CLOSE = D
          ICLOSE = i
        ENDIF
90    CONTINUE
      BULKAREA = 0.0
      SV = 0.0
      DO  100  i = 1, NC, 1
        A(i) = AMAT(ICLOSE,i)
        RL(i) = RLMAT(ICLOSE,i)
        RS(i) = RSMAT(ICLOSE,i)
        RVUG(i) = RVUGMAT(ICLOSE,i)
```

```
      TAUL(i) = TAULMAT(ICLOSE,i)
      TAUS(i) = TAUSMAT(ICLOSE,i)
*      SV = SV + 2*pi*RL(i)*TAU(i)/A(i)
      BULKAREA = BULKAREA + A(i)
100   CONTINUE
    WRITE(*,*) 'The surface area per unit volume (Sv) = ',SV
    WRITE(29,*) 'The surface area per unit volume (Sv) = ',SV
    WRITE(*,*) 'The bulk area of the network is ',
   + BULKAREA/100000000., ' sq cm.'
    WRITE(29,*) 'The bulk area of the network is ',
   + BULKAREA/100000000., ' sq cm.'
*-----------------------------------------------------------------
* Sort r(i), find min and max displacement pressures.
    N = NC
    DO  110  TOP = 1, N, 1
      MIN = RL(TOP)
      DO  105  i = TOP+1, N
        IF (RL(i) .LT. MIN) THEN
          TEMP = RL(i)
          RL(i) = MIN
          MIN = TEMP
        ENDIF
105     CONTINUE
      RL(TOP) = MIN
110   CONTINUE
    DO  111  i = 1, NC, 1
      TMP(NC+1-i) = RL(i)
111   CONTINUE
    DO  112  i = 1, NC, 1
      IF (TMP(i) .LT. 0.01) THEN
        TMP(i) = 0.01
      ENDIF
      RL(i) = TMP(i)
112   CONTINUE

    PDMIN = 2*FACIALT*14.7*100./(C*RL(1)/10000.0)
    PDMAX = 2*FACIALT*14.7*100./(C*RL(NC)/10000.0)
    INPDMAX = INT(PDMAX)
    WRITE(*,*) 'Displacement pressure for the largest
   + tube is ', PDMIN, ' psi.'
    WRITE(*,*) 'Displacement pressure for the smallest
   + tube is ', PDMAX, ' psi.'
    WRITE(29,*) 'Displacement pressure for the largest
   + tube is ', PDMIN, ' psi.'
    WRITE(29,*) 'Displacement pressure for the smallest
   + tube is ', PDMAX, ' psi.'
    CLOSE(10)
    CLOSE(11)
    CLOSE(12)
    CLOSE(13)

*-----------------------------------------------------------------
```

```
* Loop to calculate I, Pc, and Kr as a function of Sw (drainage).
      OPEN(UNIT=22,FILE='I.DAT',STATUS='NEW')
      OPEN(UNIT=23,FILE='KRW.DAT',STATUS='NEW')
      OPEN(UNIT=27,FILE='N.DAT',STATUS='NEW')
      OPEN(UNIT=28,FILE='KRNW.DAT',STATUS='NEW')
      WRITE(*,*) 'Please enter value for desired irreducible water
     + saturation.'
      READ(*,*) SWIRR
      WRITE(29,*) 'Irreducible water saturation = ',SWIRR
      WRITE(*,*) 'Please enter value for residual oil saturation.'
      READ(*,*)  SORES
      WRITE(29,*) 'Residual oil saturation = ', SORES

      IUPPER = 0.0
      KLOWER = 0.0
      SWLOWER = 0.0
      DO  114  i = 1, NC, 1
        IUPPER = IUPPER + ((RS(i)**2*(TAUL(i)*(L-2.*RVUG(i))+RL(i)))+
     +    (RL(i)**2*(TAUS(i)*(L-2.*RVUG(i))+RS(i))))/(RL(i)**2*
     +    RS(i)**2)
        KLOWER = KLOWER + pi**((L/10000.)**2)*C*(((RL(i)/10000.)**4
     +    /TAUL(i))
     +    +((RS(i)/10000.)**4/
     +    TAUS(i))))/(8.*((L/10000.-2.*RVUG(i)/10000.)**2))
        SWLOWER = SWLOWER +pi*((RL(i)**2*TAUL(i))+(RS(i)**2*TAUS(i)))
     +    *(L-2.*RVUG(i)) + (4./3.)*pi*RVUG(i)**3
114   CONTINUE
      SWLOWER = SWLOWER * (1 + (ALP/(1.-ALP)))
      IUPPER = IUPPER * (L/pi)
      M = 0
      SW = 1.00
      KW = 1.00
      ARCHIEI = 1.00

      DO  170  PC = 0.0, PDMAX, .10
117     PD = 2*FACIALT*14.7*100./(C*RL(m+1)/10000.0)
        IF (PC .GE. 50.0) GOTO 180
        IF (PC .GE. PD) THEN
          M = M + 1
          SWTOPA = 0.0
          SWTOPB = 0.0
          DO  118  i = M+1, NC
            SWTOPA = SWTOPA + (L-2.*RVUG(i))*pi*
     +        ((RL(i)**2*TAUL(i)) + (RS(i)**2*TAUS(i)))
     +        +(4./3.)*pi*RVUG(i)**3
118       CONTINUE
          SWTOPA = SWTOPA * (1.+(ALP/(1.-ALP)))
          DO  119  i = 1, M
            SWTOPB = SWTOPB + (L-2.*RVUG(i))*pi*RS(i)**2
     +        *TAUS(i)+ (ALP/(1.-ALP))*PI*(((L-2.*RVUG(i))*
     +        (RL(i)**2*TAUL(i)+RS(i)**2*TAUS(i))+
     +        (4./3.)*pi*RVUG(i)**3))
```

```
119          CONTINUE
            SW = (SWTOPA + SWTOPB) / SWLOWER
            ILOWER = 0.0
            DO  130  i = M+1, NC
              ILOWER = ILOWER + ((RS(i)**2*(TAUL(i)*
     +         (L-2.*RVUG(i))+RL(i)))+(RL(i)**2*(TAUS(i)*
     +         (L-2.*RVUG(i))+RS(i))))/(RL(i)**2*RS(i)**2)
130          CONTINUE
            ILOWER = ILOWER * (L/pi)
            ARCHIEI = IUPPER/ILOWER
            ARCHIEN = -LOG(ARCHIEI)/LOG(SW)
                    WRITE(27,*)  SW, ARCHIEN
            RHOB = RHOM*(1.0 - TEMPPHI)+ RHOW*(TEMPPHI*SW) +
     +       RHOO*(TEMPPHI*(1.0 - SW))
            WRITE(19,*)  SW, RHOB
            KWUPPER = 0.0
            DO  140  i = M+1, NC
              KWUPPER = KWUPPER + pi**((L/10000.)**2)
     +          *C*(((RL(i) /10000.)**4/
     +          TAUL(i))+ ((RS(i)/10000.)**4/TAUS(i)))
     +          /(8.*((L/10000.-2.*RVUG(i)/10000.)**2))
140          CONTINUE
            KW = KWUPPER/KLOWER
            KNWUPPER = 0.0
            DO  160  i = 1, M
            KNWUPPER = KNWUPPER + pi**((L/10000.)**2)*C*(((RL(i)
     +       /10000.)**4/
     +       TAUL(i))/(8.*((L/10000.-2.*RVUG(i)/10000.)**2)))
160          CONTINUE
            KNW = KNWUPPER / KLOWER
           IF (SW .LT. SWIRR) GOTO 180
         ELSE
           GOTO 165
         ENDIF
         GOTO 117
165        WRITE(20,*)  M, SW
         WRITE(21,*)  M, SW, REAL(PC)
         WRITE(23,*)  M, SW, KW
         WRITE(28,*)  M, SW, KNW
         WRITE(22,*)  M, SW, ARCHIEI
170   CONTINUE
180   CONTINUE
      MMAX = M
      PCMAX = PC
      CLOSE(30)
      CLOSE(31)
      CLOSE(32)
      OPEN(UNIT=35,FILE='krwimb.dat',STATUS='NEW')
      OPEN(UNIT=36,FILE='krnwimb.dat',STATUS='NEW')
      OPEN(UNIT=37,FILE='pcimb.dat',STATUS='NEW')

*---------------------------------------------------------------
```

```
* Loop to calculate Pc as a function of Sw (imbibition).
*
      DO 230 PC = PCMAX, PDMIN, -0.1
415         PD = 2*FACIALT*14.7*100./(C*RL(m-1)/10000.0)
          IF (PC .LE. PD) THEN
            M = M - 1
            SWTOPA = 0.0
            SWTOPB = 0.0
            DO 418 i = M+1, MMAX
              SWTOPA = SWTOPA + (L-2.*RVUG(i))*pi*
     +          ((RL(i)**2*TAUL(i)) + (RS(i)**2*TAUS(i)))
     +          +(4./3.)*pi*RVUG(i)**3
418           CONTINUE
            FACT = (1.-BET)+(M/(NC/(1.-BET)))
            SWTOPA = SWTOPA * (1.+(ALP/(1.-ALP)))*FACT
            DO 419 i = 1, M
              SWTOPB = SWTOPB + (L-2.*RVUG(i))*pi*RS(i)**2
     +          *TAUS(i)+ (ALP/(1.-ALP))*PI*(((L-2.*RVUG(i))*
     +          (RL(i)**2*TAUL(i)+RS(i)**2*TAUS(i))+
     +          (4./3.)*pi*RVUG(i)**3))
419           CONTINUE
            SW = (SWTOPA + SWTOPB) / SWLOWER
            KWUPPER = 0.0
            DO 440 i = M+1, NC
              KWUPPER = KWUPPER + pi**((L/10000.)**2)
     +          *C*(((RL(i) /10000.)**4/
     +          TAUL(i))+ ((RS(i)/10000.)**4/TAUS(i)))
     +          /(8.*((L/10000.-2.*RVUG(i)/10000.)**2))
440           CONTINUE
            KW = KWUPPER/KLOWER
            KNWUPPER = 0.0
            DO 460 i = 1, M
            KNWUPPER = KNWUPPER + pi**((L/10000.)**2)*C*(((RL(i)
     +       /10000.)**4/
     +       TAUL(i))/(8.*((L/10000.-2.*RVUG(i)/10000.)**2)))
460           CONTINUE
            KNW = KNWUPPER / KLOWER
          ELSE
            GOTO 470
          ENDIF
          GOTO 415
470           WRITE(35,*) M, SW, KW
            WRITE(36,*) M, SW, KNW
            WRITE(37,*) M, SW, REAL(PC)
230   CONTINUE

      END

*-------------------------------------------------------------------
*-------------------------------------------------------------------
      SUBROUTINE DISTRIB(NC,j,FLAG,SV,MIN,MAX,MEAN,ALPHA,
     + BETA, SIGMA, R)
```

```
      REAL  R(1000), MEAN, MIN, MAX
      INTEGER  FLAG, J, LOGFLAG
      IF (j .EQ. 1) THEN
        WRITE(*,*) '   (1) Single-value'
        WRITE(*,*) '   (2) Uniform'
        WRITE(*,*) '   (3) Gaussian'
        WRITE(*,*) '   (4) Beta'
        WRITE(*,*) '   (5) Lognormal'
        READ(*,*)  FLAG
      ENDIF
      IF (FLAG .EQ. 1) THEN
        IF (j .EQ. 1) THEN
          WRITE(*,*) 'Enter value of the distribution.'
          WRITE(*,*) 'A in square micrometers;'
          WRITE(*,*) 'r in micrometers;'
          WRITE(*,*) 'Tau is unitless.'
          READ(*,*)  SV
          WRITE(29,*) 'Singular Value = ', SV
        ENDIF
        DO  100  i = 1, NC, 1
          R(i) = SV
100     CONTINUE
      ENDIF
      IF (FLAG .EQ. 2) THEN
        IF (j .EQ. 1) THEN
          WRITE(*,*) 'Enter the minimum and maximum.'
          WRITE(*,*) 'A in square micrometers;'
          WRITE(*,*) 'r in micrometers;'
          WRITE(*,*) 'Tau is unitless.'
          READ(*,*)  MIN, MAX
          WRITE(29,*) 'Uniform:  min = ',MIN,', MAX = ',MAX
        ENDIF
        CALL RNUN(NC, R)
        DO  200  i = 1, NC, 1
          R(i) = (R(i)*(MAX-MIN))+MIN
200     CONTINUE
      ENDIF
      IF (FLAG .EQ. 3) THEN
        IF (j .EQ. 1) THEN
          WRITE(*,*) 'Enter the mean value (mu).'
          WRITE(*,*) 'A in square micrometers;'
          WRITE(*,*) 'r in micrometers;'
          WRITE(*,*) 'Tau is unitless.'
          READ(*,*)  mean
          WRITE(*,*) 'Enter the standard deviation (sigma).'
          READ(*,*)  sigma
          WRITE(29,*) 'Gaussian: Mu = ',MEAN,', Sigma = ',SIGMA
        ENDIF
        CALL RNNOA(NC, R)
        DO  300  i = 1, NC, 1
          R(i) = (R(i)*sigma) + mean
300     CONTINUE
```

```
      ENDIF
      IF (FLAG .EQ. 4) THEN
        IF (j .EQ. 1) THEN
          WRITE(*,*) 'Enter alpha, beta, min, max.'
          WRITE(*,*) 'A in square micrometers;'
          WRITE(*,*) 'r in micrometers;'
          WRITE(*,*) 'Tau is unitless.'
          READ(*,*)  ALPHA, BETA, MIN, MAX
          WRITE(29,*) 'Beta: Alpha = ',ALPHA,', BETA = ',BETA
          WRITE(29,*) '      Min = ',MIN,', Max = ',MAX
        ENDIF
        CALL RNBET(NC, ALPHA, BETA, R)
        DO  400  i = 1, NC, 1
          R(I) = (R(i)*(MAX-MIN))+MIN
400     CONTINUE
      ENDIF
      IF (FLAG .EQ. 5) THEN
        IF (j .EQ. 1) THEN
          WRITE(*,*) 'Enter the mean of the underlying
     + normal distribution; this method will generate normal deviates
     + with mean, mu, and standard deviation, sigma, and then
     + exponentiate the normal deviates.'
          WRITE(*,*) 'A in square micrometers.'
          WRITE(*,*) 'r in micrometers.'
          WRITE(*,*) 'Tau is unitless.'
          READ(*,*) MEAN
          WRITE(*,*) 'Enter the standard deviation.'
          READ(*,*) SIGMA
          WRITE(*,*) 'Now enter the minimum and the maximum
     + of the distribution.'
          READ(*,*) MIN, MAX
          WRITE(29,*) 'Lognormal: Mu = ',Mu,', Sigma = ',SIGMA
          WRITE(*,*) 'Enter (1) for true log-normal or (2)
     + for inverted lognormal.'
          READ(*,*) LOGFLAG
          IF (LOGFLAG .EQ. 2) WRITE(29,*) 'Lognormal inverted.'
        ENDIF
        CALL RNLNL(NC, MEAN, SIGMA, R)
        DO  500  i = 1, NC, 1
          IF (LOGFLAG .EQ. 2) THEN
            R(i) = 10.0 - R(i)
          ENDIF
          R(i) = (R(i)*(MAX-MIN)/10.0) + MIN
500     CONTINUE
      ENDIF
      RETURN
      END
*-----------------------------------------------------------------------
*-----------------------------------------------------------------------
```

Appendix B

Probability Theory of the Monte Carlo Simulation

The probability density function, or simply density function, is a mathematical expression over the range of a continuous stochastic variable. It describes the relative frequency of occurrences of a particular value of the random variable. Probabilities for intervals of a stochastic variable can be obtained by the integration of the density function. The density function f(y) for a continuous random variable y is equal to the derivative of the associated cumulative distribution function F(y), or

$$f(y) = \frac{dF(y)}{dy}.$$

It follows from the previous equation that the area under the curve between $-\infty$ and a point y_0 is equal to $F(y_0)$. Furthermore, the density function must have a non-negative range and the area underneath its curve should equal 1. These are stated mathematically below:

1.) $f(y) \geq 0$

2.) $\int_{-\infty}^{+\infty} f(y)dy = F(\infty) = 1.$

There are three terms which can be used to describe a sample of data points or a distribution:

1.) **Median** The middle value of a distribution; this value exceeds half the data points and is itself exceeded by the other half.

2.) **Mode** The one value that occurs most frequently; the most probable.

3.) **Arithmetic Mean** The average; the sum of all measured values divided by the total number of measurements.

Not all distributions are symmetric about a particular value; the skewness is a measure of the lopsidedness of the distribution. Figure B-1 shows a right-skewed distribution, the median and the mean being greater than the mode. In a left-skewed distribution, the values for the median and the mean are both less than that of the mode.

The distribution of the samples about some measure of central tendency is described by various measures of dispersion. Two of the most important are the variance, V, and its square root, the standard deviation, σ. The formulas for variance and standard deviation are given by

$$V = \frac{\sum_{i=1}^{N}(x_i - x_{mean})^2}{N},$$

$$\sigma = \sqrt{\frac{\sum_{i=1}^{N}(x_i - x_{mean})^2}{N}},$$

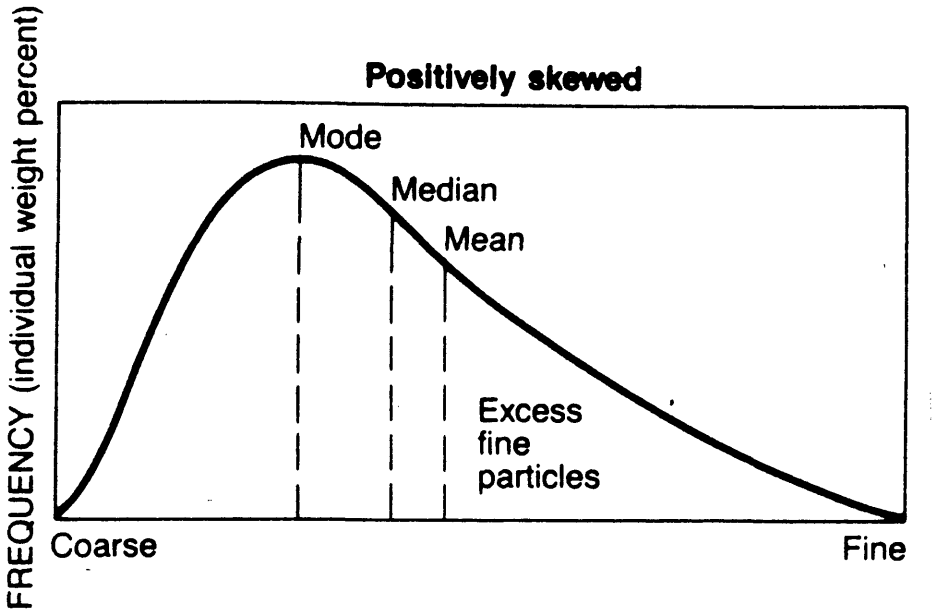

Figure B-1. Positively skewed probability density function.

where x_i represent the individual values, x_{mean} the mean value, and N is the number of data points.

The singular-value, uniform, Gaussian, and Beta distributions are now discussed separately.

The Singular-value Probability Distribution

Also known as a discrete one-value or deterministic distribution, this function allows only one value to occur. This value is, by definition, the mean, mode, and median, and the probability of occurence is 100%.

The Uniform Probability Distribution

This distribution is used to randomly select a number y, where y has an equal chance of occurrence in the interval $a \leq y \leq b$. The density function, mean and variance are given below:

$$f(y) = \frac{1}{b-a} \quad \text{if } a \leq y \leq b$$

$$0 \quad \text{elsewhere}$$

$$m = \frac{a+b}{2} \qquad \sigma^2 = \frac{(b-a)^2}{12}$$

A uniform distribution with a minumum value of 150, a mean of 175, and a maximum value of 200 is shown in Figure 10. Pseudorandom numbers from a uniform (0,1) distribution can be generated on the VAX with the IMSL subroutines RNUN (single precision) and DRNUN (double precision) as below:

CALL RNUN(NR, R)

NR = Number of random numbers to generate. (Input)

R = Vector of length NR containing random uniform values. (Output)

The Gaussian Probability Distribution

This bell-shaped curve provides accurate frequency distributions for many different scientific phenomena. The density function is characterized by two parameters, the mean, m, and standard deviation, σ,

$$f(y) = \frac{1}{\sigma\sqrt{2\pi}} e^{-(y-m)^2/2\sigma^2} \qquad -\infty < y < +\infty.$$

Figure B-2 shows several Gaussian distributions with various values of σ and μ. Pseudorandom numbers from a standard normal ($\mu = 0$, $\sigma = 1$) distribution can be generated on the VAX using the IMSL subroutines RNNOA (single precision) and DRNNOA (double precision):

CALL RNNOA(NR, R)

NR = Number of random numbers to generate. (Input)

R = Vector of length NR containing random Gaussian values. (Output)

The Beta Probability Distribution

The Beta function is useful in that it can generate bell-shaped curves that are either left-symmetric or right-symmetric. It possesses finite lower and upper limits - usually given as 0 and 1, but these can be modified. The probability density function for the Beta distribution is given by

$$f(y) = \frac{y^{\alpha-1}(1-y)^{\beta-1}}{B(\alpha,\beta)} \qquad \text{if } 0 \le y \le 1;\ \alpha > 0, \beta > 0$$

where

$$B(\alpha,\beta) = \int_0^1 y^{\alpha-1}(1-y)^{\beta-1}dy = \frac{G(\alpha)G(\beta)}{G(\alpha+\beta)}$$

where

$$G(\alpha) = \int_0^\infty y^{\alpha-1}e^{-y}dy$$

$$G(\alpha) = (\alpha-1)! \text{ when } \alpha \text{ is a positive integer}$$

The mean and variance are given by

$$m = \frac{\alpha}{\alpha+\beta} \qquad \sigma^2 = \frac{\alpha\beta}{(\alpha+\beta)^2(\alpha+\beta+1)}.$$

Figure B-3 includes graphs of beta density functions with $\alpha = 2$ and various values for β. Pseudorandom numbers following a Beta distribution can be generated on the VAX by the IMSL subroutines RNBET (single precision) and DRNBET (double precision):

CALL RNBET(NR,PIN,QIN,R)

NR = Number of random numbers to generate. (In)

PIN = α; $\alpha > 0$. (In)

QIN = β; $\beta > 0$. (In)

R = Vector of length NR. (Out)

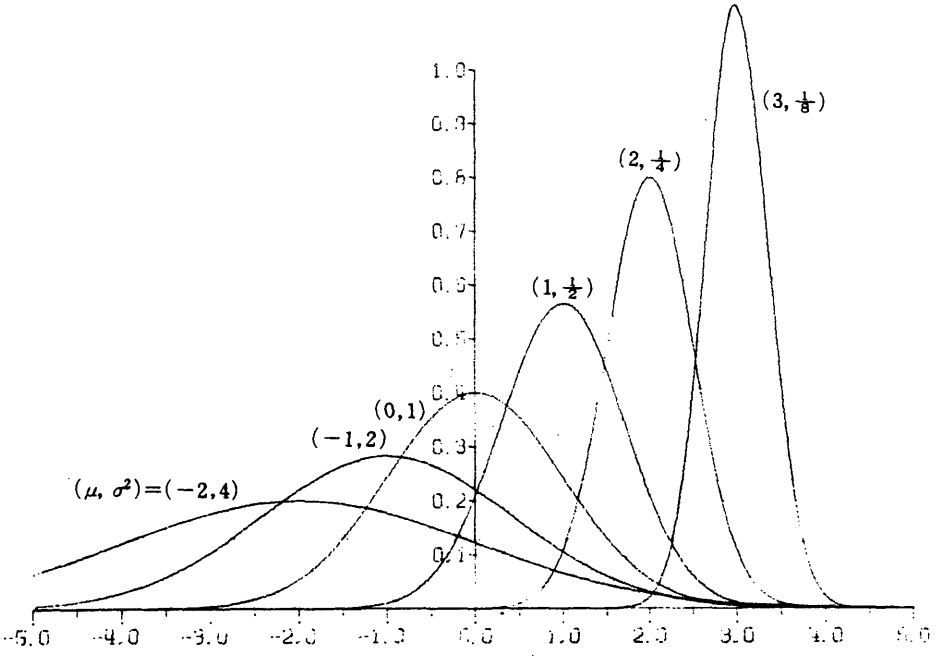

Figure B-2. Gaussian distributions with varying (μ, σ^2).

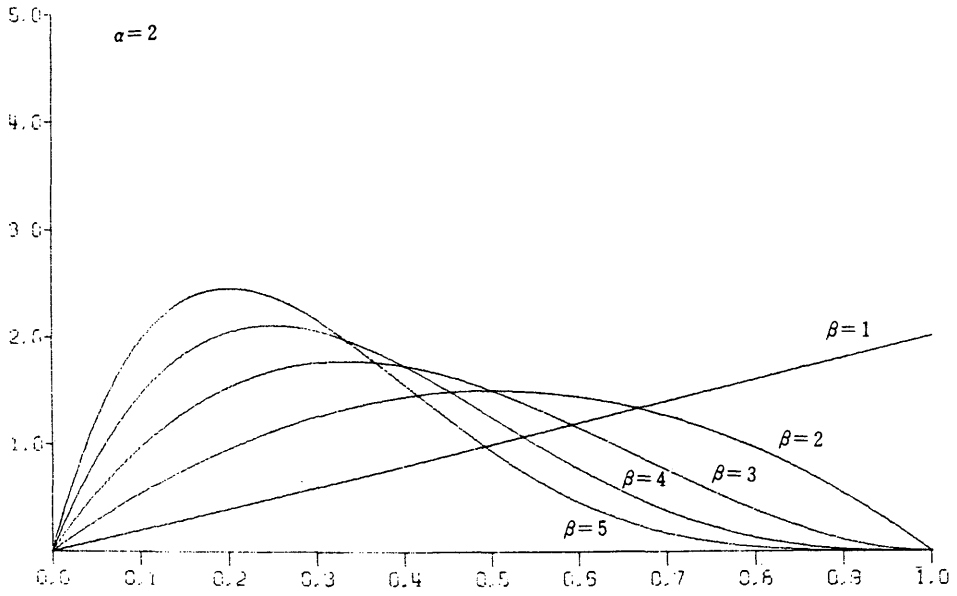

Figure B-3. Beta distributions with $\alpha = 2$ and $\beta = 1,2,3,4,5$. Note positive skewness of the (2,3), (2,4), and (2,5) distributions.